PhD Dissertation

Experimental and Numerical Investigations on the Hydraulic Characteristics of Two-phase Flow in Rock Fractures

岩盤き裂内における二相流の水理学的特性に関する数値と実験的研究

2019 年 3 月

長崎大学大学院工学研究科

王 辰

Chen Wang

Experimental and Numerical Investigations on the Hydraulic Characteristics of Two-phase Flow in Rock Fractures

Acknowledgements

I would like to express my appreciation to all those who offer their kind help during my stay in Nagasaki University. It's difficult to list all of them, but I'd like to appreciate everyone who has contributions to my research and life.

I will forever be grateful for the guidance from my supervisor—Professor **Yujing Jiang**, not only because he guided my studies, but also for the sustained support and encouragement on me which has provided me with the confidence in continuing this PhD program. The skills I learned from my professor are not only useful to the PhD studies, but also bring benefits to my lifetime.

My thanks also go to Professor **Akihide Tada** and Professor **Kiyoshi Omine**, who offered their kind suggestions to make this work better.

Assistant Professor **Satoshi Sugimoto** is appreciated for his kind help in preparing the experiments. In addition, I especially appreciate the sincere help from Professor **Bo Li,** who has offered valuable proposals to my work, especially in the period when I was confused about the research.

My fellows in Nagasaki are appreciated for their contributions to both my study and life. Thanks for the care from my tutor Dr. **Xiao Shi** and my senior Dr. **Xiaoshan Wang**, especially in the period I fell ill in 2016. Thanks for the kindness of Mr. **Xuepeng Zhang** from entrance to the university to graduation from here. Many thanks to Mr. **Changsheng Wang** and Mr. **Jiankang Liu** for their support in my experiment.

Before I came to Japan, Professor **Yaodong Jiang**, my supervisor of master course, has encouraged me to apply for this overseas study, for which I express my sincere gratitude.

Finally, I'd like to express my gratitude to my parents and brothers for their dedicated love.

Abstract

Multiphase flow is an important research task in many engineering applications, including the exploitation of conventional gas and oil resources, coalbed methane recovery, CO_2 sequestration and the exploitation of geothermal energy. Two-phase flow is the basis for understanding the multiphase flow. Two-phase flow in porous media or rock fractures tend to be investigated with seepage theories, while analysis on the two-phase flow are very dependent on the experimental equations. Experimental equations that are applicable to one kind of fracture may have significant deviations on the other fracture. In other words, a general model for describing two-phase flow in the fracture is still absent. This research is aimed at expanding the results on the hydraulic behavior of two-phase flow and making a further step to establish general equations. It investigated the hydraulic characteristics of two-phase flow in rock fractures with both experiments and numerical simulation. It is composed of two aspects: two phase flow in the single fracture and two-phase flow in the intersecting fractures, which aims at forming the basis for studying the two-phase flow in the fracture network.

In Chapter 1, the two-phase flow phenomena in rock fractures in the coalbed methane recovery and geothermal energy development are introduced, and the purposes and contents of this dissertation are introduced.

In Chapter 2, the current research status and previous researches on two-phase flow in pipes, porous media and fractures are list. Different research approaches are compared and analyzed, and the corresponding enlightenment on this research is also list.

In the Chapter 3, an experiment system developed for two-phase flow test is introduced. The experiment system is composed of the fluid supplying subsystem, the two-phase flow box and the measurement subsystem. The two-phase flow box is the core element in this system, which can seal up the rock specimens without using glue. With this experiment system, two-phase flow experiments were conducted in the single rock fractures. The results show that the flow structures in a rough fracture show more similarity to that of two-phase flow in porous media, while the flow structures in a smooth fracture were similar to that in pipes. In the rough fracture, both water and gas tend to flow in their own channels, and the flow channels are stable. The relative permeability approximately follows the Corey model, but there are some deviations, and the deviation increases with respect to the increase of water flow velocity. This is to say, the relative permeability is not only the function of saturation, but also the function of water flow velocities. The deviation from Corey model indicates that the inertial effect of water decreases the relative permeability and increases the two-phase interference. The Lockhart-Martinelli model can also fit the results well. The increase of water flow rate leads to the increase of flow turbulence, which also increases the flow interference between two phases.

In Chapter 4, a 2D numerical model of two-phase flow in the single rock fracture was established for investigating the role of fracture morphology on the two-phase pressure drop. As indicated by the experiment results, the pressure drop of two-phase flow in the single rock fracture is influenced by multiple factors. In order to quantify the role of one

factor—the fracture morphology, a 2D numerical model was established with the level set method. The simulation is conducted in a series of rough fractures, which have a normal distribution in the fracture aperture but with different standard deviations. The simulation results show that the flow structures are correlated with the fracture morphology. With the increase of the standard deviation, the flow structure becomes more tortuous. The relative permeability is also influenced by the standard deviation of the fracture aperture. This is induced by two reasons: the tortuosity degree of the flow channels and the different effects of the capillary pressure. The flow tortuosity is influenced by the aperture distribution; the larger the standard deviation, the more tortuous the flow channels will be; while the influence of capillary pressure also increases with respect to the roughness of the fracture. In addition, the impact of capillary pressure differs in different flow patterns due to the different quantities of phase interfaces. The effect of capillary pressure is more significant in bubble flow than in continuous flow. The simulation results show that the relative permeabilities of both phases are not only the function of saturation, but also the function of flow velocities and the aperture distributions (especially standard deviations).

In Chapters 5 and 6, a series of gas-water two-phase flow experiments were conducted in both the 3D intersecting fracture model and 2D intersecting fracture models. The results of experiments in the smooth 3D intersecting fracture indicate that the flow structures show more similarity to that of stratified wavy flow in pipes. The nonlinearity induced by the inertial force and turbulence in the intersecting fractures cannot be neglected. The two-phase pressure drop increases nonlinearly with respect to the gas flow rate, which is induced by the strong inertial effect in the intersecting fracture. The Martinelli-Lockhart model is no only effective for describing the two-phase flow in the single fracture, but also effective for the intersecting fractures. The phase distribution behavior at the fracture intersection was studied with the 2D models with intersecting fractures. The results show that with the increase of gas injection rates, the evolution of water and gas distribution can be classified into three stages. In different stages, the dominant factors differed. In the first stage, gas flowed as bubbles and the flow of gas bubbles was stable; gas distribution was dominated by the gas injection position; in the second stage, gas flow as larger bubbles and the phase distribution of water and gas was dominated by the difference of the inertial effect of the two phases; in the third stage, the turbulence became serious and gas flowed as slugs. The inertial effect still influenced the phase distribution, but it is no longer the dominate factor. The inertial effect tended to separate the two phases, but the turbulence tended to homogenize the phase distribution.

In Chapter 7, the conclusions in each chapter are summarized and the enlightenment on future studies are given.

Keywords: two-phase flow, rock fracture, intersecting fracture, visualized experiment, relative permeability, Lockhart-Martinelli multiplier, flow structures, level set method, phase distribution

要　　旨

混相流は炭層ガスの開発、天然ガスと石油の利用、地熱開発、二酸化炭素の貯留などの工事の中で発生する。混相流の行為を理解するため、二相流の知識は基礎である。岩盤き裂における二相流は一般的に多孔質材料の流体力学に基づいて研究されている。今岩盤における二相流の解析には実験式に依存する点が多い。いずれの実験式はあるき裂の実験データに適用しますが、他のき裂に対して誤差が大きくなる傾向がある。つまり、一般形の式はまだない。本研究はき裂における二相流の挙動に関する研究結果を拡充するため、実験とシミュレーションで岩盤き裂の水理学的特性を解明することです。本研究には「単一き裂における二相流」と「交差き裂における二相流」という二種類の内容がある。

第一章では、炭層ガスと地熱の開発に伴う岩盤き裂における二相流現象を紹介した。その上に、本研究の目的と構成を示した。

第二章では、管内、多孔質材料とき裂における二相流に関する研究現状と既往研究について記述し，各種の研究方法を分析した上に、本研究に与えたヒントを示した。

第三章では、単一き裂の二相流実験システムを紹介した。この実験システムは液体供給設備、気体供給設備、二相流ボックスと測定設備により構成される。二相流ボックスはコアな設備であるので、接着剤を使わないながら岩盤供試体を密封できる。この実験システムを使って単一き裂の気液二相流実験を行った。実験結果により、滑らかき裂における二相流の流動様式は管内における二相流の流動様式と似ていましたが、粗いき裂における二相流の流動様式は多孔質材料における二相流の流動様式と似ていた。粗いき裂における二相流は、液相と気相両方も自分の流路に流れていたので、流路が安定である。相対浸透率は大体に Corey モデルに合いますけど、すこし偏差がある。その偏差は水流速度の増加に対して増加する。相対浸透率は飽和度の関数だけではなく、水流速度の関数でもある。水の慣性は相対浸透率を減少させ、二相間の干渉を増加させる。実験結果も Lockhart-Martinelli モデルに合う。水流速度の増加は乱流の程度を増加させるので、それも二相間の干渉を増加させる。

第三章の実験結果により、二相流の水力的特徴は複数の要因に影響される。実験で単一の要因を解析することが難しいである。従って、単一き裂面の形態

が二相流水理的特性に与える影響を解明するため、第四章では等位集合方法（Level set method）で二次元シミュレーションモデルを立てた。このシミュレーションは一連の生成したき裂面に行われた。これらのき裂面の開口幅は正規分布に従いますけど、開口幅平均値と分散の値が異なる。シミュレーションの結果より、二相流の流動様式はき裂面の形態と相関する。分散値の増加に伴い、流動様式はより曲がりくねっている。相対浸透率も正規分布の分散値に影響される；これは二つの要因によって引き起こされる：一つが流路の屈曲度、もう一つが毛管圧である。正規分布の分散値の増加に伴い、流路の屈曲度が増加するので、流動中の圧力損失と相対浸透率を高める。また、き裂面の粗さの増加に伴い、毛管圧の影響も増加する。この毛管圧より発生した抵抗力が相対浸透率を減少する。また、二相間の界面の量が異なるため、異なる流動様式に毛管圧の影響は異なる。連続流により、気泡流における毛管圧の影響が大きいである。総じて言えば、シミュレーションの結果により、相対浸透率は飽和度の関数だけではなく、水流速度とき裂開口分布（特に分散値）の関数でもある。

第五章と第六章では、二次元交差き裂と三次元交差き裂における気液二相流実験を行った。三次元交差き裂の二相流実験結果により、滑らかな交差き裂における二相流の流動様式はパイプにおける成層二相流の流動様式と似ている。慣性力と乱流によって誘起される非線形性が無視できない。き裂交差点によって誘起された慣性力により、気体流量の増加に対して圧力損失が非線形的に増加する。交差き裂に対して Martinelli-Lockhart モデルは有効である。二次元交差き裂で相の分配の特徴を研究した。実験結果により、気体注入速度に伴い、水と気体の分配は 3 段階に分ける。異なる段階で分配を支配する要因が異なる。第一段階では、気体は気泡として安定的に流れていた；気体の分配は気体注入位置に支配された。第二段階では、気泡のサイズが大きくなって、気体と水の分配は二相間の慣性力の差に支配された。第三段階では、気体はスラグ流として流れていたので、乱流の程度も上がった。水と気体の分配は慣性力に影響されますけど、慣性力は唯一の要因ではない。慣性力は二つ流体を分離する傾向がありますけど、乱流は二つ流体の分配を均一化する傾向がある。

第七章では、各章の成果を総括して結論とした；その上に、未来研究の考えをしめした。

キーワード：二相流、岩盤き裂、交差き裂、可視化実験、相対浸透率、Lockhart-Martinelli 乗数、流動様式、等位集合方法、相分布

Contents

Chapter 1 Introduction

1.1 Background

Multiphase flow refers the simultaneous flow of materials with two or more immiscible phases (gas, liquid, solid), or materials with different properties but in the same phase (i.e. liquid-liquid systems) [Wang, 2012]. Multiphase flow exists in many engineering applications, such as the gas-oil exploitation, gas-oil storage and transportation, chemical engineering, coalbed methane recovery, CO_2 sequestration, contaminant transport and the exploitation of geothermal energy [Kimura, 1997; Detwiler et al., 2009; Persoff and Pruess, 1995; Sudicky and Frind, 1982; Nuske et al., 2010]. Two-phase flow is the basis for studying multiphase flow. Studies on two-phase flow can be classified into two categories: (1) Two-phase flow in pipes. In the gas-oil transportation and chemical engineering, the two-phase flow dynamics in different kinds of conduit is a critical concern, because two-phase flow shows different pressure drop characteristics from that of single-phase flow. These issues are studied with the conduit flow models and conventional theories of fluid mechanics. (2) Two-phase flow in porous media or fractures. In oil-gas recovery and coalbed methane recovery, the issues concerning two-phase flow in porous media and fractures tend to be investigated with seepage theories.

In this dissertation, the two-phase flow in fractures is investigated, which concerns the applications such as coalbed methane recovery, CO_2 sequestration and geothermal energy exploitation.

Coalbed methane is one of the extensively utilized unconventional gases, which has decreased the utilization of coal. Consequently, it is assumed as an environmentally friendly resource. More than 90% coalbed methane is stored as absorbed state in the coal seams. With the depletion of reservoir pressure, the absorbed gas changes into gaseous phase. That is to say, the exploitation of coalbed methane is accompanied with a process of gas desorption. In addition, the coal seams are initially abounded with water. The recovery of coalbed methane resources is composed of three stages [Feng, 2009]. In the first stage, water is drained out from the coal seams, which is a single-phase flow process. With the depletion of the reservoir pressure, gas in the absorbed phase begins to desorb from the coal matrix. Due to its small quantity, the gas phase is discontinuous and bubbly

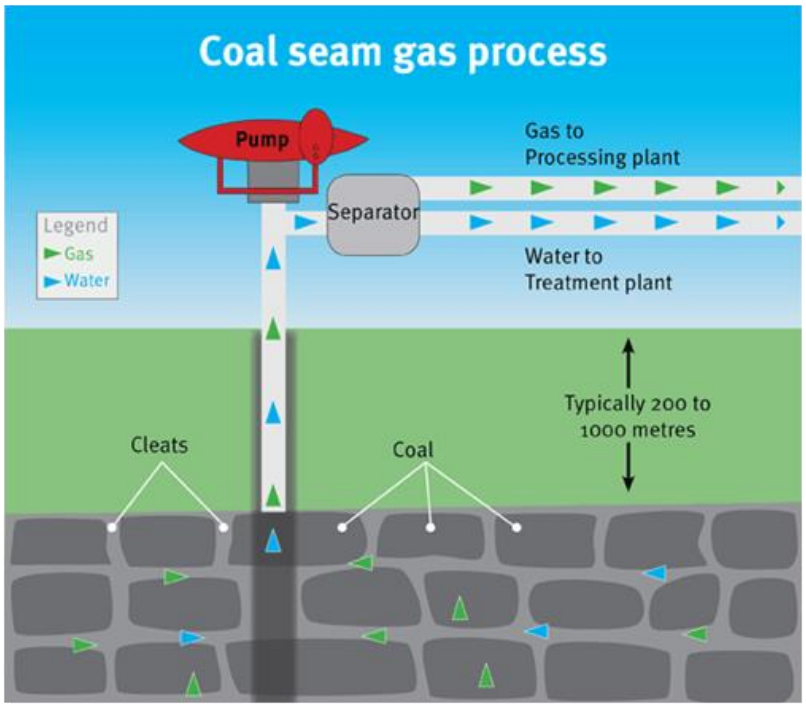

Fig. 1-1 The schematic of gas and water extraction from coal seams

flow is formed. The water and gas transport in the fractures of coal seams and the conduit of the extraction well, and they will be separated by a separator, as shown in Fig.1-1. With more gas desorbing, the gas percentage increases and the flow structures may change. In the third stage, the water depletes, and gas keeps transporting, namely the recovery process returns to a single-phase flow; but the trapped water phase may have a significant influence on the transport of gas. In the above-mentioned process, there is a transition from single-phase flow to two-phase flow in the fracture network, and the gas desorption rate varies with respect to time. Consequently, a two-phase flow with different gas-water ratios will be formed. Since the two-phase flow process influences the production rate, the water drainage rate and gas exploitation rate must be well controlled to reach an optimal recovery ratio.

CO_2 sequestration is an effective method to reduce the CO_2 emission amount into the atmosphere. The injection of CO_2 into the saline aquifers or abandoned coal seams will lead to a two-phase flow of CO_2 and saline water [Soong et al., 2004]. The injection of CO_2 into the coal seams can increase the output of coalbed methane. The injected CO_2 can be in gaseous, supercritical or liquid state. Consequently, different kinds of multiphase-phase flow can be formed, namely supercritical CO_2-water, gaseous CO_2-

water or even three-phase flow of supercritical CO_2-gaseous CO_2-water. The relative permeability of CO_2 and brine has an obvious impact on the transport of both phases and the injection efficiency. The relative permeability is influenced by many factors, for example, the increase of the viscosity ratio between the fluid pairs will make the more mobile phase (less viscous) to flow through the pore space [Bachu and Bennion, 2008]. The stability of CO_2 in the aquifers should be carefully evaluated to avoid the escape of CO_2, so before CO_2 becomes fixed through chemical reactions with the saline water, the transport of multiple phases shall be fully estimated, which requires a profound understanding of the transport mechanisms of multiphases in the fracture network or saline aquifers or coal seams.

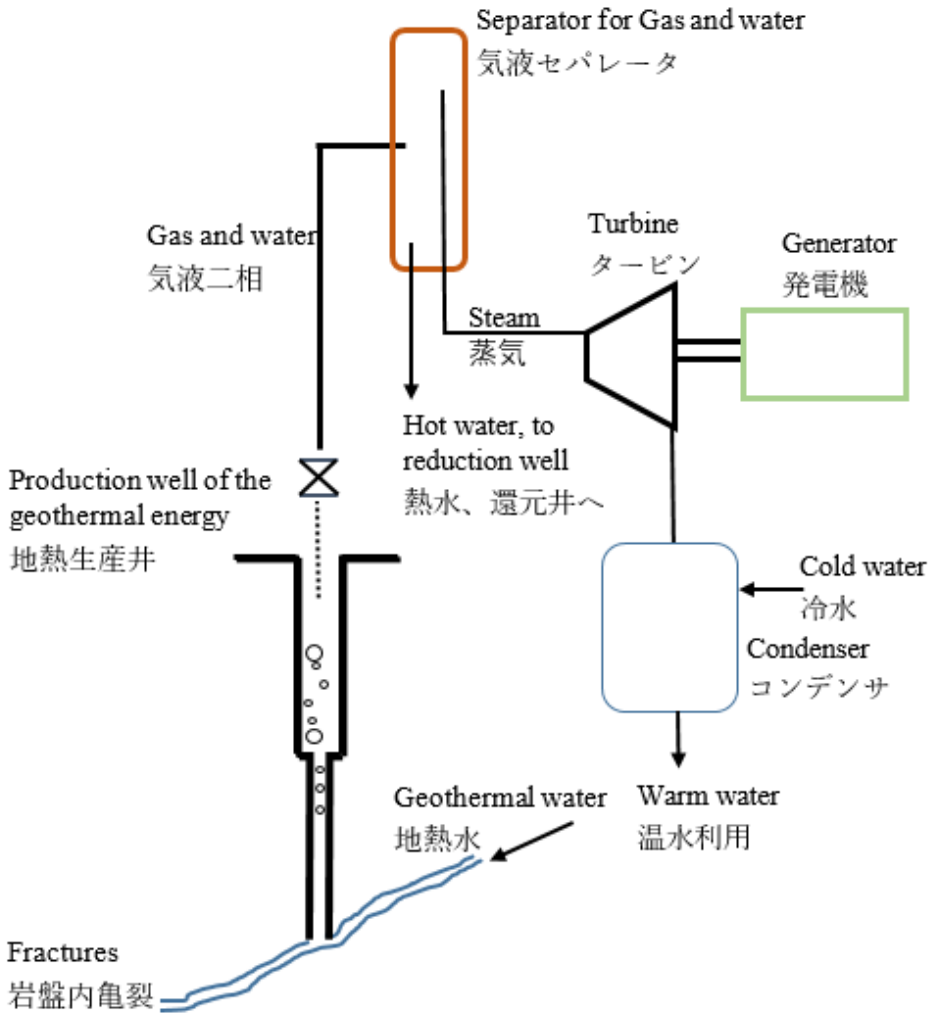

Fig. 1-2. The schematic of geothermal power plant [Kimura, 1997]

Geothermal energy is an environmentally friendly reproducible resource. Conventional method of utilizing the geothermal energy includes two steps: (1) injecting water into the rock strata through the fracture network, where steam will be produced due to the high temperature; (2) extracting the high-temperature steam and water into the earth surface to generate electricity. Because the average temperature gradient in the earth's crust is about 30 °C/km, an excavation of 10 km into the earth will provide access to the heat source of 300 °C, where the water will be in the state of steam [Kimura, 1997]. This is to say, a two-phase flow of water in liquid state and gaseous state exists in the rock fractures and the production well, as shown in Fig. 1-2. The two phases, namely water and vapor, are separated in a separator. The vapor is used for generating electricity, and the water is injected back to the underground strata. The purpose of injecting water back to the underground is to prevent it polluting the environment since the extracted water is generally brine. However, this two-phase flow process is different from the above-mentioned two-phase flow in coalbed methane recovery or oil-gas exploitation, because liquid water and steam can convert into each other according to the temperature, namely there is a phase change process along with the transport of two phases. In this process, the decrease of the two-phase pressure in the production well and the evolution of temperature are coupled with each other, which requires to be fully understood for providing basis for the design of the production well.

Compared with single-phase flow, the hydraulic characteristics of two-phase flow is influenced by more factors, including the capillary pressure, the viscous coupling and additional turbulence induced by two-phase interactions. Due to the complexity of the influencing factors, there is still not a general equation which can predict two-phase flow characteristics in all kinds of circumstances. In addition, it is also difficult for two-phase simulation to cover all the factors which influence the flow. In view of this, this dissertation has three aims: (1) To investigate the hydraulic characteristics of single fractures with experiments, and evaluate the effect of surface morphology on two-phase relative permeability and Lockhart- Martinelli multipliers; (2) To quantitatively evaluate the impact of aperture distribution on the two-phase flow concerning the effect of capillary pressure with simulation; (3) To study the applicability of Lockhart-Martinelli model in intersecting fractures with experiments. Based on the above-mentioned researches, we expect to provide a basis on studying the hydraulic characteristics of two-

phase flow in the fracture network.

1.2 Outline of the dissertation

This dissertation is divided into 7 chapters. Chapter 1 and Chapter 2 give a review on this research theme. Chapter 3 and Chapter 4 study the hydraulic characteristics of two-phase flow in single fractures, with experiment and simulation respectively. Though the experiment includes more pressure-drop mechanisms than the simulation, Chapter 4

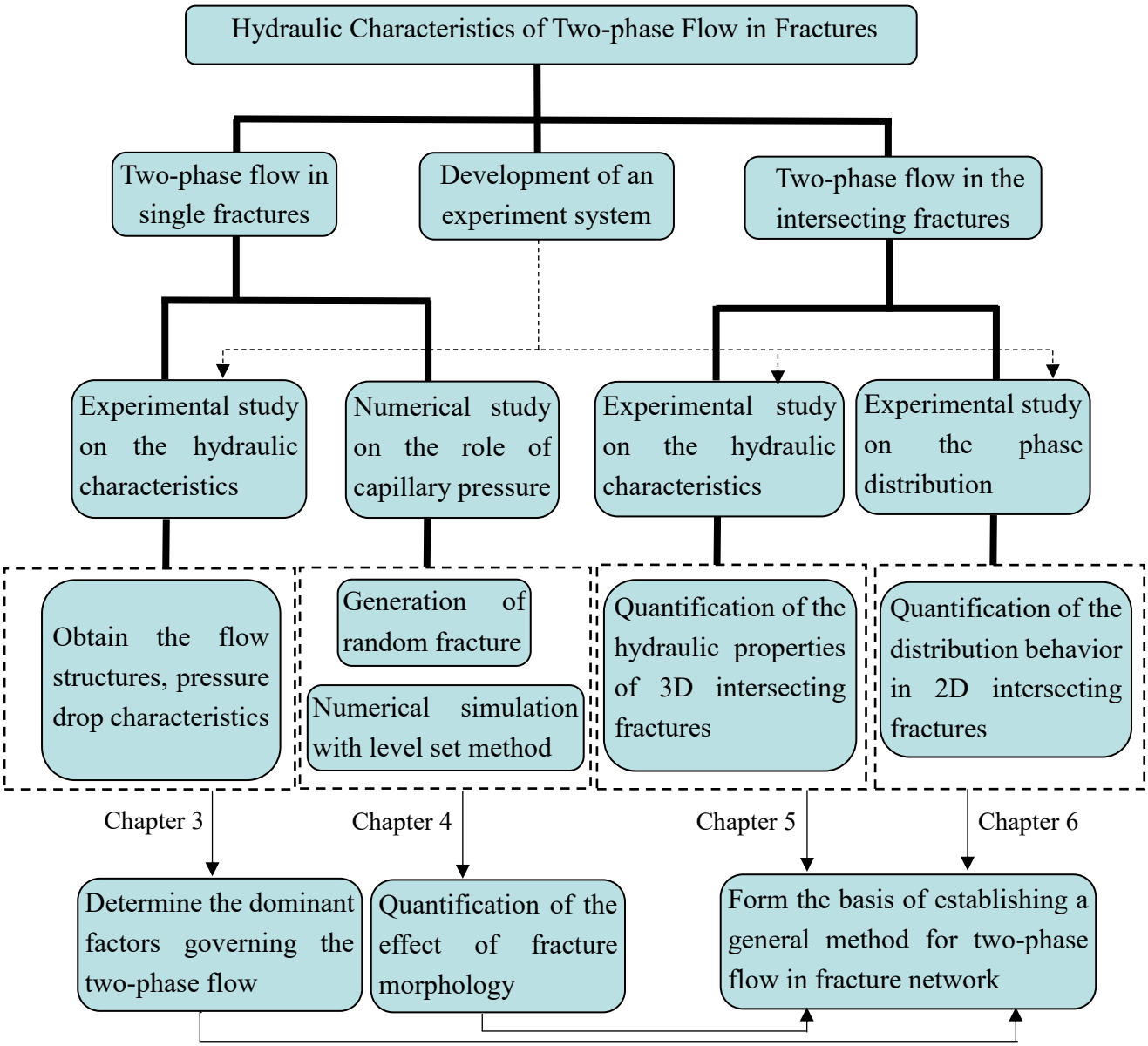

Fig. 1-3 Dissertation structure

provides reference with quantitative analysis on the effect of capillary pressure. Chapter 5 and Chapter 6 investigate the two-phase flow hydraulic characteristics and distribution behavior, respectively. They are outlined as the following:

Chapter 1 introduces the engineering applications of two-phase flow in fractures and states the significance of the research.

Chapter 2 lists the theoretical and empirical models for two-phase flow in conduit, porous media and fractures. Most of the approaches in two-phase flow are covered here. Many of them are derived from the experiments, and the derivations are also simply introduced.

Chapter 3 firstly introduces the experimental apparatus developed by the author; the core part—two-phase flow box and the corresponding sealing techniques are introduced in detail. Then the experiment procedures, results of tests in two different fractures are list. The effect of the fracture surface morphology on the relative permeability and phase multipliers is discussed.

Chapter 4 introduces a two-dimensional numerical model for simulating two-phase flow in a single fracture with the level set method. The effect of capillary pressure and fracture aperture distribution on the relative permeability is discussed.

Chapter 5 introduces the experimental apparatus and procedures of two-phase flow tests in intersecting fractures. The applicability of the method in single fractures (Lockhart-Martinelli multipliers) in intersecting fracture is investigated. Furthermore, the influence of fracture intersections on the Lockhart-Martinelli multipliers is also discussed.

Chapter 6 investigates the two-phase flow distribution behavior in intersecting fractures by experiments. The inertial effect, intersecting angle on the distribution characteristics are analyzed.

Chapter 7 lists the conclusions. In addition, future numerical and experimental researches are recommended.

Chapter 2 Reviews on the studies of two-phase flow

Studies on two-phase flow can be divided into three types: (1) Two-phase flow in pipes, which refers to the two-phase flow in large-scale tubes, such as the gas-oil transportation conduit. This kind of studies are conducted on the basis of the conventional theories of fluid mechanics. (2) Two-phase flow in porous media, such as the gas-water two-phase flow in the matrix of coal seams. This kind of studies are based on the theory of poromechanics. (3) Two-phase flow in the fractures, such as the gas-water two-phase flow in the fractures of coal seams, CO_2-water two-phase flow in the fractures of saline aquifers. Under many circumstances, the flow in fractures exists together with that in porous media since many porous media are abundant of fracture network.

In this dissertation, we investigate the two-phase flow in fractures. The studies of two-phase flow in the fractures mainly borrow the methods of two-phase flow in porous media, namely poromechanics, since they show much similarity to each other [Fourar and Lenormand, 1998; Brooks and Corey, 1964]. But some researchers also tried to use the theories in conduit flow, and they found some correlations between the flow regime and the pressure drop characteristics [Fourar and Bories, 1993]. To illustrate the relationship between different approaches, a systematical introduction is given in the following sections. This helps understand the origins of different research methods that are used in investigating two-phase flow in fractures.

2.1 Approaches of two-phase flow in pipes

As mentioned above, two-phase flow in conduit are studied on the basis of conventional fluid mechanics, that is to say, the fundamental mass conservation equations and momentum conservation equations shall be established for the fluids. However, compared with single-phase flow, more difficulties or complexities remain in the two-phase problems remain, as indicated in the following aspects: (1) Besides the conservation equations and momentum equations, additional equations also require to be established, such as the interactions between two phases (mass transfer, energy transfer); (2) Much of the energy transfer occurs at the two-phase interfaces, however, the interfaces are always moving, which adds to the difficulty of calculation. (3) The distribution of two phases can be of different forms. Suppose a gas-water two-phase flow in which the gas

and water accounts for 50%, respectively, the distribution of two phases can be the even distribution of gas bubbles in water, or both gas and water flow continuously in their respective channels, which is knows as stratified flow. This is called as flow structure. Difference in flow structures leads to different mechanical (pressure drop of flow) performance, mass transfer performance and heat transfer performance.

Due to the above-mentioned complexities, until now there is still not a general equation that can cover all kinds of two-phase flow issues. Taking the problem of moving interface as an example, some methods track the two-phase interface to accurately estimate the interactions between two phases, such level set method, phase field method, and VOF method. In the future, it may be possible to code the Navier-Stokes equations for each of phases and compute every detail of a multiphase flow and the position of every interface [Brennen, 2005]. This will lead to very accurate calculation results. But this kind of calculation is far beyond the capacity of present computers. Consequently, macroscopic calculation models, which are more applicable to compute large-scale two-phase flow problems, should be established. In this section, some typical methods are list as the following.

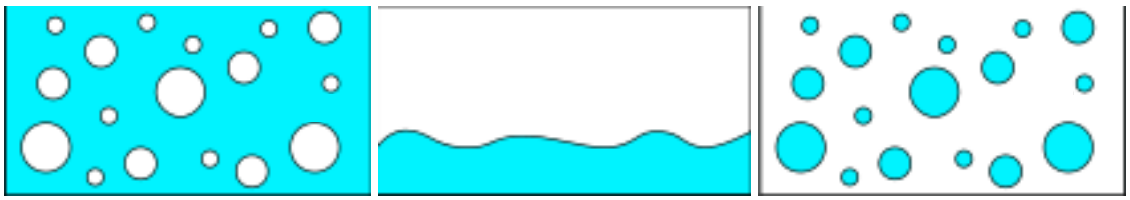

Fig. 2-1 Flow structures—bubble flow, stratified flow, droplet flow

2.1.1 Homogenous model and the friction factor

Homogenous model is a simple method for the calculation of two-phase conduit flow. In this method, two-phase flow is treated as single-phase flow by homogenizing the parameters of two phases into that of a hypothetical single-phase. In this “sing-phase flow”, all the critical variables and parameters are the average of the original two phases. The flow of this “single-phase” fluid is assumed to follow the rules of classical fluid mechanics, therefore, the two-phase flow can be calculated with the sing-phase fluid mechanics. The density of the two-phase mixture is defined as Equation 2-1, in which ρ,

ρ_α, ρ_β are the density of the mixture, density of phase α and density of phase β, respectively. q_α, q_β are the flow rate of phase α and phase β, respectively.

$$\rho = \frac{\rho_\alpha q_\alpha + \rho_\beta q_\beta}{q_\alpha + q_\beta} \tag{2-1}$$

The viscosity of the two-phase mixture is defined as Equation 2-2, in which μ, μ_α, μ_β are the viscosity of the mixture, phase α and phase β, respectively. χ is the mass fraction factor, which is defined as $M_\alpha / M_\alpha + M_\beta$, M is the mass flow rate.

$$\mu = \frac{\mu_\alpha q_\alpha + \mu_\beta q_\beta}{q_\alpha + q_\beta} \tag{2-2}$$

The two-phase Reynolds number is defined as Equation 2-3, in which h is half of the hydraulic diameter, in which V is the velocity of the mixture, defined as $(q_\alpha+q_\beta)/A$, where A is the area of the cross section. The two-phase pressure gradient is derived as Equation 2-4 (with the acceleration components neglected), in which the C_f is the friction factor, d is the hydraulic diameter. The homogeneous model aims to seek for the correlation between C_f and Re_2. With an appropriately established correlation [Fourar and Bories, 1993], the pressure drop of two-phase flow can be predicted.

$$\mathrm{Re}_2 = \frac{2hV\rho}{\mu} \tag{2-3}$$

$$\frac{dp}{dx} = 2C_f \rho \frac{V^2}{d} \tag{2-4}$$

2.1.2 Lockhart-Martinelli model and the multipliers

Lockhart-Martinelli model is derived by accounting for the property that the two-phase pressure drop is always than that of single-phase pressure drop with the same flow rate. Two critical parameters are defined to evaluate this property, as indicated in Equations 2-5 and 2-6. Here, φ_L is the liquid multiplier. It is defined as the square root of the ratio between the two-phase pressure drop (dp/dx) and the single-phase pressure drop of the liquid $(dp/dx)_L$. φ_G is the gas multiplier, which is defined as the square root of the ratio between the two-phase pressure drop (dp/dx) and the single-phase pressure drop of the gas $(dp/dx)_G$.

$$\varphi_L = \frac{dp/dx}{(dp/dx)_L} \tag{2-5}$$

$$\varphi_G = \frac{dp/dx}{(dp/dx)_G} \tag{2-6}$$

These definitions are similar to that of relative permeabilities (as will be illustrated in Section 2.2), which are defined as the ratio between the two-phase permeability and the single-phase permeability. Both the multiplier and the relative permeability are the ratio between the two-phase transport capacity and the single-phase transport capacity. However, the difference lies in that the multipliers in Lockhart-Martinelli model accounts for the inertial effect. This is because in calculating the single-phase pressure drop $(dp/dx)_L$ and $(dp/dx)_G$, the inertial effect is accounted for by using the Forchheimer's law. A suitable model which can describe the evolution of Lockhart-Martinelli multipliers can be used to model the two-phase flow, especially for calculating the pressure drop. This will be introduced in Chapter 5 in detail.

2.2 Approaches of two-phase flow in porous media

2.2.1 Extended Darcy's law and relative permeability

The main difference between the two-phase flow in porous media and the single-phase flow in porous media is that: the permeability of single-phase flow a constant and it is considered as a property of the porous medium itself [Brooks and Corey, 1964]; but the effective permeability of two-phase flow is not only influenced by the property of the porous medium, but also the properties of both fluids and the interactions between them. This difference gives enlightenment about the approaches of studying two-phase flow in porous media: to extend the equations of single-phase flow by considering the two-phase interactions, and to extend the effective permeability as the function of the property of the medium and the interactions between two phases. The most commonly adopted alternative is to extend the Darcy's law.

Darcy's law is the basis of hydrogeology, which is formulated by Henry Darcy, a French engineer, from the experiments on the flow of water through beds of sand. It is also derived theoretically from the Navier-Stokes equations via homogenization [Whitaker, 1986]. This law indicates a linear correlation between the pressure drop and the superficial velocity of water fluid in porous media, as shown in Equation 2-7, where

u refers to the superficial velocity, k is the permeability, μ is the dynamic viscosity, Δp is the pressure drop of fluid flow, L is the flow distance.

$$u = -\frac{k}{\mu}\frac{\Delta p}{L} \tag{2-7}$$

Darcy's law is widely adopted to calculate the single-phase flow in porous media in engineering applications. The extended Darcy's Law is assumed effective for describing the two-phase flow in porous media [Scheidegger, 1974]. Compare with Darcy's law, a critical parameter—relative permeability is introduced to the extended Darcy's law to include the interference and interaction between two phases. The extended Darcy's law was firstly proposed by Wyckoff and Botset [1936], as indicated in Equation 2-8. The subscript α refers to different phases; u, k, μ are same as that defined in Equation 2-7; ∇p is the pressure gradient, which is proportional to $\Delta p/L$ defined in Equation 2-7; k_r is the relative permeability of each phase.

$$u_\alpha = -\frac{kk_{r\alpha}}{\mu_\alpha}(\nabla p_\alpha) \tag{2-8}$$

The relative permeability is a critical parameter in two-phase flow, because it is an evaluation of the interactions between the two phases. Quite a significant part of the studies on two-phase flow in porous media or fractures are about the evolution the relative permeability and different kinds of conclusions are obtained. That is because there are many kinds of two-phase interactions, such as the capillary pressure, viscous coupling induced by the different viscosities of phases. Since the relative permeability is influenced by multiple factors, different models are proposed to describe the evolution of relative permeability. They are introduced in detail in the next section.

2.2.2 Models for relative permeability

Commonly-used models of relative permeability of two-phase flow in porous media include the X-model, the viscous-coupling model and the Brooks-Corey model [1964]. The X-model has been used to simulate reservoir behaviors for its priority in simplicity [Gilman and Kazemi, 1983; Thomas et al., 1983]. This model is derived based on the assumption that each phase flows in its own channel, so that no interference between two phases exist in their simultaneous flow. Consequently, the relative permeability of each phase equals its saturation, as indicated in Equation 2-9 and Fig. 2-2.

$$k_{rw} = S_w \tag{2-9a}$$

$$k_{rg} = S_g \tag{2-9b}$$

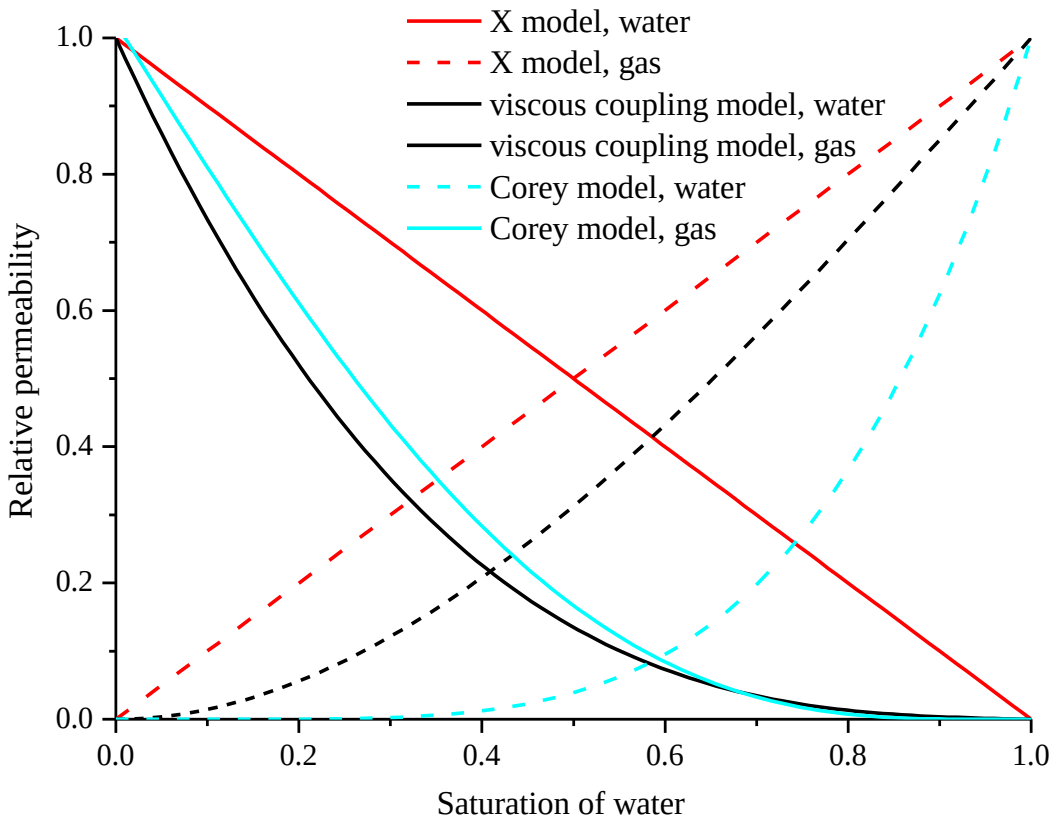

Fig. 2-2 Evolution of relative permeability with respect to saturation in X-model, viscous model and Corey model ($\mu_w = 1.01\times10^{-3}$ Pa·s; $\mu_{nw} = 17.9\times10^{-6}$ Pa·s in the viscous coupling model)

However, the interference between phases cannot be neglected in many occasions. The viscous-coupling model accounts for the interaction between phases induced by the viscosity difference. It is derived by integrating Stokes' equation. It is assumed that the fracture is a small sized conduit, in which the wetting phase flows at both sizes (contacting the wall) and the nonwetting phase flows in between. The relative permeability is derived as Equation 2-10, in which μ_w and μ_{nw} are the viscosity of wetting phase and non-wetting phase, respectively. Note that the relative permeability of nonwetting phase is dependent on the viscosity ratio between two fluids.

$$k_{rw} = \frac{S_w^2}{2}(3 - S_w) \tag{2-10a}$$

$$k_{rg} = (1 - S_w)^3 + \frac{3}{2}\frac{\mu_g}{\mu_w} S_w (1 - S_w)(2 - S_w) \tag{2-10b}$$

The Corey model is a commonly used approach in porous media [Corey, 1954], in which capillary pressure plays a dominant role on the relative permeability. It suggests stronger phase interference than viscous coupling model. The relative permeabilities are described as Equation 2-11, in which the $S_{w,r}$ and $S_{nw,r}$ are the residual saturation of wetting phase and non-wetting phase, respectively.

$$k_{rw} = \left(\frac{S_w - S_{wr}}{1 - S_{wr} - S_{gr}}\right)^4 \tag{2-11a}$$

$$k_{rg} = \left(1 - \frac{S_w - S_{wr}}{1 - S_{wr} - S_{gr}}\right)^2 \left[1 - \left(\frac{S_w - S_{wr}}{1 - S_{wr} - S_{gr}}\right)^2\right] \tag{2-11b}$$

The diversity of various models indicates that their difference is induced by different mechanisms. In the next section, we introduce a series experimental and numerical studies in fractures, in which the results conform to different models.

2.3 Typical studies on two-phase flow in the rock fracture

Studies on two-phase flow in fractures can be divided into two categories, namely the displacement mechanisms [Babadagli et al, 2015] and simultaneous flow of two phases in the fractures or porous media [Fumagalli and Scotti, 2013; Hauge and Aarnes, 2009]. These two categories of studies have something in common, because the flow is under the same influence of the two-phase interactions, such as the capillary pressure. However, these two kinds of studies correspond to different types of engineering background. For example, in the gas and oil recovery, the simultaneous flow of oil and gas exists in the previous stage of exploitation, while the displacement process exists in the stage of water displacing oil. In this dissertation, we focus on the simultaneous flow of two phases.

Methods of studying two-phase flow in fractures are of two types: (1) To borrow the theories and approaches of two-phase flow in porous media. In this method, fracture is assumed as two-dimensional porous media [Pruess and Tsang, 1989]. (2) To borrow the approaches of two-phase flow in conduit. This is on the basis that the flow structures in

fractures are similar to that in conduit in some experiments [Fourar and Bories, 1993]. Different methods and the corresponding typical researches are introduced as the following.

2.3.1 Studies that conform to X-model, viscous coupling model, Corey model

Conventional theories on the two-phase flow in porous media, which is based on the concept of relative permeability, has been widely used to describe the two-phase flow in fractures. Romm [1966] conducted the kerosene-water two-phase flow tests in parallel artificial fractures. The fracture is composed of parallel bands with alternate wettability. The results confirm to X model, indicating negligible two-phase interference. Analysis on the production data of a geothermal field by Pruess et al [1983] also supports the X model. Mahoney and Doggandt [1997] also showed similar results. Fourar and Bories [1998] investigated the air-water flow in parallel artificial fractures, and the relative permeability complies with viscous-coupling model. Fourar and Bories [1995] also observed results that conform to viscous coupling model. Their experiment was conducted with air and water in parallel glass plates, in which the aperture was about 1mm. Diomampo [2001] conducted N_2-water flow experiment in smooth-walled fractures, and the results conform to the Corey model. This indicates that in some cases the two-phase flow behavior in fractures is a limiting case of that in porous media.

2.3.2 Studies that shows stronger interference than Corey model

Persoff and Pruess [1995] conducted air-water two-phase flow in rough-walled fractures, and they observed that the sum of relative permeabilities was much less than 1 at intermediate saturations. This indicates a more severe phase interference than Corey model. Watanabe et al. [2014] conducted a series of experiments with decane-water and nitrogen-water in real fractures with different wettability values. They also observed a stronger phase interference and proposed a new v-type relative permeability model. Pruess and Tsang [1990] conducted a numerical study in a fracture to study the effect of capillary pressure on the relative permeability. The fracture aperture follows a log-normal distribution. Their results also indicate that the two-phase interference is stronger than that of Corey model. All of the above three studies indicate that in some cases the Corey model, which is originally proposed for porous media, is not applicable to fractures. This

may be because in 2D porous media (fractures) the chance of one phase bypasses the other phase is larger than in 3D porous media.

This indicates that the three models for porous media shall be revised for application in fractures due to the difference between 2D porous media (fractures)and 3D porous media.

2.3.3 Studies with novel models of relative permeability

Conventional models for relative permeability are mainly expressed as the function of saturations, which neglects the contributions of fracture roughness. In consideration of this deficiency, Chen [2005] established the correlation between the flow structures and the relative permeability in single fractures through visualization experiment. Based on this correlation, the permeability was expressed as the function of both saturation and flow tortuosity. The flow tortuosity is a parameter that is related to flow structures. Since the flow tortuosity is also a reflection of the fracture roughness, the influence of fracture roughness is included in the expression of relative permeability.

Besides the viscous coupling and capillary pressure, the inertial effect also influences the two-phase flow hydraulic characteristics. However, the influence of inertial effect is not included in the above-mentioned three models of relative permeability. Experiments by Radilla et al [2013] show that the relative permeabilities not only rely on saturation, but also the flow regimes. They expressed the relative permeability as the function of both saturation and Reynolds number.

The above two studies indicate that the X model, viscous coupling model and Corey model are not enough for describing the two-phase flow in fractures, because the three models fail to include the influence of fracture morphology and the inertial effect.

2.3.4 Studies with models of two-phase flow in conduit

Fourar and Bories [1993] observed the evolution of flow structures of bubble flow, fingering bubble flow, complex flow, film flow and drop flow in their experiment. Because the inertial force cannot be neglected in their experiment, they abandoned the relative permeability model which cannot account for the inertial force. Since the evolution of the flow structures show similarity to that of two-phase flow in conduit, they tried to use the models developed for two-phase flow in conduit, which account for the

inertial effect. Their results show that both the Lockhart-Martinelli model and homogeneous model can predict the two-phase friction factor, and the homogeneous model fit the experiment data better than the Lockhart-Martinelli model over the entire range of pressure gradients. But the deficiency is that their model for the rough fracture was only applicable to the only one rough fracture which was used in their experiment. The applicability to other fractures was not investigated.

To conclude, the effect of fracture morphology is not included in this model for predicting two-phase pressure drop.

2.4 Motivations of this research

From this review, we conclude that some shortages in the researches remain in:

(1) Different experiments show different results about the evolution of relative permeabilities. Some testing results follow the X-model [Romm, 1966, smooth fracture with alternative stripes], some follow the viscous model [Fourar and Bories, 1995, smooth fracture], some follow the Corey model [Diomampo, 2001, both smooth and rough fracture;], while some indicate more severe two-phase interactions than Corey model [Persoff and Pruess, 1995, rough fracture]. Since different researchers use specimens with different fracture surface morphologies, it is believed that different performances are induced by the difference in the surface morphology or roughness of the fractures. Consequently, the effect of fracture roughness on the relative permeability remains to be further investigated quantitatively.

(2) The X-model, viscous model and Corey model are all expressed as the function of saturations, as indicated in Equations 2-9, 2-10 and 2-11. However, the hydraulic characteristics of two-phase flow are influenced by many factors, such as the viscous force, the capillary pressure, the inertial effect etc. Compared with single-phase flow, there are more influencing factors. It is difficult to quantify the effect of a single factor with experiments. In addition, the fracture roughness also has effect on the relative permeability. The effect of fracture roughness should be quantitively evaluated.

Consequently, this dissertation seeks for additional results on the effect of fracture surface morphology on the two-phase flow characteristics. The experimental study used smooth and naturally rough fractures to evaluate the surface roughness on the relative permeabilities and Lockhart-Marinelli multipliers. This helps understand what factor

(capillary pressure, viscous coupling, inertial effect et al.) is the dominant one in different kinds of fractures. To quantitatively evaluate the capillary pressure effect in different fractures, simulation with level set method, which accounts for the effect of capillary pressure, is conducted in the generated random rough fractures. Detailed descriptions are given in the following chapters.

Chapter 3 Development of an experiment system and experimental studies on the hydraulic characteristics of two-phase flow in the single rock fractures

In present engineering applications, calculations of hydraulic properties in two-phase flow are still highly dependent on empirical or semi-empirical equations obtained from experiments. However, the empirical equations that can reproduce the experiment data on a certain fracture specimen may have errors on other specimens. Sometimes researchers have obtained results that show quite different evolution forms of relative permeability [Romm, 1966; Persoff and Pruess, 1995; Diomampo, 2001; Watanabe, 2015]. This is because two-phase flow in a fracture is influenced by multiple factors, which add to the difficulty on establishing a general equation. This chapter aims at expanding the experimental results and making a further step to establish a general model. Firstly, an experiment system which can conduct visualized two-phase flow experiments is introduced. By analyzing both the flow structures and the pressure drop characteristics, the two-phase hydraulic properties in this certain rock fracture are concluded.

3.1 Development of an experiment system

3.1.1 Reviews on experiment systems for two-phase flow

In many engineering applications, the multiphase flow tends to be an important issue. Due to the complexity of two-phase flow, a universal equation for describing all the two-phase flow problems is still absent, which indicates that the empirical or semi-empirical equations obtained from the experiments are still important in practice use. At the present stage, experimental studies remain to be a significant method to gain more insight about the two-phase flow mechanisms. What's more, the two-phase flow in fractures is more complicated considering the influence of the fracture roughness or aperture on the fluid flow.

In addition, sealing the specimens remains to be a principle difficulty in a two-phase flow experimental apparatus. The sealing process tends to be time-consuming or difficult. Generally, there are two kinds of sealing methods: mechanical sealing and sealant sealing. Mechanical sealing refers to compacting the specimens and the flow box with the mechanical force. This method is time-saving and convenient. But in many situations, the

sealing effect is not good. Water or gas leakage may happen at some junctions. Sealing the specimens with sealant is generally with good effect, but it's time-consuming in assembling the specimens because some time is required for solidification of the sealant. When replacing the specimens, it takes time to remove the used sealant, meaning that this method is also costly. What's more, in natural rock masses, fractures tend to have shear displacements. However, it's quite hard to apply shear displacements in existing apparatuses since it causes more difficulties in sealing.

Some researchers have already developed certain experimental apparatuses for two-phase flow in fractures. Liang et al [2016] has developed "An visualized experimental system for two-phase flow in fractured rocks". In this system, a T-type fracture intersection model was designed as the two-phase flow channel, as shown in Fig. 3-1. This fracture intersection model can be viewed as an element of the fracture network, namely a special combination of two single fractures intersecting at 90°. The fracture surface is to be carved in a machine tool to simulate the natural rough surface of the fracture. However, in this fracture intersection, the flow of water and gas is under the gravitational effect and buoyancy in the vertical fracture, while the flow in the horizontal fracture is not influenced by this effect. Consequently, there are too many impact factors which influence the two-phase flow characteristics in this fracture intersection model, which increases the difficulty of analyzing the influence of different factors based on the measured data such as the pressure, the flow rate and the flow structures. Fan et al [2017] developed "An experimental system for two-phase flow in fracture network", in which experiments can be conducted in fracture networks. In addition, an effective method for

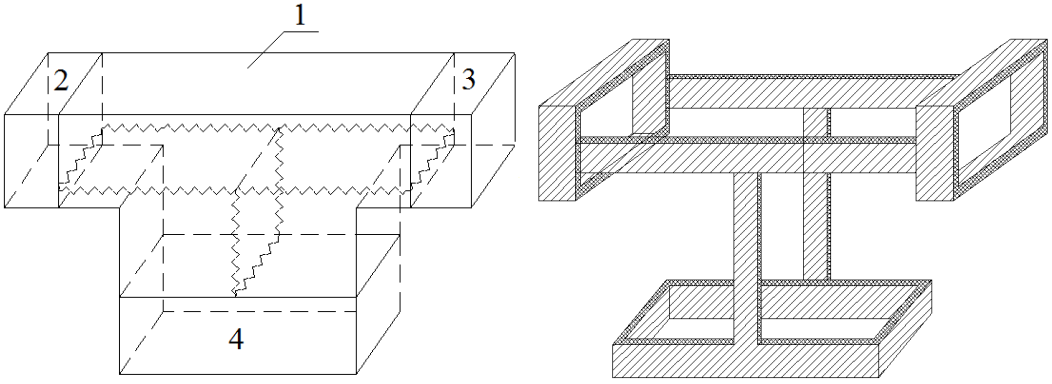

(a) The fracture specimen (b)The sealing rubber

Fig. 3-1 The T-type fracture apparatus [Liang et al. 2016]

dealing with the mixed water and oil has been proposed. Two-phase flow itself is influenced by many factors such as the water-gas ratio, the aperture fracture, the fracture roughness etc. In the fracture network, more factors characterizing the network structure are introduced to influence the flow process. Due to the complicity of different impact factors, study on the two-phase flow in single fractures is still necessary.

Diomampo [2001] has designed a system for conducting gas-water two-phase flow experiments in single fractures. The core device of this system is a two-phase flow apparatus, which consists of a smooth glass plate as the upper plate for the convenience of observing the flow structures, and an aluminum plate as the bottom. There are two groups of ports acting as the water injection ports and the gas injection ports, respectively. Viton is placed between the bottom and upper plates for sealing. A couple of pressure measurement ports and temperature measurement ports are set in the bottom plate. A wire mesh is inserted in between the two plates of the apparatus, which is assumed to represent the rough fracture. However, the rough surface of the wire mesh is different from that of the real fractures in rock specimens. On the other hand, shear displacement between two rock specimens will lead to a totally different aperture distribution, which will induce serious influence on the fluid flow. With this apparatus, the flow tests in the rock fracture with different shear displacements and different apertures can't be conducted.

In this section, a newly developed experimental system is introduced. The core component of this system is a two-phase flow box, in which two rock specimens can be put in. One of the specimens is transparent for the convenience of observing the flow structures. With the specially designed sealing structure of the two-phase flow box, good sealing effects can be acquired. Since we can assemble the specimens without using sealant, the assembling process is time-saving and economical. The aperture and shear displacement between two specimens can be assigned as different values. With this system, experiments can be conducted to investigate the gas-water two-phase flow characteristics in single fractures with different roughness degrees, different shear displacements, and different apertures.

3.1.2 The experiment system

The experimental system is shown in Fig. 3-2, which includes four subsystems: the water supply subsystem, the gas supply subsystem, the two-phase flow box and the

measurement subsystem. The water supply subsystem includes a peristaltic pump and a pulse damper. The peristaltic pump can inject water at a specified flow rate in the range of 0-2000 mL/min, as shown in Fig. 3-3. The flow rate and pressure of the water from the peristaltic pump is always fluctuating. This is because water is injected by squeezing the flexible tube with a rotor in the peristaltic pump. To decrease this fluctuation, a pulse

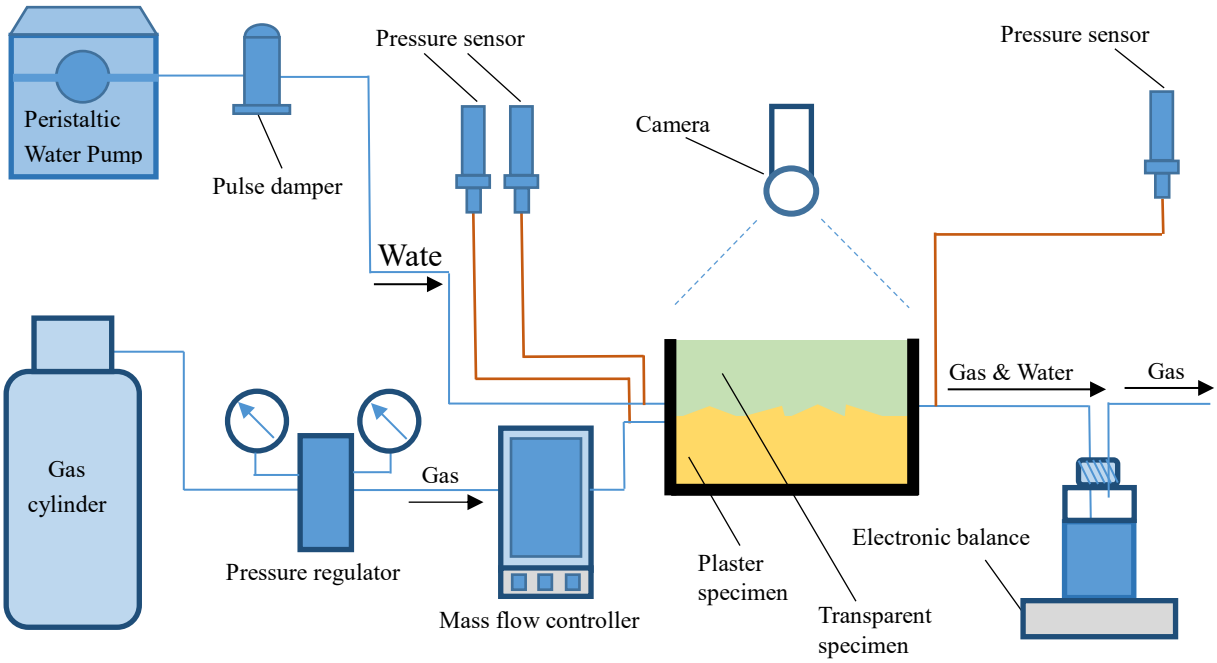

Fig. 3-2 The schematic of the experimental system

Fig. 3-3 The peristaltic pump

Fig. 3-4 The pulse damper

damper is connected to the pump. As shown in Fig. 3-4, the pulse damper has an inlet (at the bottom) and an outlet (in the above). Inside the pulse damper, the upper space is filled with air while water flows through the lower space. Due to its great compressibility, the air will swell and contract periodically, whereby the fluctuation of water pressure and flow rate will be decreased. Consequently, water flows out of the outlet with stable flow rate and pressure. With the peristaltic pump and the pulse damper, water can be stably injected to the two-phase flow box at a specified flow rate.

The gas supply subsystem includes a gas cylinder, a pressure regulator and a mass flow controller. Nitrogen is supplied from the gas cylinder, in which the initial pressure is within 0~14 MPa. With the pressure regulator, the gas pressure can be decreased to be the value within 0~0.2 MPa to protect the mass flow controller, since the mass flow controller cannot bear a pressure over 1 MPa. The mass flow controller can inject gas into the two-phase flow box at a specified rate between 0~5000 mL/min. The two-phase flow box is the core component of the experimental system. Two rock specimens can be put into the flow box, and one of the specimens is transparent for the convenience of obtaining the flow structures. The measurement system includes the pressure sensors, the camera and the electronic balance. They are used for obtaining the flow pressure of both phases, the flow structures and flow rate of water, respectively. This experimental system has the following advantages: (1) To conduct the visualized two-phase flow experiments in single fractures, meaning that the flow structures can be captured; (2) Rock specimens with different roughness degrees can be used in the system to study the influence of roughness on the two-phase flow characteristics; (3) The specimens can be placed with different apertures to investigate its influence on the two-phase flow; (4) The specimens can be placed with different shear displacements to investigate its influence on the two-phase flow; (5) A specially designed mechanical sealing method is used to seal the specimens. Sealant is not needed in the process of assembling or replacing the specimens, and consequently it's time-saving and economical. With this experimental system, the two-phase flow characteristics can be quantitatively studied to understand the two-phase flow mechanisms in engineering applications such as coalbed methane recovery, CO_2 sequestration and nuclear waste storage.

Since the two-phase flow box is the core component in the experiment system, it is introduced in the next section in detail.

3.1.3 Two-phase flow box

The two-phase flow box is manufactured with stainless steel. It is composed of one pedestal, two long-edge side plates, one fixed short-edge plate, one mobile short-edge plate, two L-modules, five pieces of rubber sheets, spacing shims, displacement shims and other accessories. After assembling the above-mentioned components, mechanical force can be applied on the specimens by tightening the screws, whereby the specimens can be sealed. As shown in Figs. 3-5 and 3-6 (a), the components include:

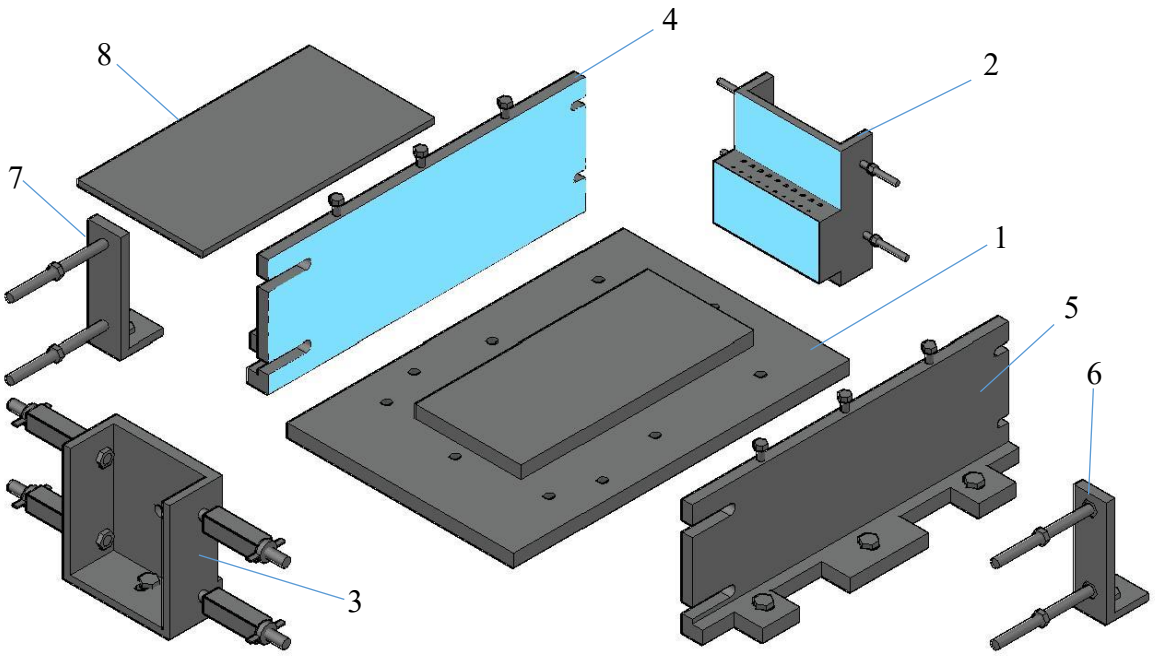

Fig. 3-5 The components of the two-phase flow box

1--Pedestal. The pedestal has a raised baseplate, on which the specimens will be put on. The length of the baseplate is 220 mm, which is 20 mm longer than the length of the specimen (200 mm). Several tapping holes are set on the pedestal, which are used for fixing the pedestal with other components.

2--Fixed short-edge plate. The fixed short-edge side plate can be fastened on the pedestal. A rubber sheet is pasted on the inside of this plate. There are 10 water injection poles and 10 gas injection poles on the plate. The height of the gas injection pores and water injection poles is 50 mm, which is identical to the thickness of one specimen; in this way the gas and water can be directly injected into the fracture between the two specimens.

3--Mobile short-edge plate. The mobile short-edge side plate is also fastened on the pedestal, but the position can be adjusted. By adjusting its position, the specimens can be compacted. A rubber sheet is pasted on the inside of this plate. There is an outlet on the mobile short-edge side plate for discharging the water and gas, as shown in Fig.3-7.

4,5—Long-edge plates. Two long-edge plates are also fastened on the pedestal. Rubber sheets are pasted on the inside of the plates.

6,7—L-modules. Two L-modules are fastened on the pedestal. They are connected to the mobile short-edge plate by the bolts. By screwing up the bolts, the position of the mobile short-edge plate can be adjusted to compact the specimens.

8—Transparent acrylic plate (not shown in Figs. 3-5 and 3-6). This acrylic plate is fastened on the long-edge plates with bolts. It is used for controlling the vertical displacement of the upper specimen under the water and gas pressure. It is made transparent for the convenience of observing the flowing structures.

In Fig. 3-5, the blue parts refer to the rubber sheets, which are used for sealing up the specimen. Fig. 3-6 (b) shows the physical picture of the two-phase flow box. Figs. 3-7 shows the side view (in the direction of width), in which the outlet of fluids is clearly shown. Figs. 3-8 and 3-9 show the vertical view and the side view (in the direction of length) of the two-phase flow box.

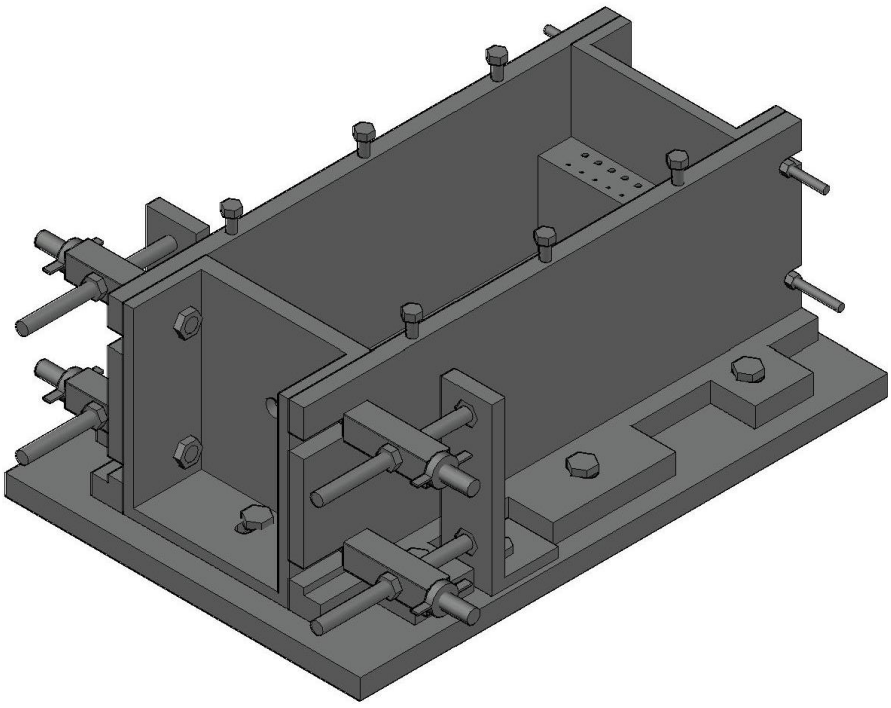

(a) Schematic (oblique view)

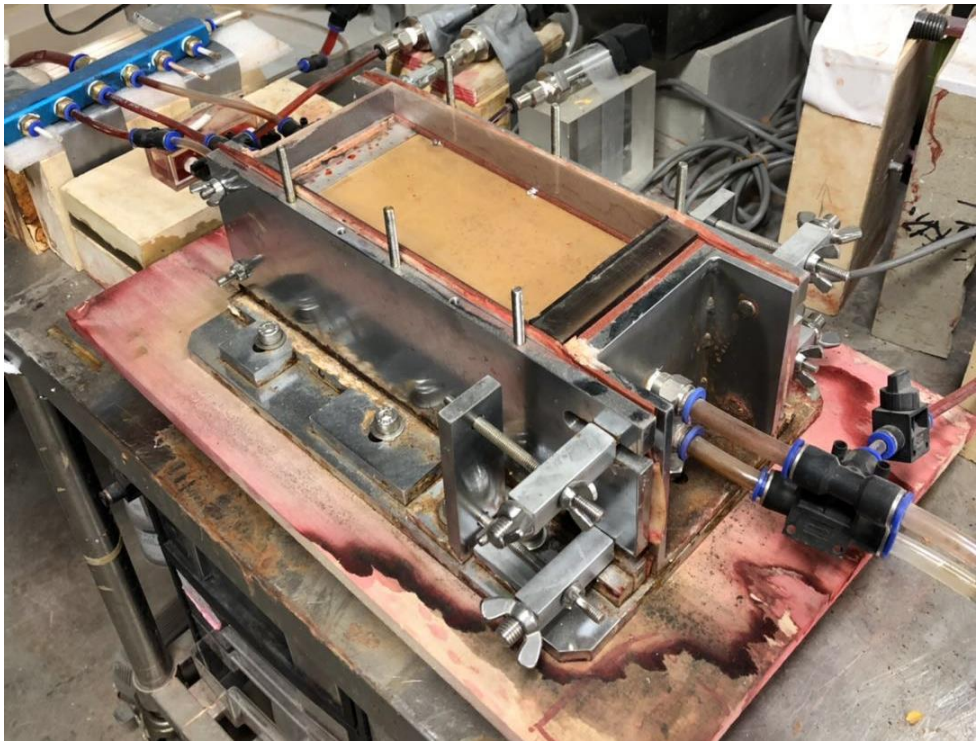

(b) The physical picture

Fig. 3-6 The assembled two-phase flow box

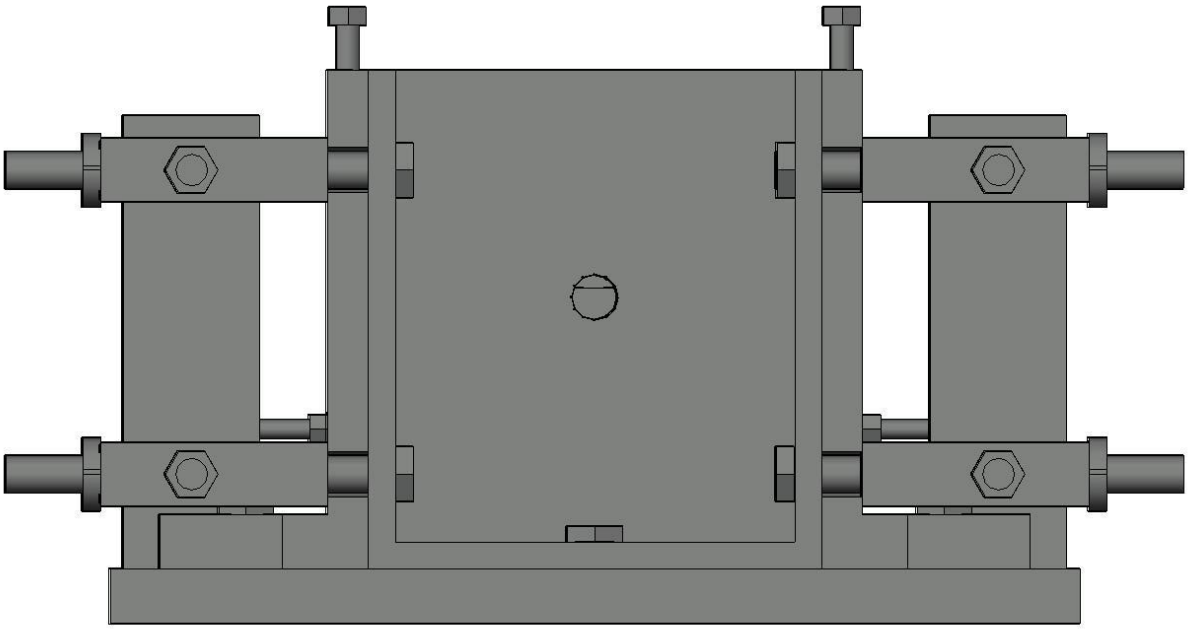

Fig. 3-7 Two-phase flow box--side view (in the direction of width)

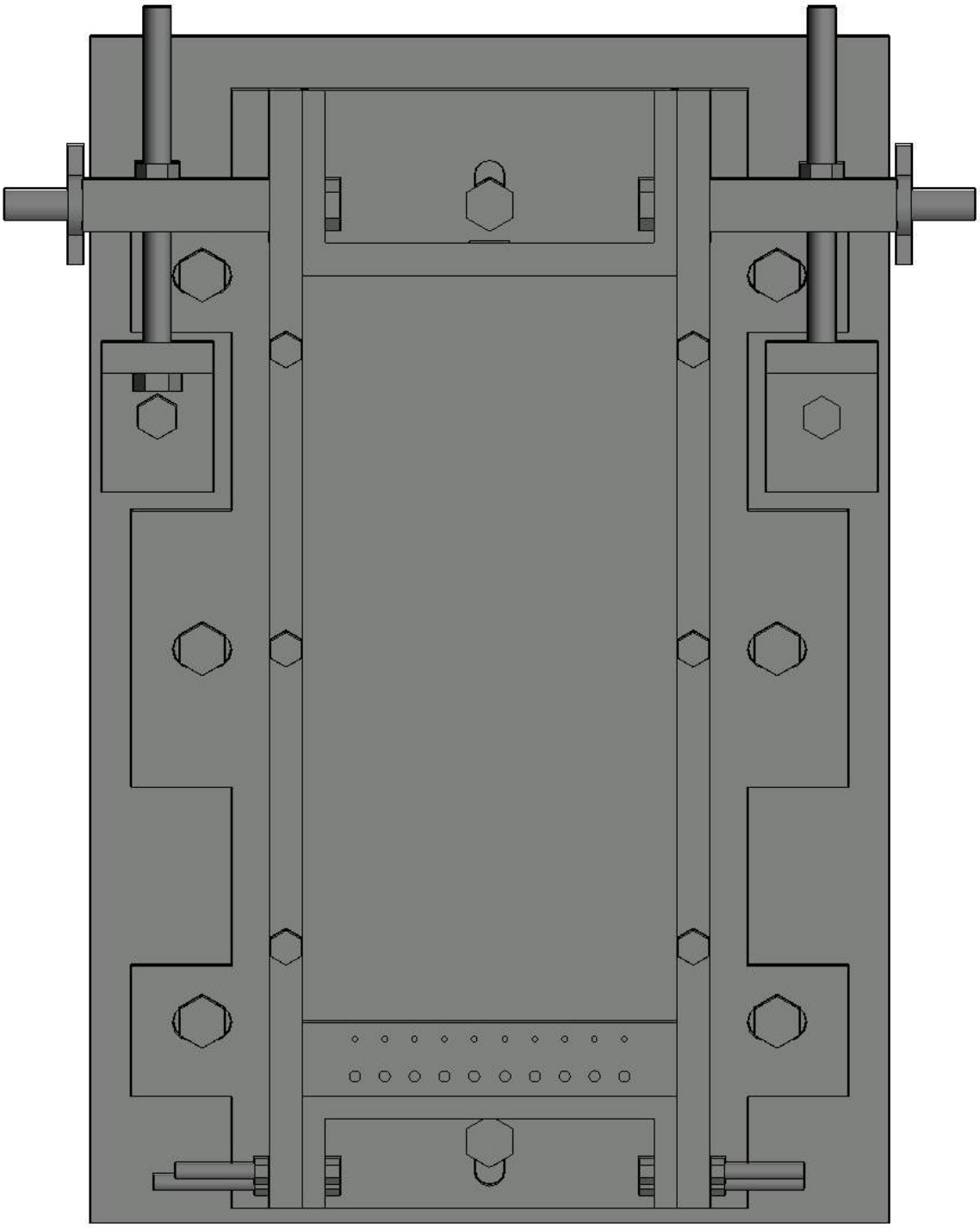

Fig. 3-8 Two-phase flow box in vertical view (without specimens)

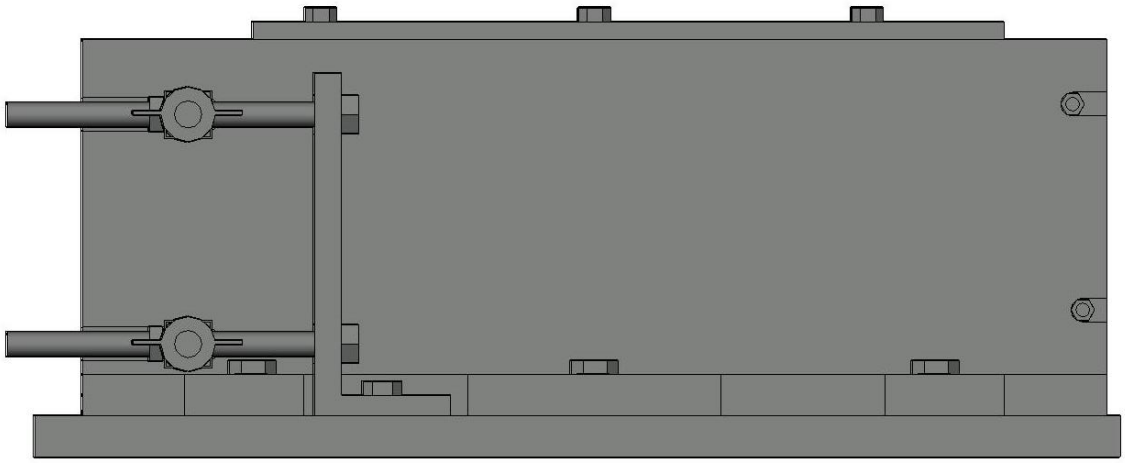

Fig. 3-9 Two-phase flow box--side view (in the direction of length)

The bottom specimen is placed alongside the bulge of the fixed short-edge plate. For the purpose of sealing, shim blocks should be placed alongside the upper specimen. Fig. 3-10 shows the side view of the two-phase flow box, in which the specimens (indicated by the blue lines) do not have a shear displacement. One shim-block is placed alongside the upper specimen for sealing. The length of this shim-block is 20 mm. Fig. 3-11 shows the side view of the two-phase flow box, in which the specimens (indicated by the blue lines) have a shear displacement. Two shim blocks, whose sizes are different from that in Fig. 3-10, are placed alongside the upper specimen. Actually, the length of Shim-block 1 can be 0.5 mm, 1 mm, 1.5 mm, 2 mm, 3 mm, 5 mm; and the length of Shim-block 2 can

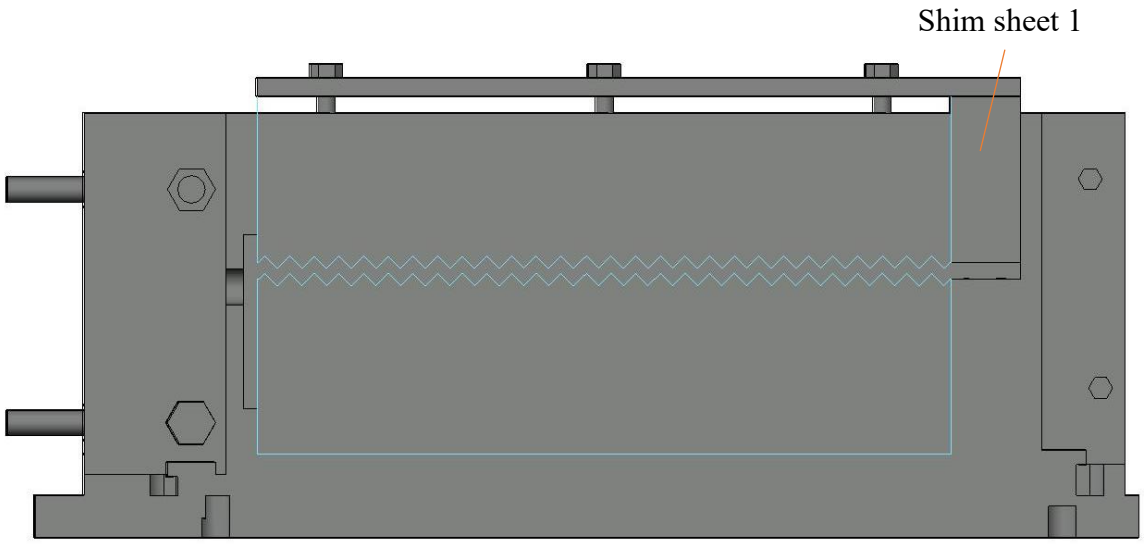

Fig. 3-10 Side view of the flow box (no shear displacement)

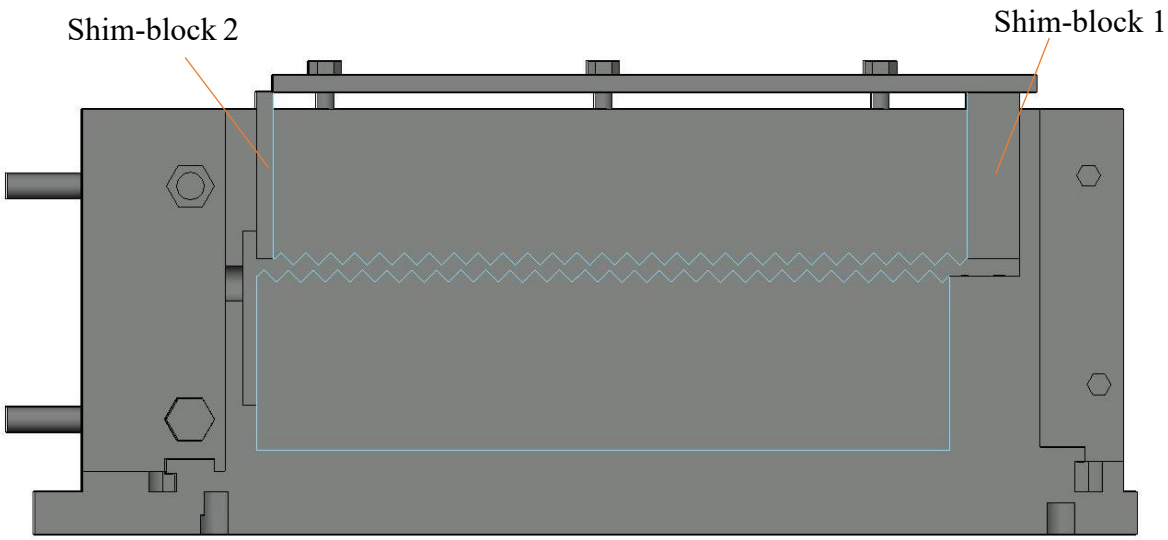

Fig. 3-11 Side view of the flow box (with shear displacement)

be 19.5 mm, 19 mm, 18.5 mm, 18 mm, 17 mm, 15 mm. In this way, the upper specimen can be placed with different shear displacements.

The specimens are specially manufactured to obtain the natural fracture surface. The bottom specimen can be a natural rock specimen or a plaster specimen which is cast with the natural rock specimen. The upper specimen is transparent, which is cast with the bottom specimen. The size of either specimen is 200 mm×100 mm×50 mm. Specimens with different JRC (Joint Roughness Coefficient) values can be put into the two-phase flow box to investigate the influence of the fracture roughness on the flow.

3.1.4 Measurement techniques

The measurement subsystem includes an electronic balance, a camera and three pressure sensors. Theoretically, if the surface tension between gas and water can be neglected, the gas pressure should be identical to that of water at the same location. But our experiments are to be conducted in a small aperture of the fracture, in which situation the surface tension is important, the gas pressure and water pressure should be respectively measured. Therefore, two of the pressure sensors are respectively connected to the gas inlet and water inlet. One pressure sensor is connected to the outlet. Since water and gas will flow out of the box through the only outlet, gas and water will pass the pressure sensor successively, so the pressure values will fluctuate more seriously. The

response time of the pressure sensors is 20 ms, which is small enough to measure the fluctuation of the fluids' pressure. The data of pressure sensors are transmitted and save in the data logger, as shown in Fig. 3-12. The data logger can be connected to 10 pressure sensors, and it can save 6 months' pressure data. All the pressure data are corresponding to the time. When conducting the experiment, the time ranges of each testing round shall be recorded.

Fig. 3-12 The data logger

A separation bottle is connected to the outlet of the two-phase flow box. Two fluids (gas and water) flow into the separation bottle, and water remains in the bottle while gas flows out of it. The separation bottle is placed on the electronic balance, which is used for measuring the water mass that flows out of the outlet. The data recording interval is 1 s, and the data are transmitted into the computer. With these data, the water flow rate can be calculated. The gas flow rate can be indicated on the digital screen of the mass flow controller. The flow structures are recorded with the camera. Since the flow structures are always varying, at each testing round 15 pictures are taken to obtain the average values of saturation.

3.2 Two-phase flow experiment in the single rock fracture

3.2.1 The testing procedures

In this experiment, there are several testing rounds. In each round, the gas injection rate

and water injection rate remain a constant value. The testing procedures include:

(1) Assemble the specimens in the two-phase flow box. Rubber sheets are pasted on all the four side plates in the aim of sealing water and gas. Then screw up all the bolts. The rubber sheets can be reused as long as no air/water leakage occurs. Fig.3-6(a) shows the schematic of the assembled two-phase flow box (without specimens) and Fig. 3-6(b) shows the physical picture (with specimens).

(2) Test the sealing effect. Water and gas are injected into the two-phase flow box. A flowmeter is connected to the separation bottle to check whether the flow rate indicated by the mass flow controller is identical to that indicated by the flowmeter. If no water leakage happens and the gas flow rate indicated by the gas flowmeter is identical to that indicated by the mass flow controller, the sealing effect is assumed to be good.

(3) Conduct single-phase flow tests of water. This procedure is to obtain the single-phase hydraulic properties of the fracture, such as the intrinsic permeability. At each testing round, the water injection rate is kept constant. The data log will not be started until the flow test has been commenced for 5 minutes.

(4) Conduct the two-phase flow tests. At each testing round, water injection is firstly started by turning on the peristaltic pump. When all the space in the fracture is filled with water, gas injection will be started. When the two-phase flow reaches a stable state, the data log is started, which includes the pressure data, the water mass and the flow structures. The water mass in the separation bottle starts to be recorded by activating the recording button in the software on the computer. The data logger keeps recording the pressure data as long as it is power on, so we just keep down time range of the pressure data of each round by manual recording. After the experiments, we just need to pick out the pressure data at each testing round according to the time ranges. At the same time of pressure and water mass recording, photos are taken with the camera. In each testing round, 15 photos are taken because the flow structure is always varying. The data log in each testing round lasts 1 minute for the convenience of obtaining average values.

There are two principles for judging whether the two-phase flow has reached a stable state. The first one is to observe the flow structures. If the flow structure is not stable, the data log won't be started. The second one is to observe the evolution of the pressure data indicated by the pressure data logger. If the pressure data fluctuates stably within a certain range, it means that the stable state has been achieved. Generally, when gas injection is

started, the pressure of each sensor will increase during the fluctuation.

When a new testing round begins, repeat the above steps.

(5) When all the tests are finished, turn off the peristaltic pump, the mass flow controller, the electronic balance, the computer, the pressure data-logger. Close the valve of the gas cylinder. Disassembly and clean the two-phase flow box to prevent rust. Put away all the devices in preparation for future use.

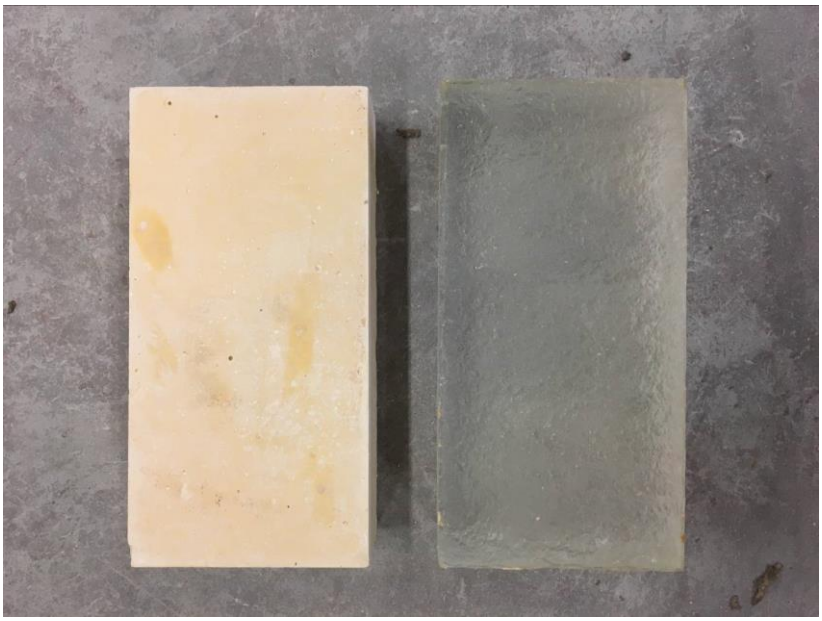

(a) Specimens

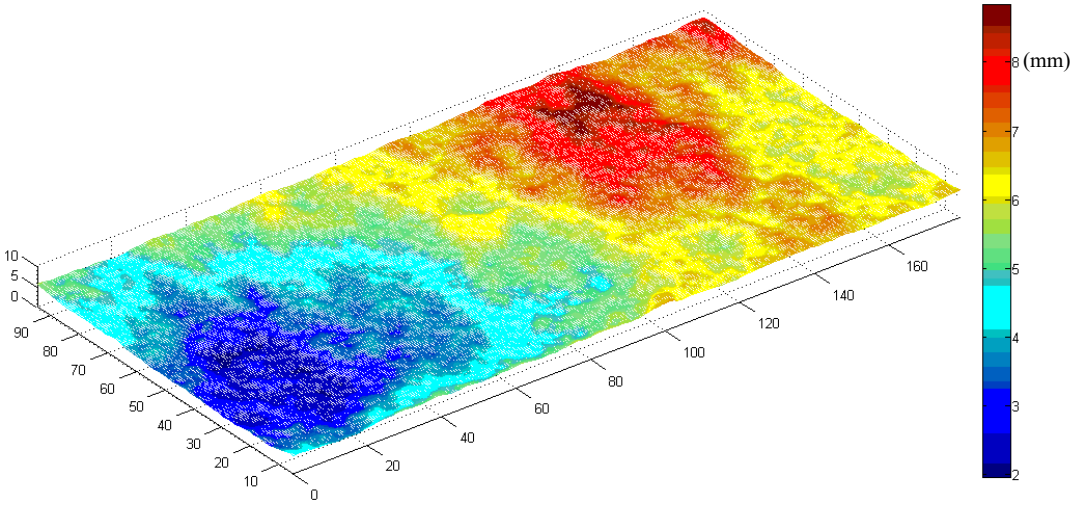

(b) The aperture distribution of the rough specimen

Fig. 3-13 Specimens used in the experiment

Two pairs of specimens are selected for test: one pair of smooth specimens and one pair of rough specimens. The specimens selected for the test are shown in Fig. 3-13(a). The lower specimen is smooth, which is made of plaster. The upper specimen is rough, which is made of transparent resin. The rough surface is made by replicating the rough surface of a sandstone fracture. The aperture distribution of the rough surface of the resin specimen is shown as Fig. 3-13(b).

3.2.2 Calculation of the hydraulic aperture and intrinsic permeability

In single-phase flow, the conductivity of fluid is dominated by permeability, which is one of the intrinsic properties of rock fractures. The hydraulic aperture of the fracture is an important parameter to evaluate the conductivity of fluid flow in fractures. In low-velocity fluid flow, the hydraulic aperture is usually calculated with Darcy's law and the cubic law, as indicated by Equation 3-1.

$$-\frac{\Delta P}{L}=\frac{\mu}{K}\frac{Q}{A}=\frac{12\mu Q}{h^3 w} \tag{3-1}$$

$\triangle P$ is the pressure drop; L is the length of flow channel; A is the cross area of the fracture; Q is the flow rate; K is the permeability, which equals $h^2/12$; μ is the dynamic viscosity of water, which is 1.5×10^{-3} Pa at 5 C°. However, this equation is not applicable when the flow velocity is high, in which the nonlinearity of fluid flow cannot be neglected. In these conditions, the Forchheimer's law is generally used, as shown in Equation 3-2.

$$-\frac{\Delta P}{L}=\frac{12\mu Q}{h^3 w}+B\frac{\rho}{h^3 w}Q^2 \tag{3-2}$$

The single-phase tests are conducted with both water and nitrogen. The evolution of pressure drop with respect flow rate of single-phase flow in the rough fracture is shown as Fig. 3-14. The experiment data are well fit with Equation 3-2. It shows that the pressure drop increases nonlinearly with respect to flow rate. The nonlinearity of water flow is more severe than that of gas, due to the more significant inertial effect of water. The hydraulic aperture calculated by Equation 3-2 with water the test result is 1.276 mm, while it is 1.088 mm with the gas test result. This difference may be induced by many factors. The values of viscosity adopted for calculation are just estimated values by referring the reference. In addition, the pressure of gas single-phase is too small, which may be easily overlapped by other errors. Consequently, the difference is acceptable, and

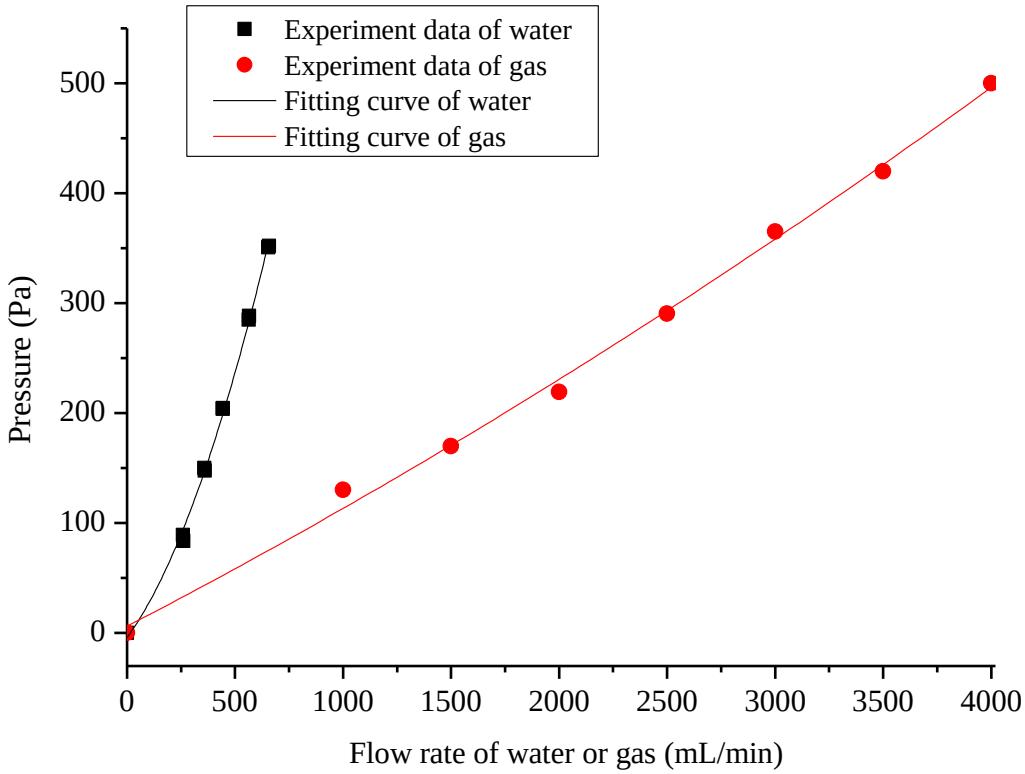

Fig. 3-14 The Pressure-Flow rate relationship in the rough specimen (single phase of water and gas)

we adopt the value of 1.276 mm by assuming that the test results of water single-phase are more accurate.

3.2.3 Calculation of the relative permeability and phase multipliers

The relative permeability is defined as the ratio of the permeability of a certain phase in a two-phase flow and the corresponding permeability in a single-phase flow. It is usually adopted as the parameter for evaluating the magnitude of two-phase interference. However, the method for calculating the relative permeability (extended Darcy's law) does not account for the inertial effect of fluid flow, so the Lockhart-Martinelli model is also adopted in many researches. The critical parameters of Lockhart-Martinelli model are the water phase multiplier, and the gas phase multiplier, as defined in Equations 3-3a and 3-3b. These two parameters are defined as the ratio of the pressure drop of a certain fluid in two-phase flow and the pressure drop in single-phase flow. Their evolution is generally analyzed with the evolution of a parameter χ. χ is defined as the ratio of the

pressure drop of one fluid and that of the other fluid in the state of single-phase flow, as shown in Equation 3-4. It represents the relative importance of one fluid to the other fluid [Fourar and Bories, 1993]. The evolution of the relative permeability and phase multipliers is analyzed in the next section.

$$\Phi_w = \frac{dP/dx}{(dP/dx)_w} \tag{3-3a}$$

$$\Phi_g = \frac{dP/dx}{(dP/dx)_g} \tag{3-3b}$$

$$\chi = \frac{(dP/dx)_w}{(dP/dx)_g} \tag{3-4}$$

3.3 The testing results

3.3.1 Evolution of the flow structures

The evolution of flow structures in the both specimens is shown in Fig. 3-15. The left column shows the original photos, in which the red parts refer to water and the while parts refer to gas. The water is dyed as red in order to form distinct different color from gas, for the convenience of binarization. The right column shows the binarized photos, in which the black parts refer to water and the while parts refer to gas. As shown in Fig. 3-15(I), the evolution of flow structures in the smooth specimen shows similarity to that of two-phase flow in pipes. With the increase of gas flow rate, the flow structure evolved from bubble flow to continuous flow; in addition, there is no trapped gas phase, which means that the capillary pressure does not take effect in the flow. However, in the rough specimen, as shown in the area marked by the blue circle in Fig. 3-15(II)a, gas was trapped and become immobile phase. All the photos in Fig. 3-15(II) shows that both water and gas tended to flow in fixed channels; gas mainly flowed in the upper the channel and was trapped in certain areas; while water flowed in the lower channel. The flow structures in the rough specimen show more similarity to that of two-phase flow in porous media, namely that the both phases flow in the fixed channels, respectively. The flow structures didn't have much change with respect to different gas-water ratios. There was not an obvious evolution process from bubble flow to continuous flow. This contrasts the results by Fourar and Bories (1993). In their study, an evolution of flow structures from bubble flow to continuous flow was observed. One reason that lead to this difference may be that

Original photo Binarized photo

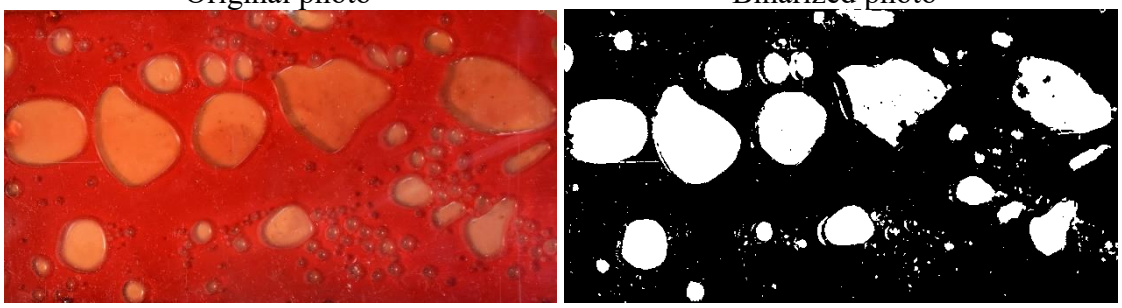

(a) *Gr* = 500 mL/min

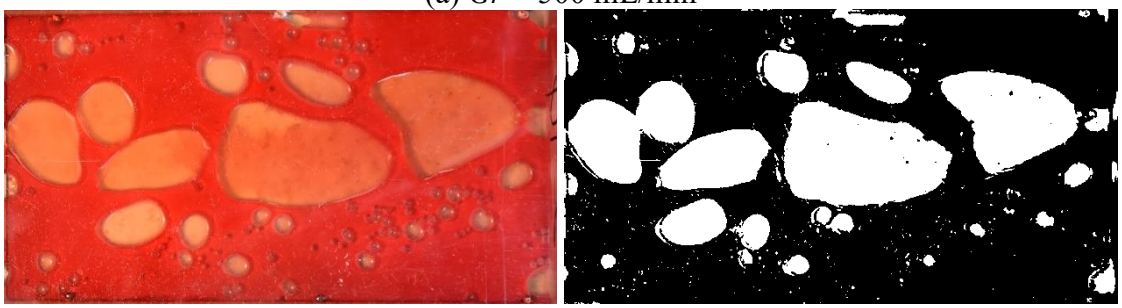

(b) *Gr* = 750 mL/min

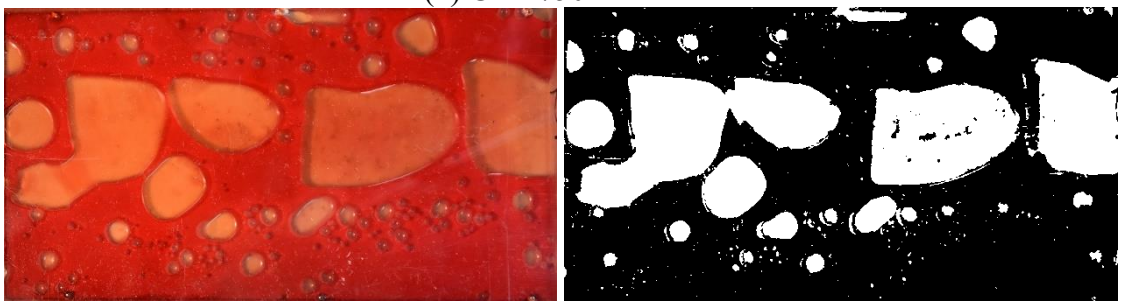

(c) *Gr* = 1000 mL/min

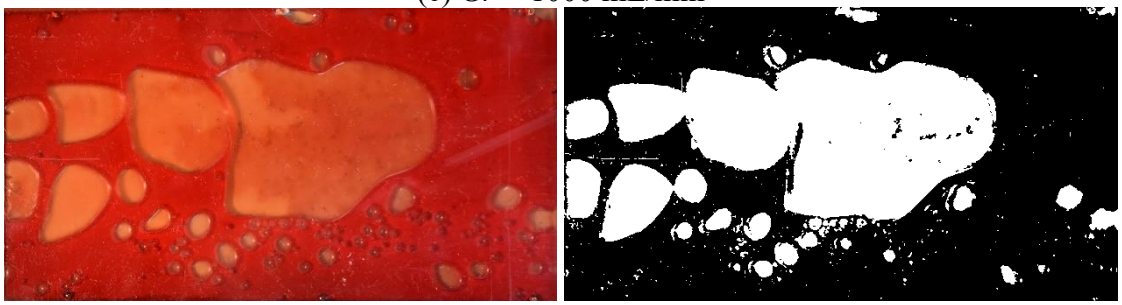

(d) *Gr* = 1250 mL/min

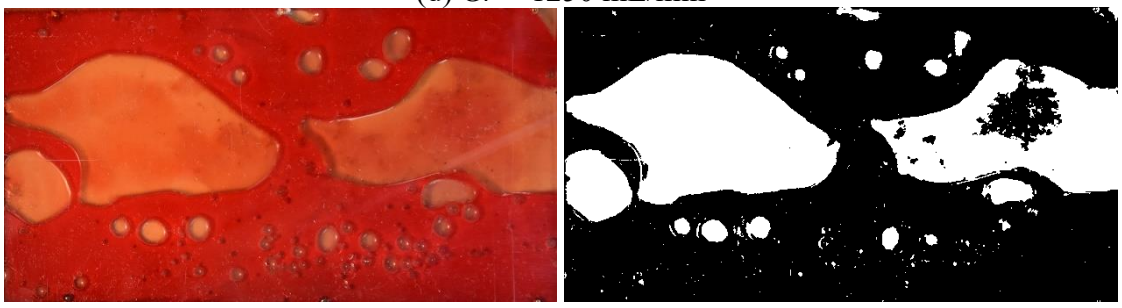

(e) *Gr* = 1500 mL/min

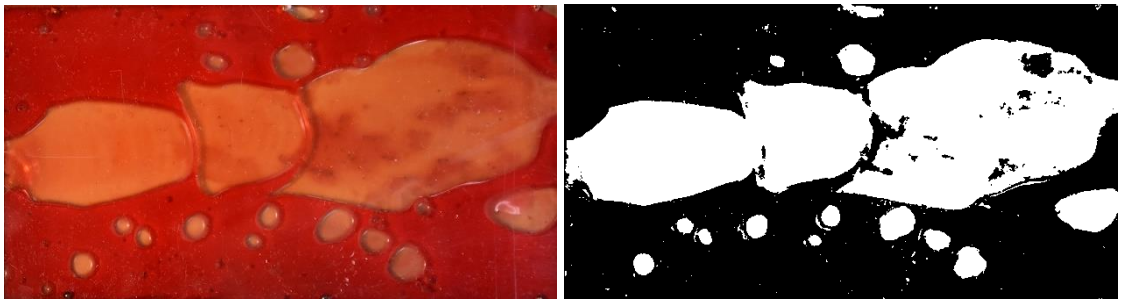

(f) *Gr* = 1750 mL/min

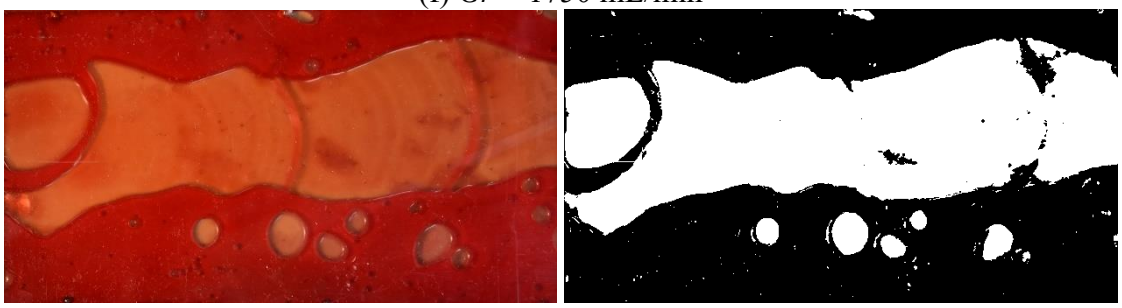

(g) *Gr* = 2000 mL/min

I. The flow structures at *Wr* = 600 mL/min in the smooth specimen

Original photo Binarized photo

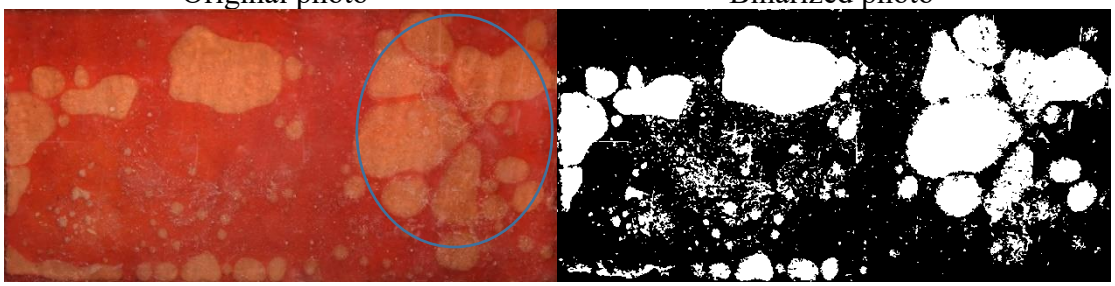

(a) *Gr* = 500 mL/min

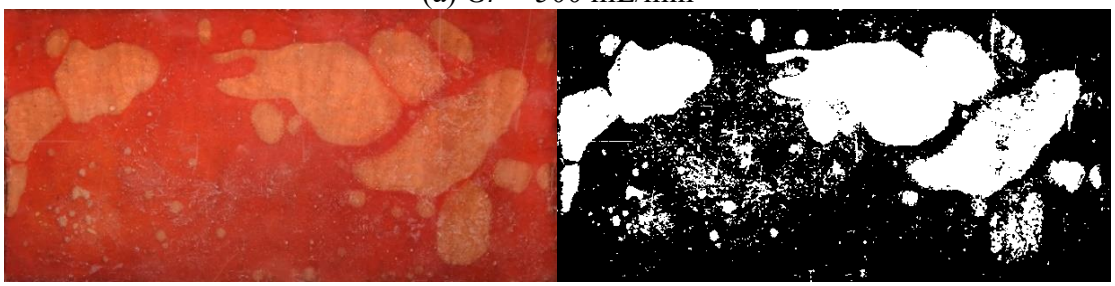

(b) *Gr* = 750 mL/min

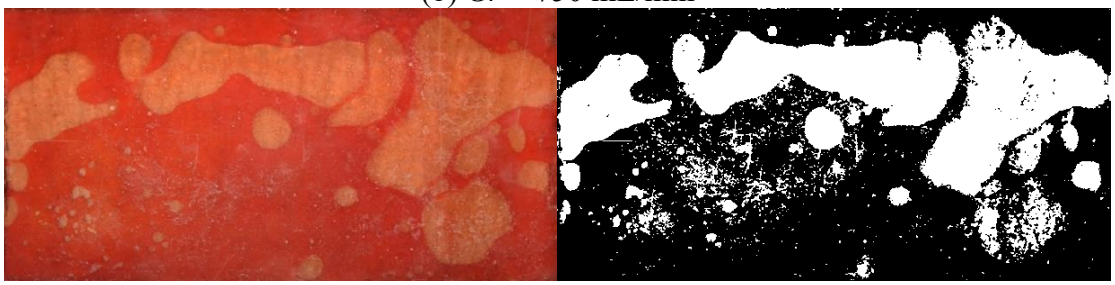

(c) *Gr* = 1000 mL/min

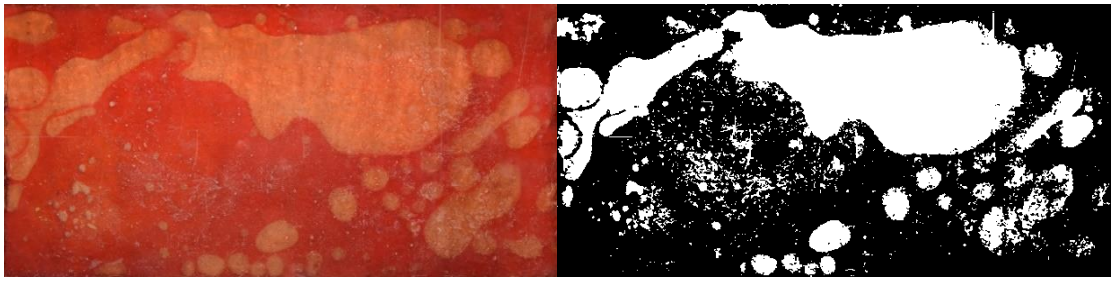

(d) *Gr* = 1250 mL/min

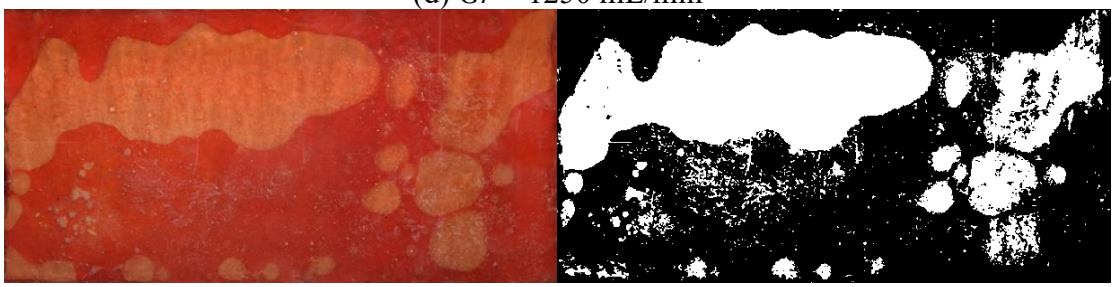

(e) *Gr* = 1500 mL/min

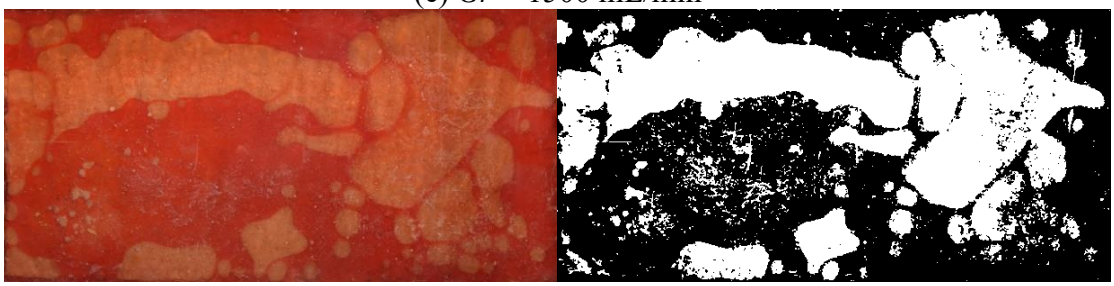

(f) *Gr* = 1750 mL/min

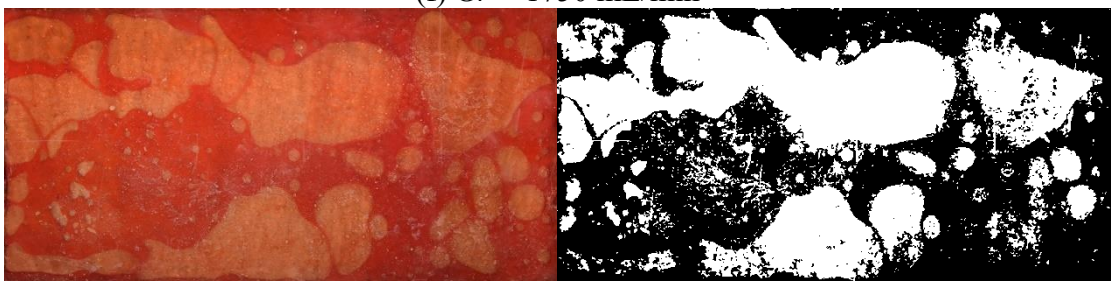

(g) *Gr* = 2000 mL/min

(II) The flow structures at *Wr* = 300 mL/min in the rough specimen

Fig. 3-15 The evolution of flow structures

the rough specimen used in our experiment is quite different from theirs. In our experiment, the rough specimen has a totally identical surface morphology to that of a natural fracture (sandstone). However, the rough specimen used by Fourar and Bories was made artificially by gluing a layer of glass beads to the glass plates. In the specimen with a natural fracture surface, the capillary pressure is significant; but in the specimen made by Fourar and Bories, the roughness is different from a natural fracture surface, and the effect of capillary pressure is different. This leads to the difference in flow structures.

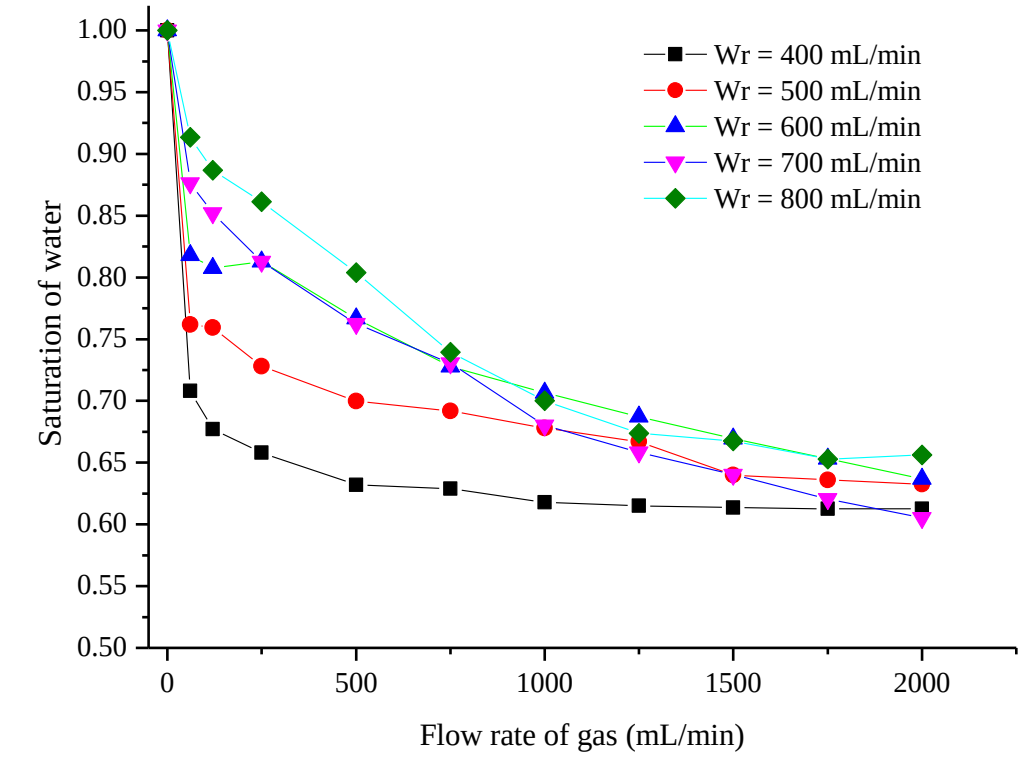

(a) Smooth specimen

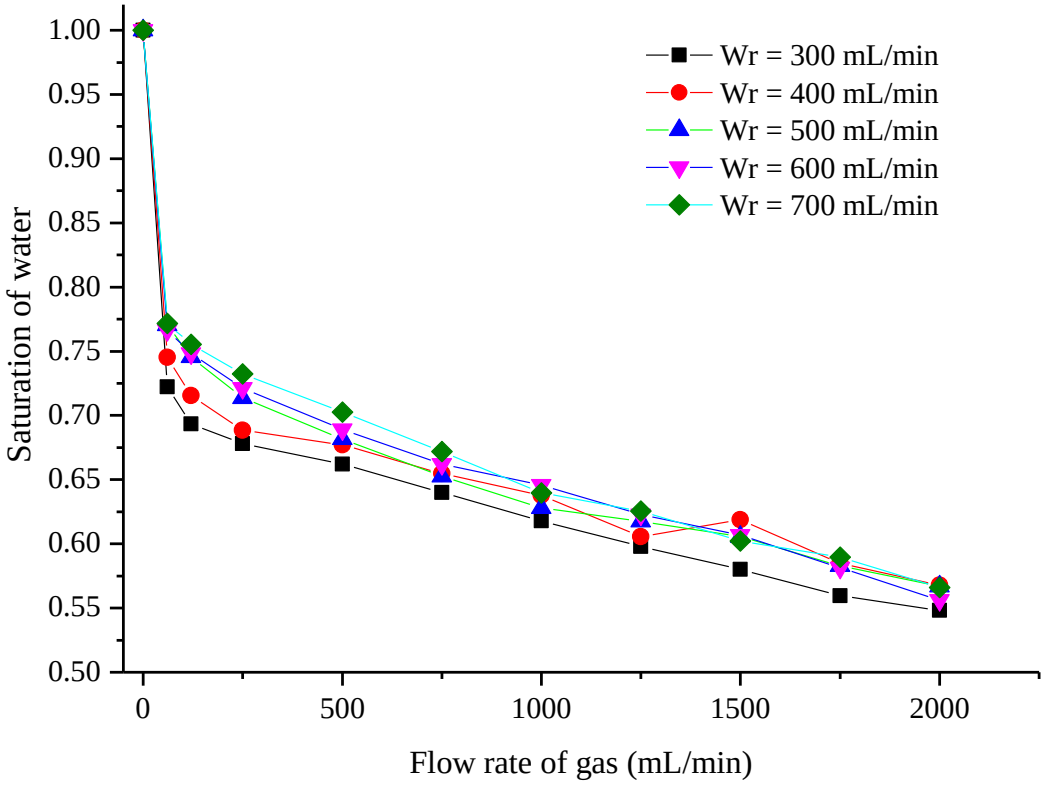

(b) Rough specimen

Fig. 3-16 The evolution of water saturations with respect to the flow rate of both phases

Fig. 3-16 shows the evolution of water saturation with respect to gas flow rate in both specimens. Each curve represents the case at the same water flow rate. The evolution styles of saturation in the smooth specimen show quite much difference from that in the rough specimen. As shown in Fig. 3-16(a), the 5 different curves with different water flow rates evolve in different ways. At the same gas flow rates, for example when G_r = 500, the saturations at different curves have significant different. However, Fig. 3-16(b) shows that at different water flow rates, the evolution patterns of saturation are almost the same. At a certain gas flow rate, the saturations at different curves are close to each other. This is because the flow in the rough specimen shows similarity to that of two-phase flow in porous media. Each phase flowed in their own channel. The trapped immobile phase accounts for a certain percentage in the total saturation, so the change of saturation induced by increasing the water flow rate is not obvious. To summarize, the different evolution patterns of saturation in the two specimens reveal that the capillary pressure only takes effect in the two-phase flow in the rough specimen. This revels that there is some difference in the two-phase interference between the two specimens. This will also lead to difference in the hydraulic properties of two-phase flow.

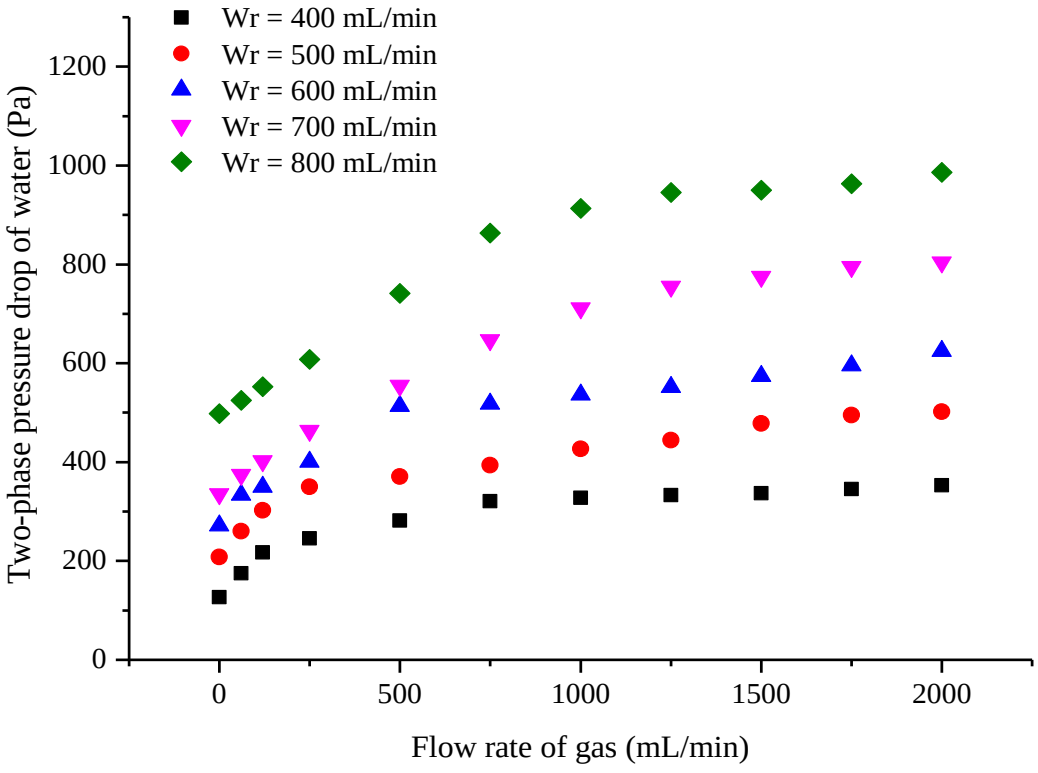

(a) Smooth specimen

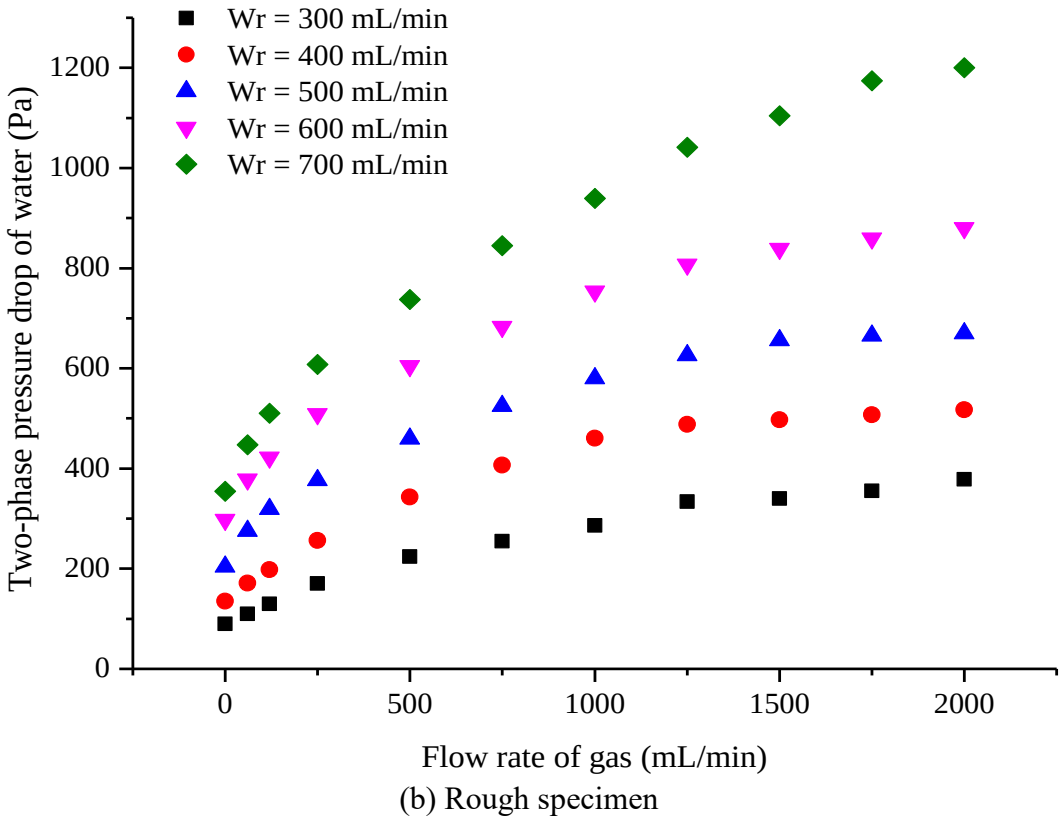

(b) Rough specimen

Fig. 3-17 Relationship between the pressure drop and flow rate in two-phase flow

Fig. 3-17 shows the evolution of two-phase pressure drop with respect to flow rates of water and gas. In both specimens, it shows a nonlinear relationship between the pressure drop and the gas flow rate. This nonlinearity is induced by the fact that the pressure drop induced by water accounts for more percent than that of gas. However, the nonlinearity is different in these two specimens. As shown in Fig. 3-17(a), even though increasing the gas flow rate would lead to an increase of pressure drop, but the pressure drop induced by gas flow accounts for a relatively small percentage. When gas flow rate is over 1000 mL/min, the increase of pressure drop induced by increasing gas flow rate is not obvious; but in the rough specimen, as shown in Fig. 3-17(b), when the gas flow rate is over 1000 mL/min, the pressure drop keeps increasing obviously with respect to gas flow rate. This means that in the rough specimen, the interactions between water and gas were more significant. In the rough specimen, when the gas flow rate was increased, the additional pressure drop is not only contributed by the flow of gas itself, but also by the serious phase interference such as the turbulence.

3.3.2 Evolution of the relative permeability

Fig. 3-18 shows the evolution of relative permeability with respect to saturation of water. For the convenience of comparison, the curves of X-model, viscous model and Corey model are also drawn in the figure. The curve of Corey model is with an assumption of $S_{w,r} = 0.01$ and $S_{nw,r} = 0.12$. The Corey model is expected to fit our experimental results in the rough specimen since this model considers the capillary effect.

Fig. 3-18(a) shows the evolution of relative permeability in the smooth specimen. It shows that all the experiment data are lower than both the viscous model and the Corey model, indicating a stronger phase interference than both models. Since the viscous coupling model indicates the two-phase interference induced by viscous coupling force between two phases and Corey model indicates the two-phase interference induced by capillary pressure, the experiment data indicate that there are other factors that would increase the pressure drop and correspondingly decrease the relative permeability. Fig. 3-18(a) shows that the relative permeability at $W_r = 400$ mL/min is larger, while the relative permeability at $W_r = 500$, 600, 700, 800 mL/min are close to each other. This may be induced by the inertial effect at high water flow rates. When the water flow rate is high, the inertial effect becomes more serious and it leads to more pressure drop and decreases the relative permeability.Theoretically, there should be no inertial effect in the smooth specimen, but any change in the flow channel will cause inertial effect of fluid flow, such as the change of flow channel size from the box inlet to the specimen.

Fig. 3-18(b) shows that the experiment data in the rough specimen fit the Corey model well, indicating that the capillary pressure is a dominant effect in our experiment. However, the curves with different water flow rates fail to fall on the same curve. This indicates that the relative permeability is not only the function of saturation, but also the dependent on the flow rate. This is to say, in addition to the capillary force, other factors also have influence on the relative permeability. By analyzing the curves in Fig. 3-18(b), it is found that at the same gas flow rate, the relative permeability increases with respect to the decrease of water flow rate. This means that the larger the water flow rate, the larger the two-phase interference. This is believed to be influenced by the inertial effect, because the inertial effect increases with respect to the increase of water flow rate. In addition, the turbulence will also increase with respect to the increase of water flow rate, and the

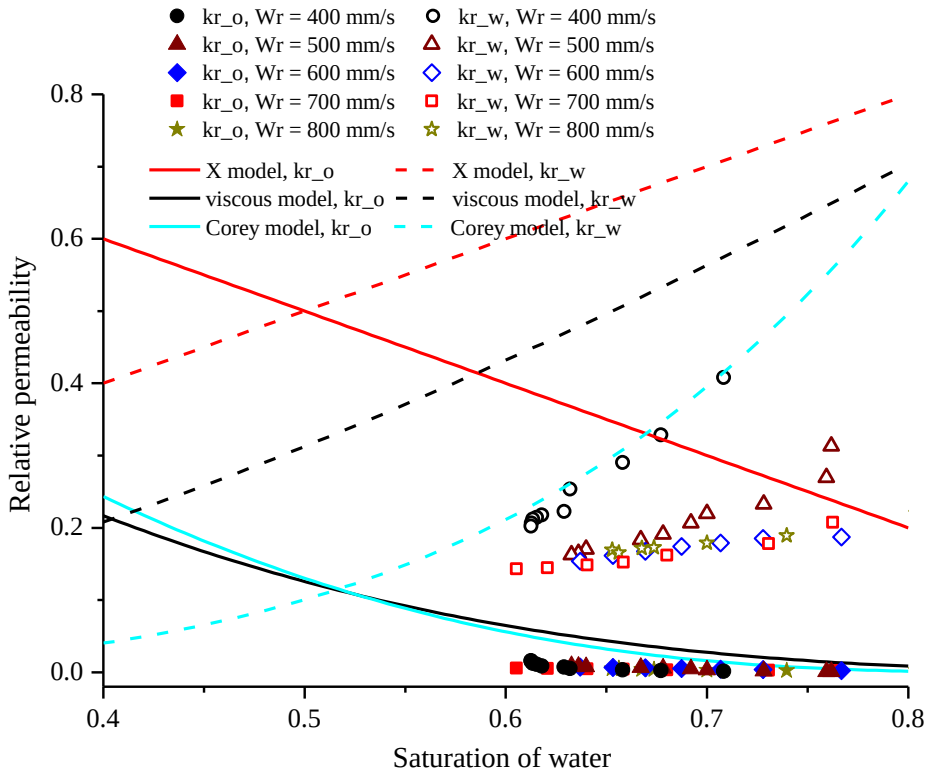

(a) Smooth specimen

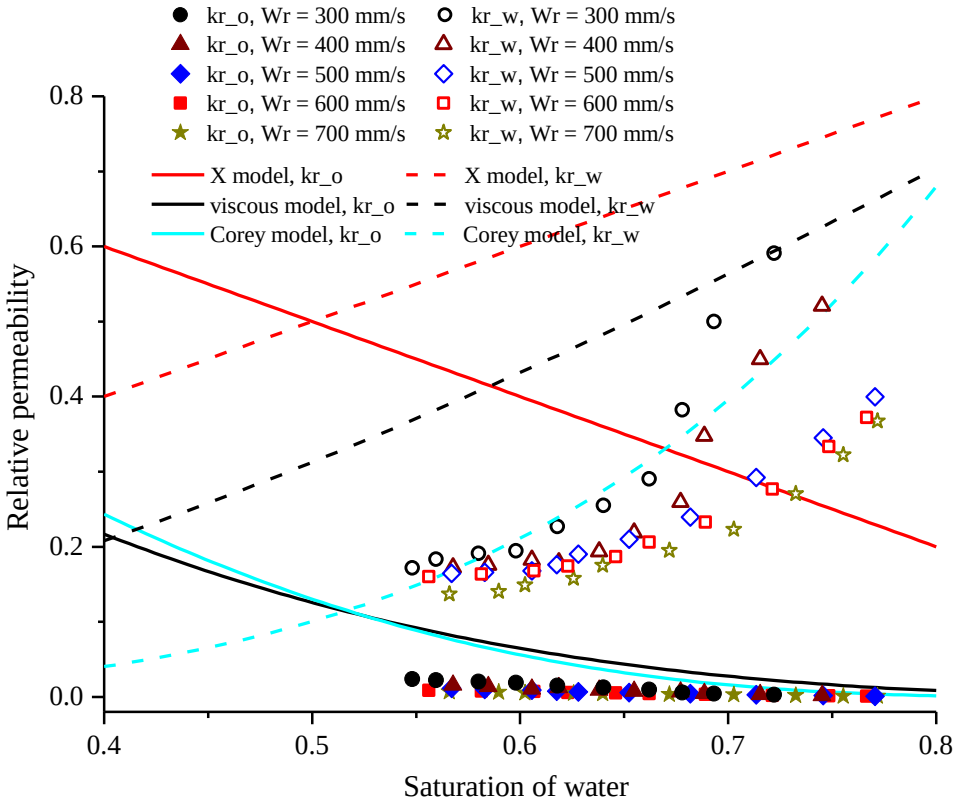

(b) Rough specimen

Fig. 3-18 The evolution of relative permeability

two-phase interference will also be increased.

3.3.3 Evolution of the phase multipliers

Since the extended Darcy's law is not perfect in describing the two-phase flow hydraulic characteristics with the concept of relative permeability, the Lockhart-Martinelli model is also adopted with an attempt to fit the experiment results. Delhaye et al [1981] proposed an empirical correlation between Φ_w, Φ_g and χ, as shown in Equations 3-5. C is a parameter that indicates the flow regime of each phase. When C = 5, both liquid and gas are laminar; when C = 10, liquid is turbulent and gas is laminar; when C = 12, liquid is laminar and gas is turbulent; when C = 20, liquid is turbulent and gas is turbulent.

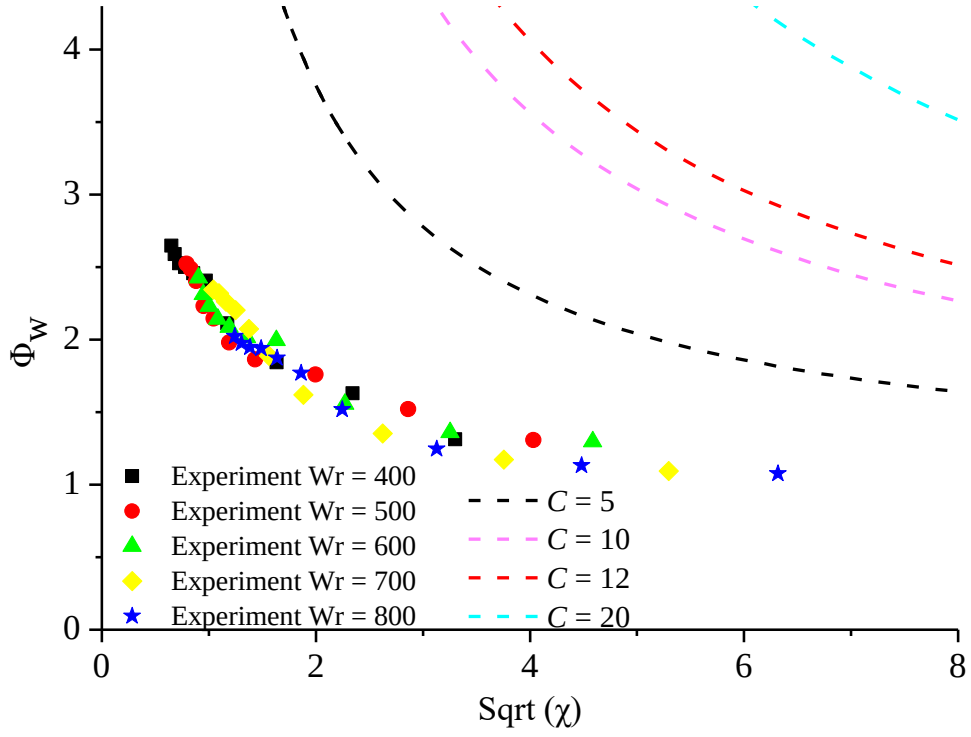

(a) Φ_w

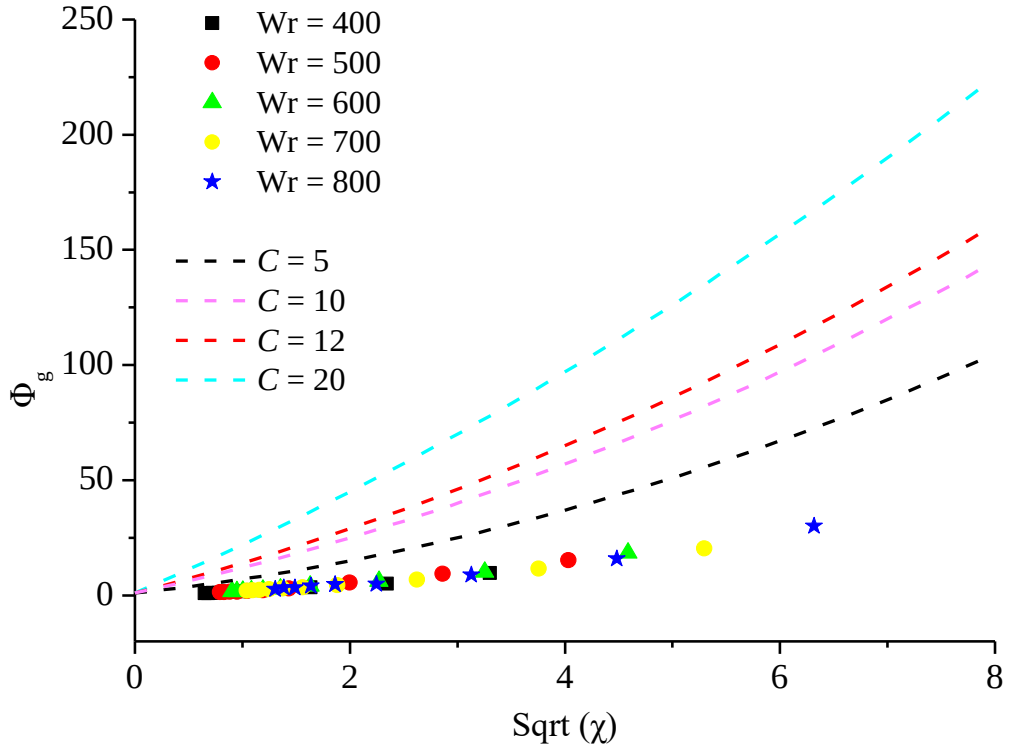

(b) Φ_g

Fig. 3-19 Evolution of phase multipliers Φ in the smooth specimen

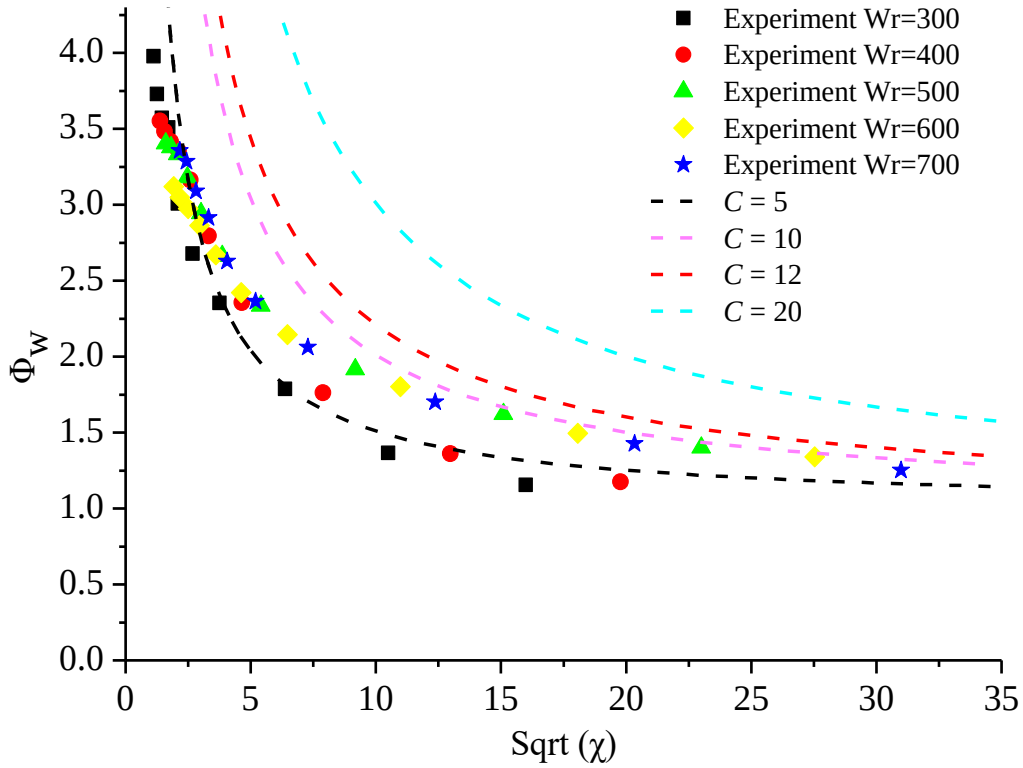

(a) Φ_w

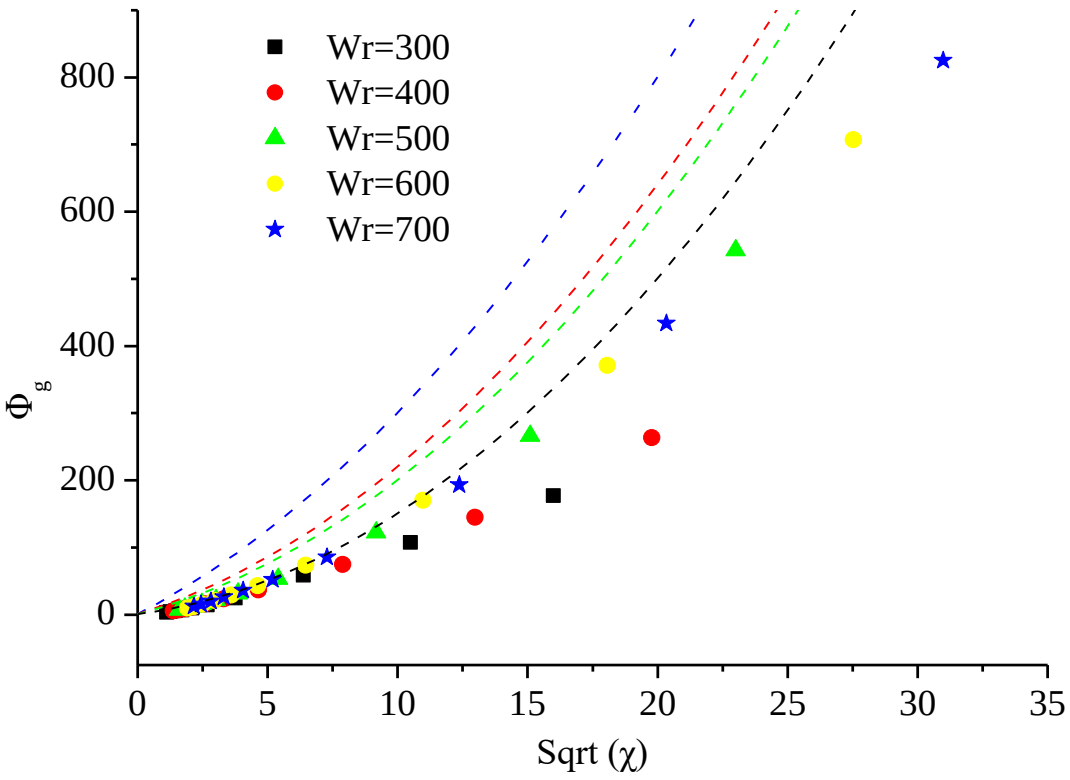

(b) Φ_g

Fig. 3-20 Evolution of phase multipliers Φ in the rough specimen

$$\Phi_w = 1 + \frac{C}{\sqrt{\chi}} + \frac{1}{\chi} \tag{3-5a}$$

$$\Phi_g = 1 + C\sqrt{\chi} + \chi \tag{3-5b}$$

Figs. 3-19 and 3-20 show the evolution of phase multipliers of both phases with respect to χ in both specimens. Fig. 3-19 shows that the different groups of data (with different water flow rates) almost fall on the same curve, indicating the effectiveness of the Lockhart-Martinelli model. The data are lower that the curve of C = 5, which means both phases are laminar. Fig. 3-20 shows that the test data of flow in the rough specimen are also close to the curve of *C* = 5. However, the data with different water flow rates don't fall on the same curve. As shown in Fig. 3-20(b), as the water flow rate increases from 300 mL/min to 700 mL/min, the value of *C* increases. This indicates that the turbulence increases with the increase of water flow rate.

3.4 Summary

(1) In the smooth fracture, the flow structures show more similarity to that of two-phase

flow in pipes, while the flow structures in rough fractures are more similar to that in porous media. In the rough fracture, the flow structures didn't have much change at different gas-water ratios. Both water and gas tend to flow in their own channels, and the flow channels are stable. A significant amount of gas was trapped in the areas with small apertures, indicating that the capillary pressure is a significant resistivity in the flow.

(2) The relative permeability in the rough specimen approximately follows the Corey model, which confirmed that the pressure drop is in this rough fracture is dominated by the capillary pressure. However, the curves with different water flow rates fail to fall on the same curve, namely there are some deviations from the Corey model, and the deviation increases with respect to the increase of water flow velocity. This is to say, the relative permeability is not only the function of saturation, but also the function of water flow velocities. The deviation from Corey model indicates that the inertial effect of water decreased the relative permeability and increases the two-phase interference. However, the relative permeability in the smooth specimen also indicates that the inertial effect cannot be neglected in the flow.

(3) The Lockhart-Martinelli model can also fit the results well. For flow in the smooth fracture, all the data almost fall on the same curve; but for the rough fracture, the increase of water flow rate leads to the increase of flow turbulence, which also increases the flow interference between two phases. This confirmed that the two-phase flow interference is not only influenced by the fluid inertial effect, but also the flow turbulence. For the rough fracture, the increase of water flow rate leads to obvious turbulence, while in the smooth fracture the change of turbulence with respect to the increase of water flow rate can almost be neglected.

Chapter 4 Numerical investigation on the two-phase flow in single rock fractures: the effect of capillary pressure and fracture morphology

The previous chapters revealed that the pressure drop characteristics of two-phase flow are influenced by many factors, such as the properties of fluids, the capillary pressure, the fracture morphology etc. When the flow is influenced by multiple factors, it is difficult to quantify the effect of a single factor; however, in experiments the multiple factors always coexist. In order to quantify the effect of the fracture morphology on the hydraulic properties of two-phase flow, in this chapter, the behavior of liquid-liquid two-phase flow in rough fractures is investigated with the level set method by numerical simulation. The simulation was conducted in fractures with different aperture distributions. The flow structures show that the aperture distribution is correlated with the flow tortuosity and leads to different evolution patterns of relative permeabilities. The above-mentioned effects are quantitatively studied in this chapter.

4.1 Introduction of level set method in two-phase flow simulation

4.1.1 Introduction of the level set method

The level set method is a numerical method for tracking the interface and shape modeling, which is proposed by Stanley Osher and James Sethian in 1980s. This method is widely applicated in computational fluid dynamics, image processing, optimization calculation, and computational geometry etc.

Two-phase flow simulation with level set method is governed by Equations 4-1 and 4-2. Equation 4-1a is the Navier-Stokes equation, in which $\boldsymbol{u}$ is the fluid velocity, ρ is the fluid density, t is time, $\boldsymbol{I}$ is the unit matrix, μ is the dynamic viscosity of the fluid, $\boldsymbol{F_{st}}$ and $\boldsymbol{F_g}$ are the volumetric force ($\boldsymbol{F_{st}}$ is the capillary pressure, which only exists in multiphase phase flow). This equation is assumed as an effective method for describing fluid transport in single-phase flow. In order to describe two-phase flow with Equation 4-1a, some modifications are required. In other words, the density and viscosity in Equation 4-1a should not be a constant value of a certain fluid, but a variable which can switch from the density or viscosity of one phase to that of the other phase. This is realized by

Equations 4-1b and 4-1c. In Equation 4-1b, μ_1 refers to viscosity of Fluid 1 and μ_2 refers to that of Fluid 2; V_f is the volume fraction of Fluid 2; μ is the resultant viscosity, which is a variable; it can be either the viscosity of Fluid 1 or Fluid 2 according the fluid type.

$$\rho\frac{\partial \boldsymbol{u}}{\partial t}+\rho(\boldsymbol{u}\cdot\nabla\boldsymbol{u})=\nabla\cdot[-p\boldsymbol{I}+\mu(\nabla\boldsymbol{u}+\nabla\boldsymbol{u}^{T})]+\boldsymbol{F}_{st}+\boldsymbol{F}_{g} \tag{4-1a}$$

$$\mu=\mu_1+(\mu_2-\mu_1)V_f \tag{4-1b}$$

$$\rho=\rho_1+(\rho_2-\rho_1)V_f \tag{4-1c}$$

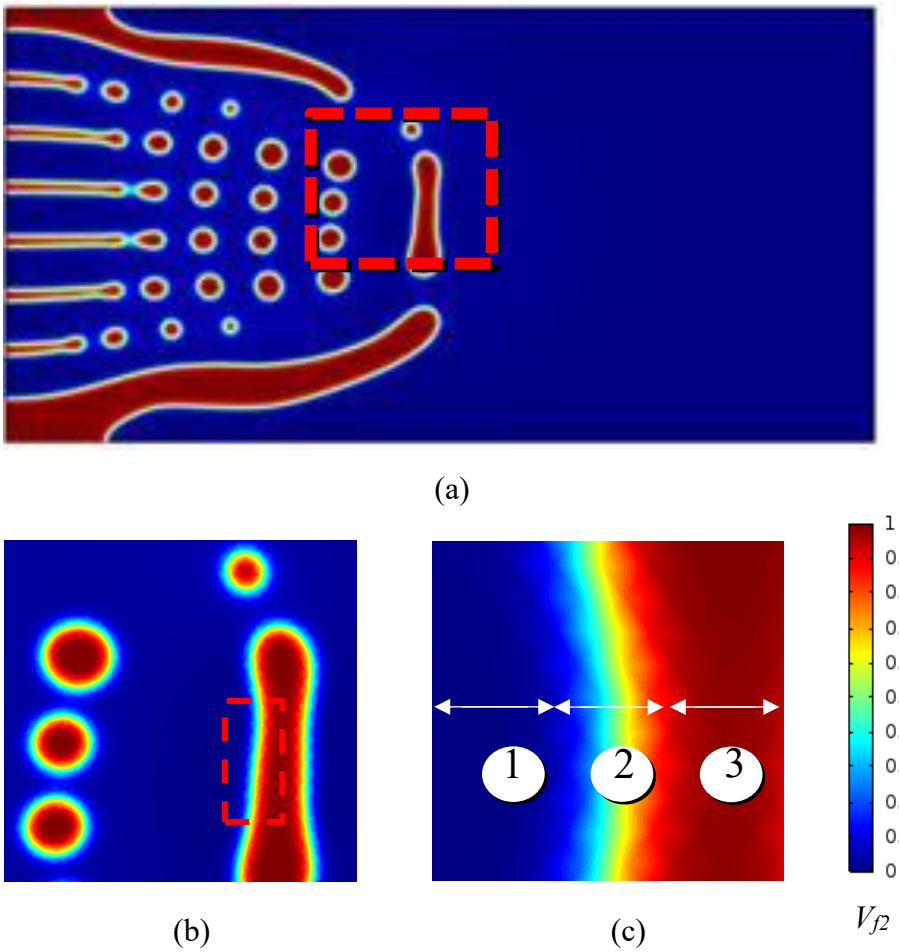

(a)

(b) (c)

Fig. 4-1 A case of the distribution of two phases in level set method (The value of V_{f2})

Fig. 4-1 shows an example of the distribution of two phases in a simulation with level-set method. The color indicates the value of V_{f2}, namely the fraction of Fluid 2. It accordingly also indicates the phase type. The blue parts refer to Fluid 1, namely V_{f2} is 0; while the red parts refer to Fluid 2, namely V_{f2} is 1. By expanding Fig. 4-1a to Fig. 4-2b

and further to Fig. 4-2c, the structure of two phases and their interface can be clearly shown. In Fig. 4-1c, Area 1 refers to Fluid 1, Area 3 refers to Fluid 2, while Area 2 refers to the interface between these two fluids where the value of V_{f2} changes gradually from 0 to 1.

$$\frac{\partial \varphi}{\partial t} + \nabla(\varphi \cdot \boldsymbol{u}) = \gamma \nabla \cdot [\varepsilon \nabla \varphi - \varphi(1-\varphi)\frac{\nabla \varphi}{|\nabla \varphi|}] \tag{4-2}$$

Equation 4-2 is an auxiliary equation to the Navier-Stokes equation. The fluid phase is tracked by this equation with the critical variable φ-the level set variable. In the level set method, φ ranges from 0 to 1. The fluid will be Fluid 1 when φ is 0; the fluid will be Fluid 2 when φ is 1; the fluid will be the interface of the two fluids when $0<\varphi<1$. Consequently, φ is identical to the fraction of Fluid 2, namely $\varphi = V_{f2}$. The level set variable is directly related to the variation of fluid properties--density and viscosity, as shown in Table 4-1; in this way φ is used to track the fluid type. γ is the reinitialization parameter. It determines the amount of reinitialization or stabilization of the level set function. ε is a controlling parameter which regulates the thickness of the region where φ varies from 0 to 1, namely it is the interface thickness. Generally, ε can be assigned as the half of the largest mesh size. The value of φ in Equation 4-2 will be imported to the density, viscosity and capillary pressure in Equation 4-1, while the value of $\boldsymbol{u}$ in Equation 4-1 will be imported to Equation 4-2; in this way, Equations 4-1 and 4-2 are coupled with each other. The flow of two phases can be tracked.

Table 4-1 Relationship between level set variable, fluid type and physical properties

Level set variable	Fraction of Fluid 1	Viscosity	Density	Type of fluid
$\varphi=0$	$V_f=0$	$\mu=\mu_1$	$\rho=\rho_1$	Fluid 1
$0<\varphi<1$	$0<V_f<1$	within $\mu_1 \sim \mu_2$	within $\rho_1 \sim \rho_2$	Interface
$\varphi=1$	$V_f=1$	$\mu=\mu_2$	$\rho=\rho_2$	Fluid 2

4.1.2 Derivation of the 2D model of level set method

In COMSOL Multiphysics, the default equation for calculating fluid transport in the level set method is the Navier-Stokes equation. However, the Navier-Stokes equation is

used for calculating the fluid flow in 3D space and the calculation load is too heavy for an ordinary computer. Therefore, in this chapter, we would like to simulate two-phase flow in a single fracture with a 2D numerical model in order to reduce the computation load. Consequently, the fluid transport equation-Equation 4-1 is replaced with the Reynolds equation [Watanabe et al, 2015], which is the 2D form of Darcy's law. It is shown in Equation 4-3, in which b is the fracture aperture, P is the pressure, μ is the viscosity. This equation is only valid on the assumption that the flow is slow enough that the flow nonlinearity (inertial effect) can be neglected.

$$\nabla \cdot [\frac{b^3}{12\mu} \nabla P] = 0 \tag{4-3}$$

$$P_c = \frac{2\gamma \cdot \cos\alpha}{b} \tag{4-4}$$

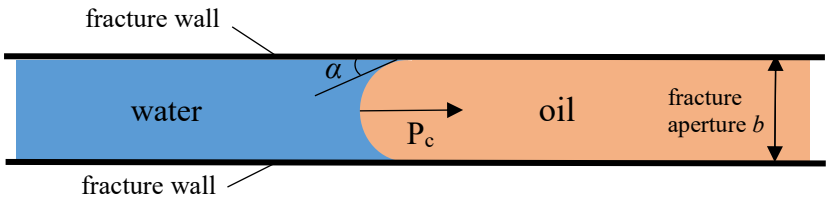

(a) Capillary pressure in a 1D case

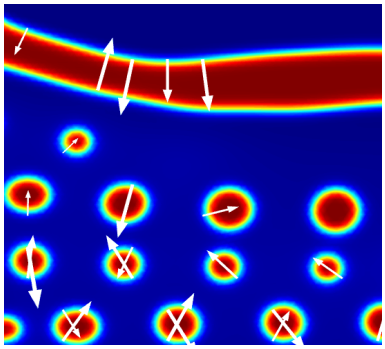

(b) Direction of the capillary pressure in a 2D case

Fig. 4-2 Schematic of the capillary pressure

Equation 4-3 is the original form of Reynolds equation for single-phase flow. In two-phase in fractures or porous media, there is an additional term--the capillary pressure. Watanabe et al [2015] included the term of capillary pressure into the Reynolds equation. Generally, the capillary pressure between the wetting and non-wetting phase is given as

Equation 4-4. γ is the surface tension between wetting phase and non-wetting phase; α is the contact angle between the fracture wall and the wetting phase meniscus, as shown in Fig. 4-2(a). Both γ and α are constant in this model, while b is a variable which depends on the location in the fracture surface.

In this study, a similar method is adopted, in which the capillary pressure is expressed as a volumetric force $\boldsymbol{F_{st}}$, as shown in Equation 4-5. Equation 4-5 is the two-dimensional form of Equation 4-4, in which $\boldsymbol{n}$ is the normal direction of the phase interface, as shown by the arrows in Fig. 4-2b. $G = \varphi(1-\varphi)$, which is an auxiliary term for discrimination. The effect of G is to ensure that the capillary pressure only exists in the interface, namely in either Phase 1 ($\varphi = 0$) or Phase 2 ($\varphi = 1$), G is zero and accordingly $\boldsymbol{F_{st}}$ is zero, too. This is simplified from the CFD modules of COMSOL Multiphysics, in which the capillary pressure has a term of $|\nabla\varphi||\varphi(1-\varphi)|$ for specifying the interface [Comsol, 2011].

$$\boldsymbol{F}_{st} = \frac{2\gamma \cdot \cos\alpha}{b} G \cdot \boldsymbol{n} \tag{4-5}$$

$$\nabla \cdot [\frac{b^3}{12\mu}(\nabla P + \boldsymbol{F}_{st}] = 0 \tag{4-6}$$

Strictly speaking, the values of φ in the phase of Fluid 1 or Fluid 2 are not strictly 0 or 1 in the Level set method, because there is an diffusion term in Equation 4-2; in addition, in order to have a good convergence for numerical calculation, sometimes the thickness of the interface is too thick, as shown in Fig. 4-3a. Since the values fluid properties are all the function of φ, such as the viscosity and density (Equation 4-1), the accuracy of the φ values will have a significant influence on the fluid transport calculation. In order to

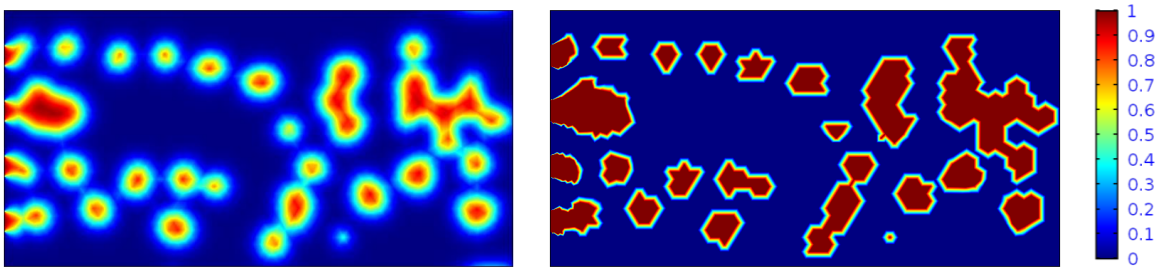

(a) Original phase distribution (φ) (b) Phase distribution after smooth processing

Fig. 4-3 Smoothing processing

resolve this, the values of φ are processed with a smoothing function to reduce the areas with a φ value within 0~1, namely the interface areas. The phase distribution after smooth processing is shown as Fig. 4-3b. It shows that the phase interfaces become more clear the interface thickness is controlled into a reasonable value.

4.2 Model description

4.2.1 Geometry and boundary conditions

In this chapter, the simulation was conducted on two series of fractures, named as Model 1 and Model 2 respectively. Both series of the fractures are automatically generated. The fracture in Model 1 is generated with the spatial frequency generation method, while the fractures in Model 2 are generated with the normal distribution method. The geometry of the numerical models is shown as Fig. 4-4. The width is 100 mm. The length is 200 mm for Model 1 and 300 mm for Model 2. The upper and lower boundaries are set as no flow conditions. Both water and oil are injected from the left boundary. Five water inlets and four oil inlets are arranged alternatively. Both water and oil are injected with constant velocities. Both fluids flow out from the right boundary, namely the outlet. The outlet is assigned with a constant pressure of 0 Pa.

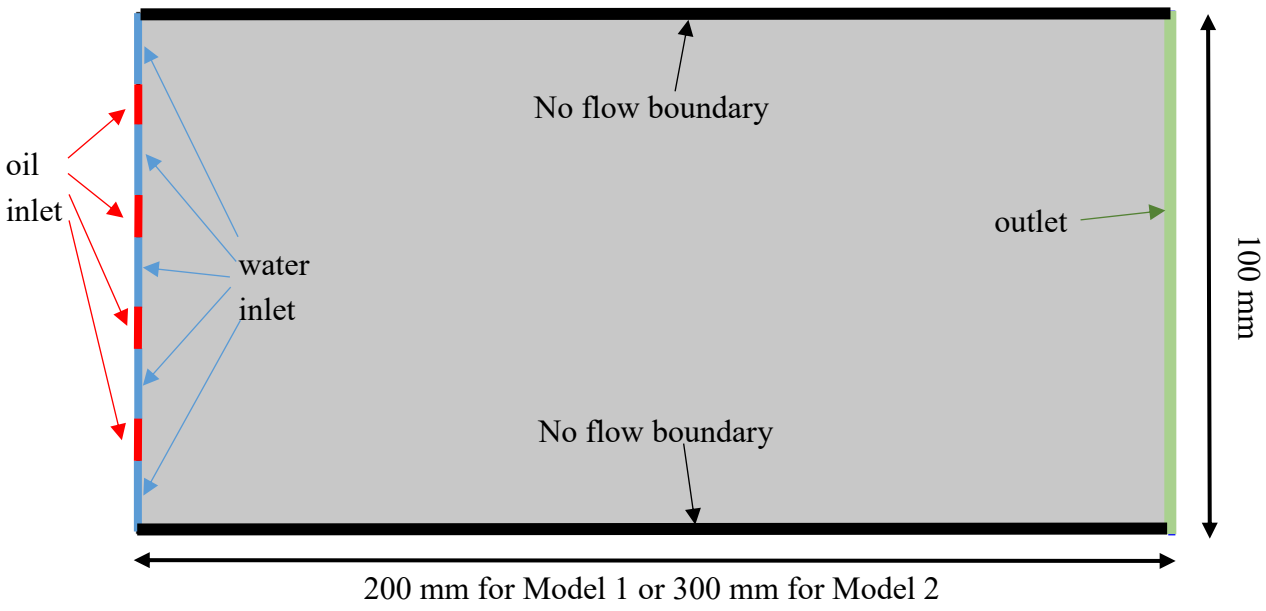

Fig. 4-4 Geometry of the numerical models

The domain is initially saturated with water, and the initial pressure is 0 Pa. The injection velocities of both water and oil are gradually increased from 0 to a stable value with the Heaviside function, in order to improve the convergence of calculation.

Since this is a 2D model, the fracture aperture b is assigned as a parameter on each point. In Model 1, the fracture aperture is a randomly rough surface, which is generated with the spatial-frequency method. In this method, the randomly rough surface is synthesized with a sum of trigonometric functions [Sjodin, 2017]. This method is similar to the Fourier series method. Here we introduce the method.

4.2.2 The randomly rough surface generated with the spatial-frequency series

In many physical problems, such the electromagnetic wave propagation, the oscillation frequency is a critical parameter. Different oscillation frequencies form different kinds of electromagnetic waves, such as infrared rays, visible light and ultraviolet rays. Sinusoid wave is a kind of electromagnetic wave, in which both the magnetic field and electric field evolve as the sinusoidal function with respect to time and space, as shown in Fig. 4-5. This evolution can be described by the cosine function as $\cos(2\pi ft)$ or $\cos(2\pi fx)$, in which f is the frequency. The former indicates the evolution with respect to time while the later indicates the evolution with respect to space.

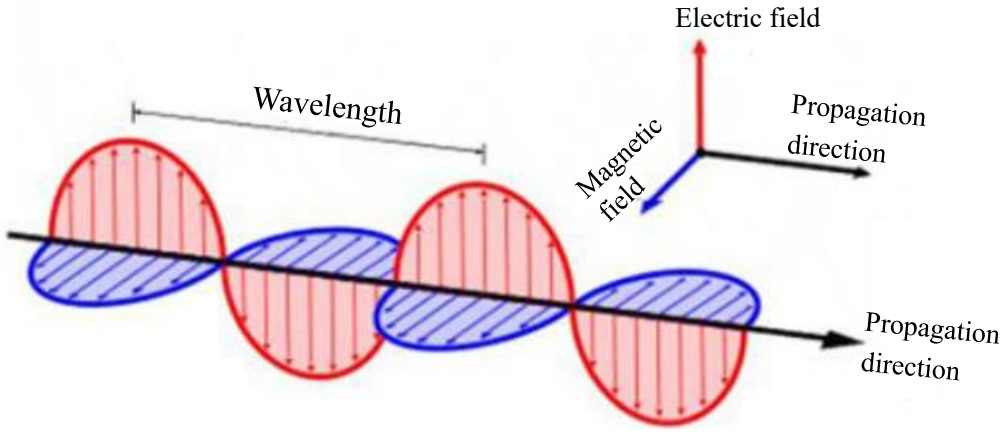

Fig. 4-5 The propagation of a sinusoidal electromagnetic wave

As is known, any curve can be constituted by a sum of Fourier series. A randomly rough surface can be regarded as to be composed of a series of fundamental waves as $\cos(2\pi fx+\phi)$, in which ϕ is the phase angle. If ϕ is a uniform random variable, the

surface will have randomness. In all, $\cos(2\pi fx+\phi)$ represents the spatial oscillation with a certain frequency for each value of f; a large f represents the high-frequency spatial oscillation, while a small f represents the low-frequency spatial oscillation. The sum of all the spatial oscillation functions will constitute a random curve.

$$f(x)=\sum_{m} A_m \cdot \cos(2\pi mx+\phi) \tag{4-7a}$$

$$f(x)=\sum_{m,n} A_{m,n} \cdot \cos[2\pi(mx+ny)+\phi] \tag{4-7b}$$

Equation 4-7a shows the oscillation function series, which can generate a 1D randomly rough curve. x is the coordinate in the 1D system. Just by extending the coordinate system into a 2D system, it can be extended to the oscillation function series for a 2D randomly rough surface, as shown in Equation 4-7b. Here it should be noted that each spatial oscillation function has a corresponding amplitude A_m or A_{mn}. A_m or A_{mn} is a mark of the weight of each oscillation frequency. For a rough surface or curve, different distributions the weight (the amplitude A_m or A_{mn}) of each oscillation frequency will generate different roughness morphology. For natural fractures, the amplitude A_m or A_{mn} is not evenly distributed in each oscillation frequency, but low-frequency oscillations tend to have a larger amplitude A_m than the high-frequency oscillations. Consequently, A_m or A_{mn} shall not be uniformly distributed with respect to m and n. For a 2D natural surface, A_{mn} can be

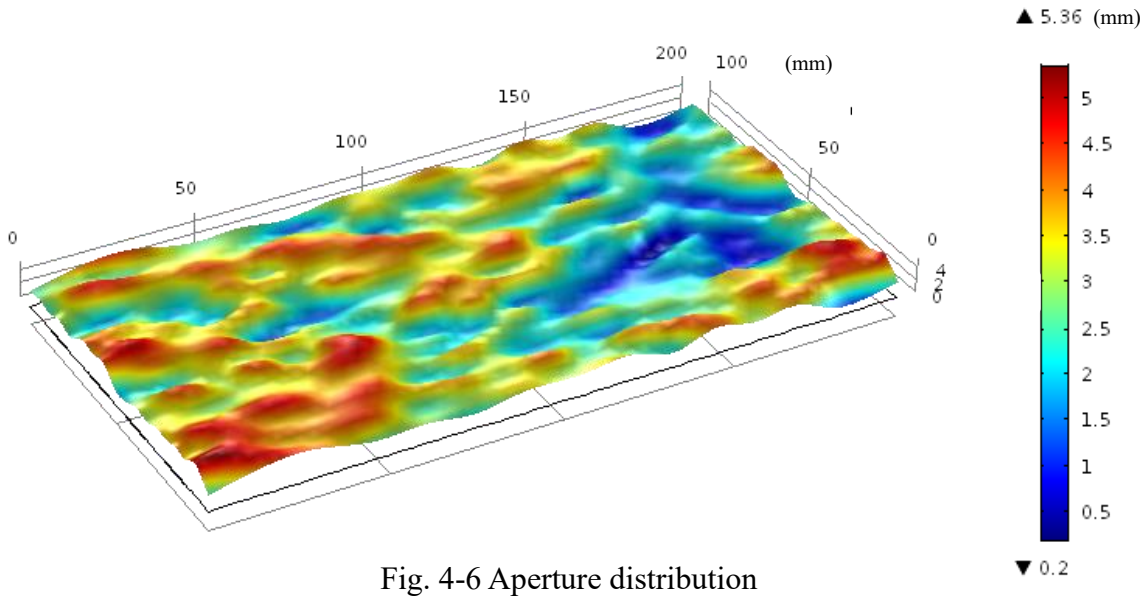

Fig. 4-6 Aperture distribution

adopted as $1/(m^2+n^2)^{\beta/2}$, so that the amplitude A_{mn} attenuates with respect to the increase

of m and n. β is a parameter that determines the morphology of the surface roughness, and it is correlated to the fractal dimension of the surface [Peitgen and Saupe, 2012].

With the above-mentioned method, a fracture is generated. β is assigned as 1, which generated the fracture roughness shown as Fig. 4-6. The irregularity in the figure shows the randomness of the fracture aperture. To clearly show the values of aperture, the fracture surface is colored. The color in the legend indicates the magnitude of fracture aperture. Red indicates a large value of aperture, while blue indicates a small value of aperture. The maximum aperture is 5.36 mm, while the minimum aperture is 0.2 mm. The areas with a small aperture (smaller than 2 mm) mainly concentrate in the right part, around the coordinate of (50, 150). This area would have larger capillary pressure according to Equation 4-5(a). The nonwetting phase is difficult to get into or pass these areas and the flow will be impeded, which is expected to add to the two-phase interference. This will be shown in the simulation results.

In Model 2, three series of fractures are generated, and the aperture of each fracture follows a normal distribution. The three series of fractures have an average aperture (μ) of 0.6 mm, 1.1 mm and 2.1 mm, respectively. In each series, there are four fractures and they have a standard deviation (σ) of 0.5, 1, 1.5, 2, respectively, in order to investigate the effect of different aperture distributions on the hydraulic characteristics of water-oil two-phase flow.

4.3 Evolution of the flow structures and relative permeability

4.3.1 The role of capillary pressure on the two-phase flow

In Model 1, the simulation is conducted at five water injection velocities and five oil injection velocities, including 20 mm/s, 50 mm/s, 100 mm/s, 200 mm/s, Consequently, there are 25 cases. The role of capillary pressure is investigated by analyzing the evolution of flow structures and the relative permeability.

Fig. 4-7 shows the flow structures and the velocity distribution when *Or* (oil injection velocity) is 20 mm/s. *Wr* (water injection velocity) ranges at 20 mm/s, 100 mm/s, and 500 mm/s. The phase distribution is shown in the pictures in the left column, in which the red or bright-colored speckles are oil, while the blue speckles are water. It's clear that the flow structures show some similarity to the two-phase flow in conduit. Since the oil injection rate is small as 20 mm/s, the oil phase is discontinuous and bubble flow is

formed. With the increase of water injection rate, the oil bubbles become smaller.

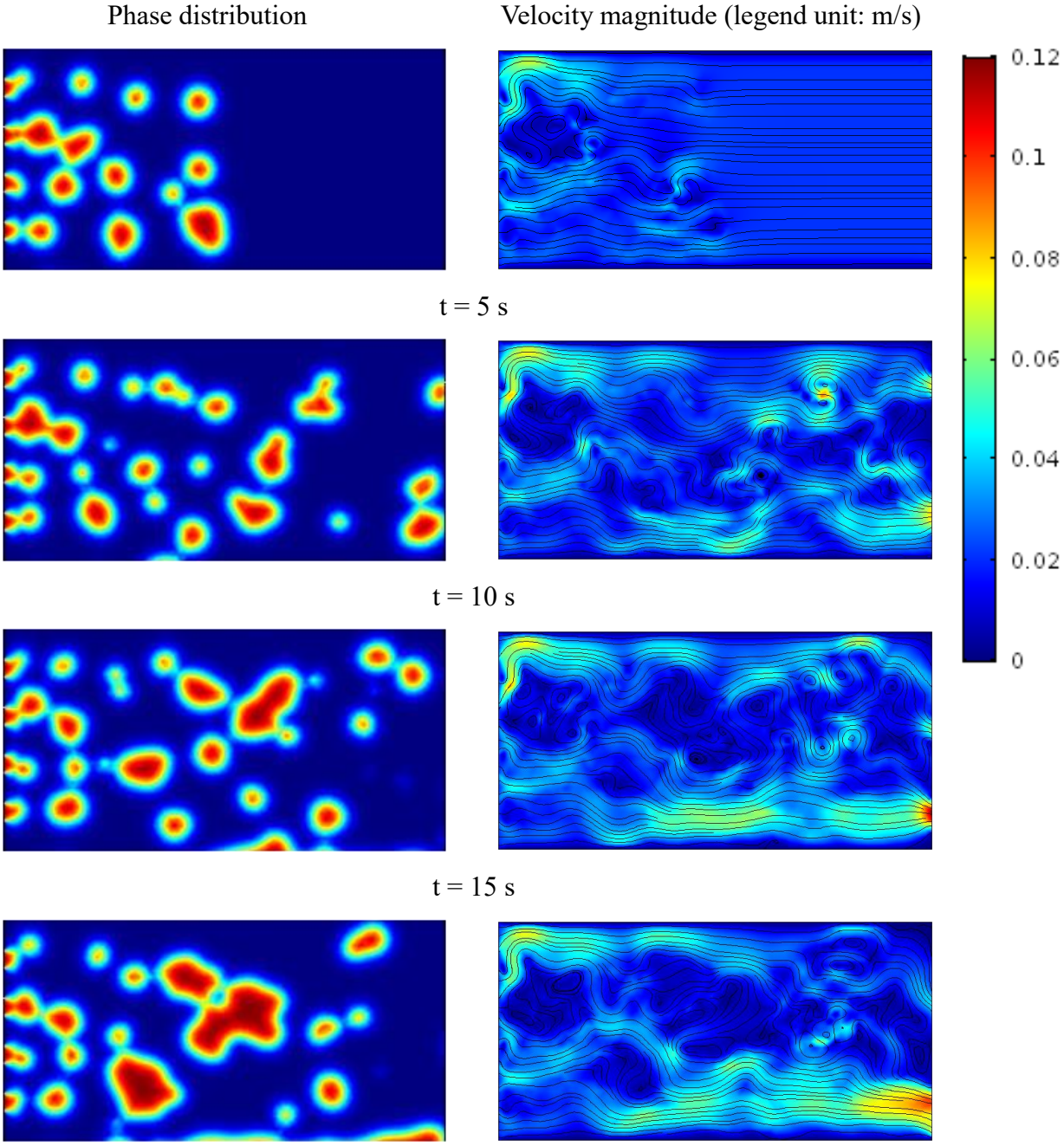

(a) *Wr* = 20 mm/s, *Or* = 20 mm/s

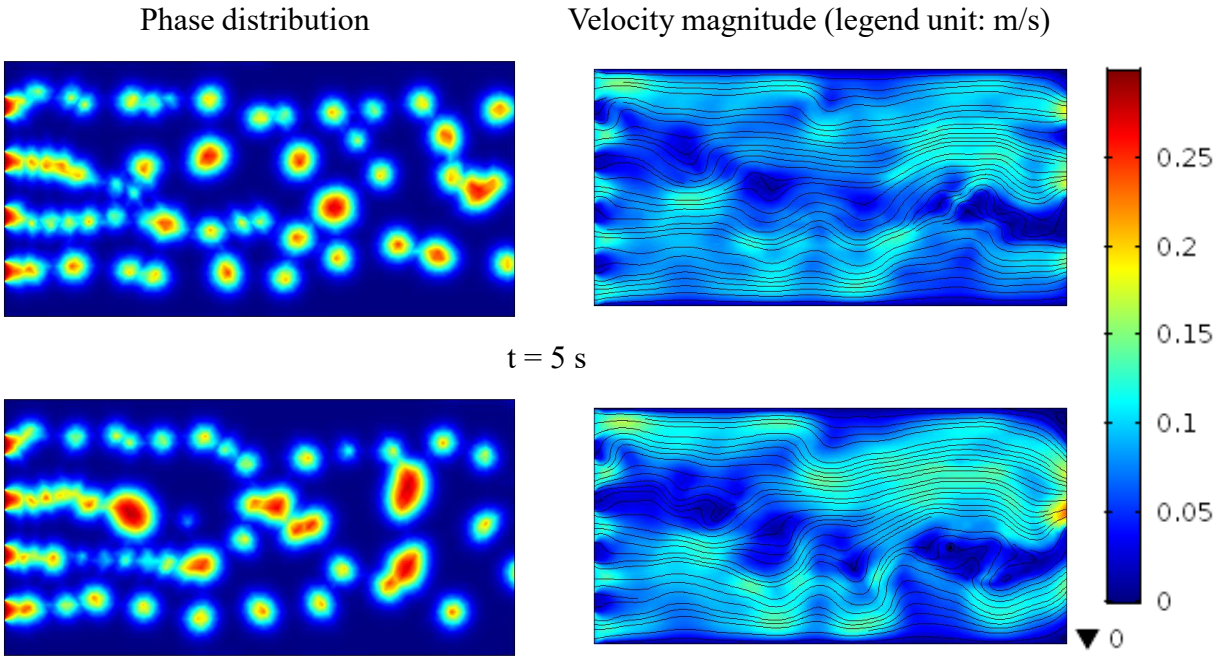

(b) *Wr* = 100 mm/s, *Or* = 20 mm/s

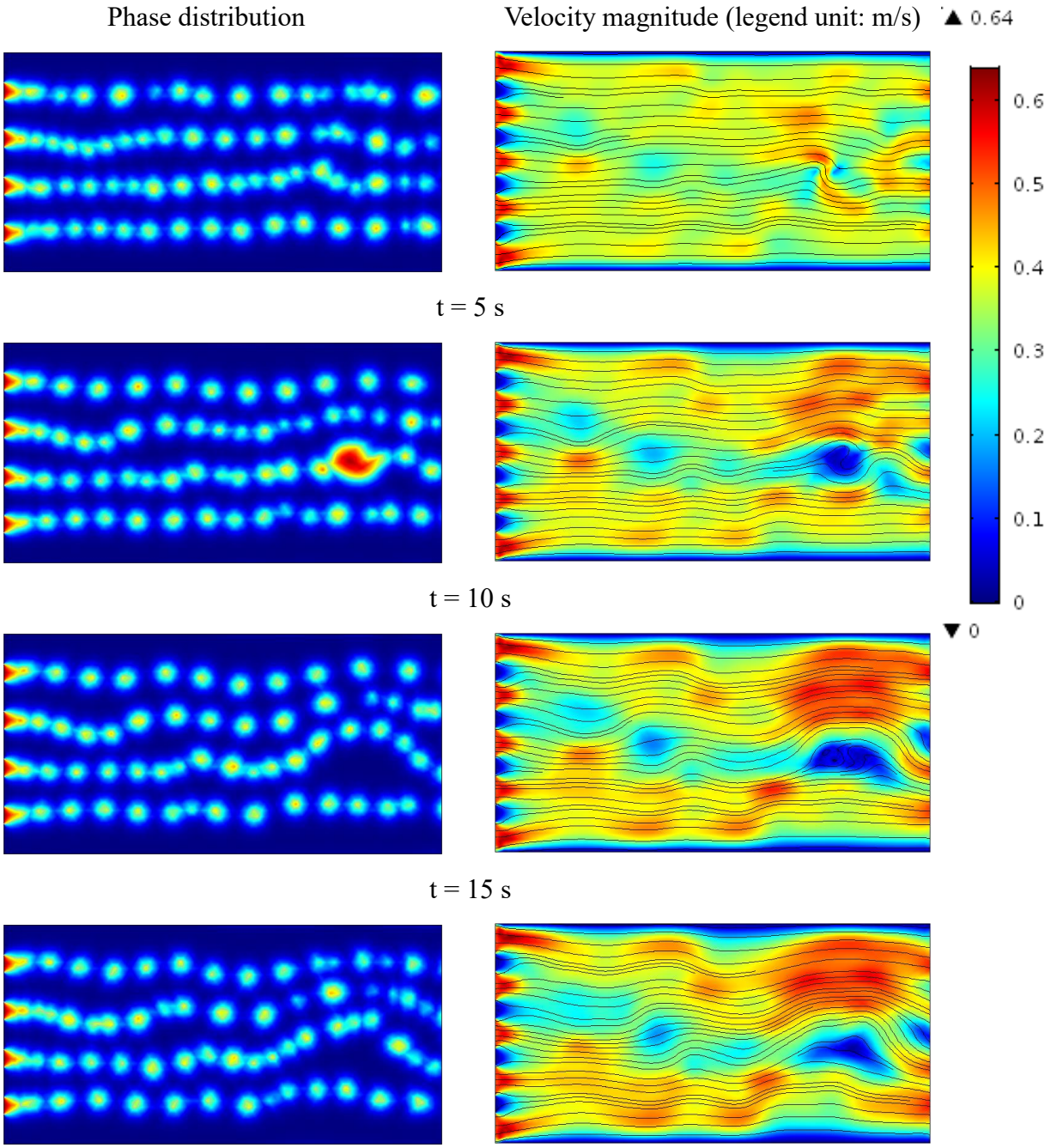

(c) *Wr* = 500 mm/s, *Or* = 20 mm/s

Fig. 4-7 The flow structures and velocity distribution in Model 1, *Or* = 20 mm/s

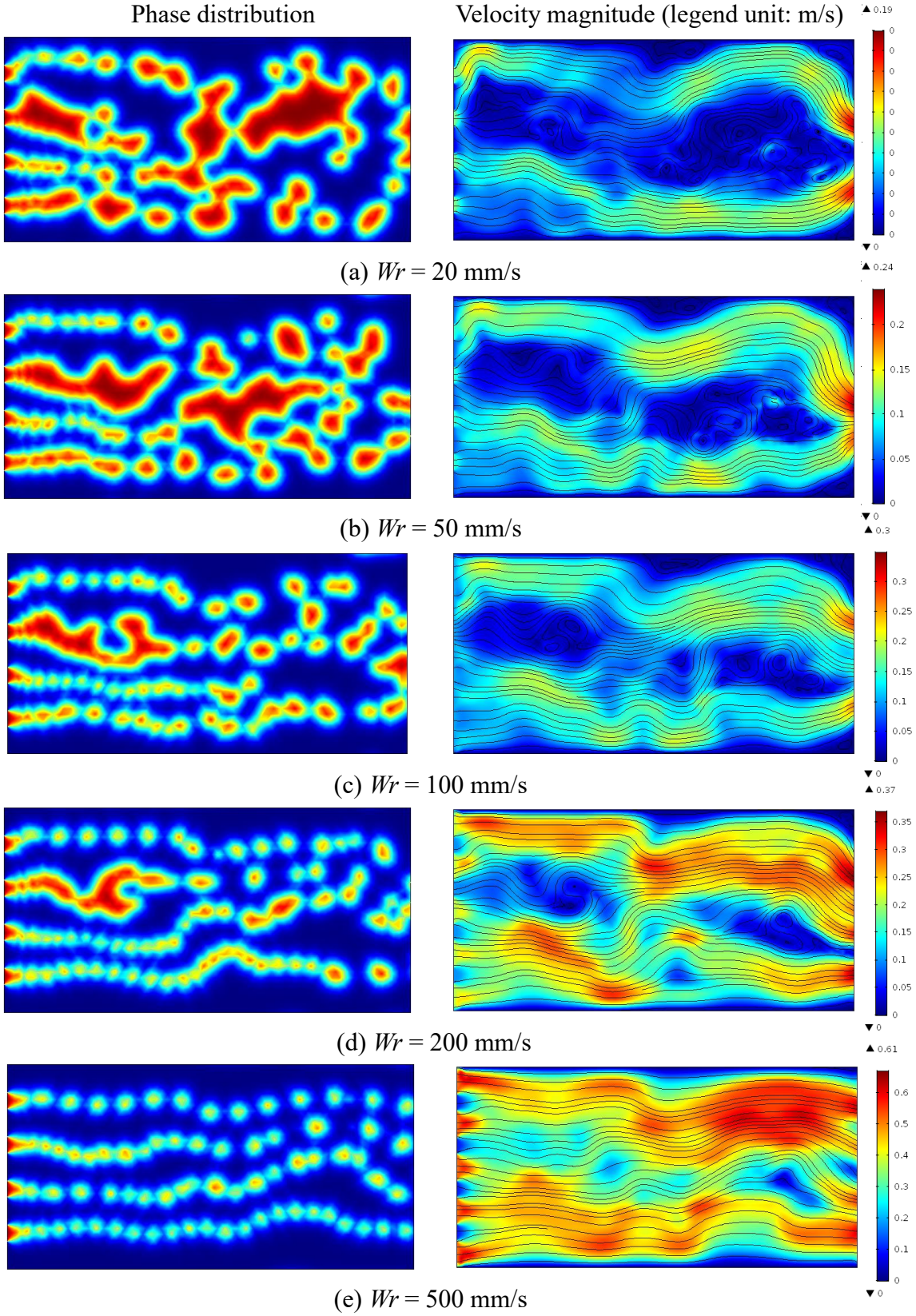

(a) *Wr* = 20 mm/s

(b) *Wr* = 50 mm/s

(c) *Wr* = 100 mm/s

(d) *Wr* = 200 mm/s

(e) *Wr* = 500 mm/s

Fig. 4-8 The flow structures and velocity distribution, *Or* = 100 mm/s

Phase distribution Velocity magnitude (unit: m/s)

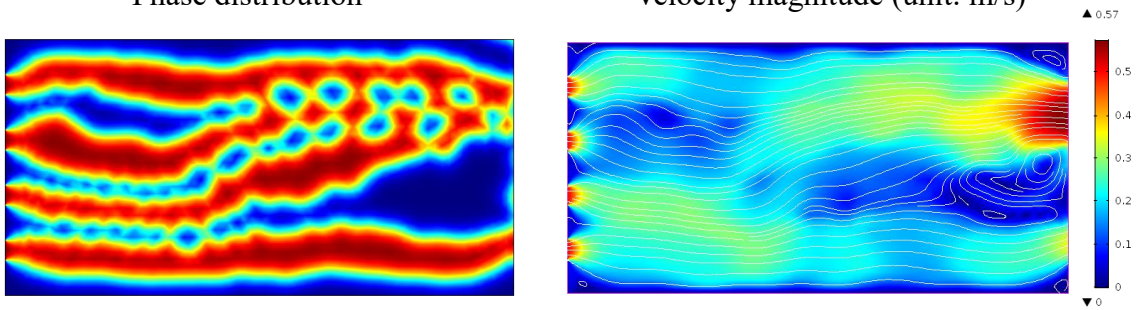

(a) *Wr* = 20 mm/s

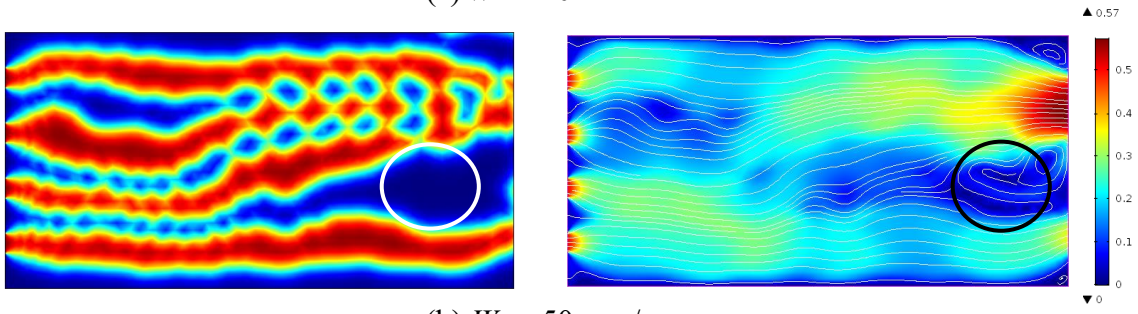

(b) *Wr* = 50 mm/s

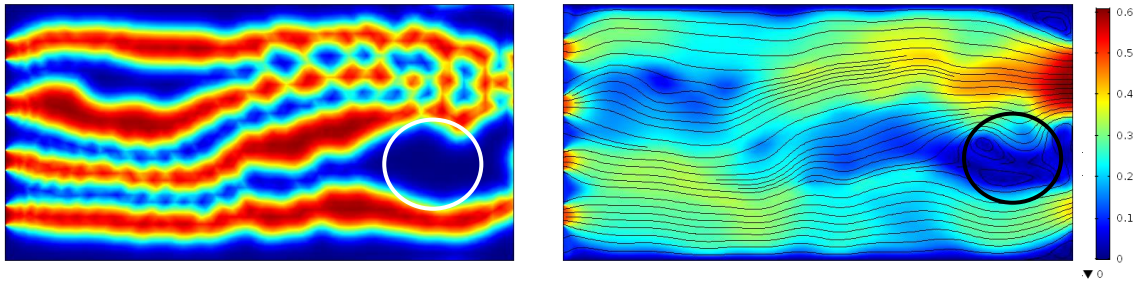

(c) *Wr* = 100 mm/s

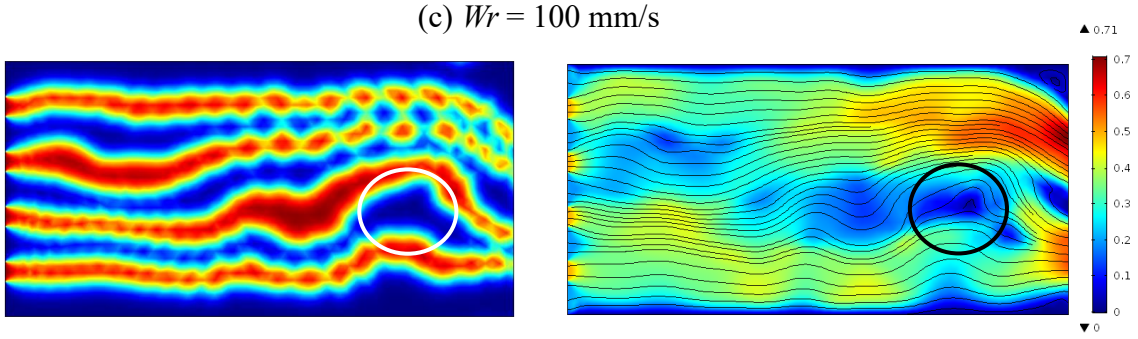

(d) *Wr* = 200 mm/s

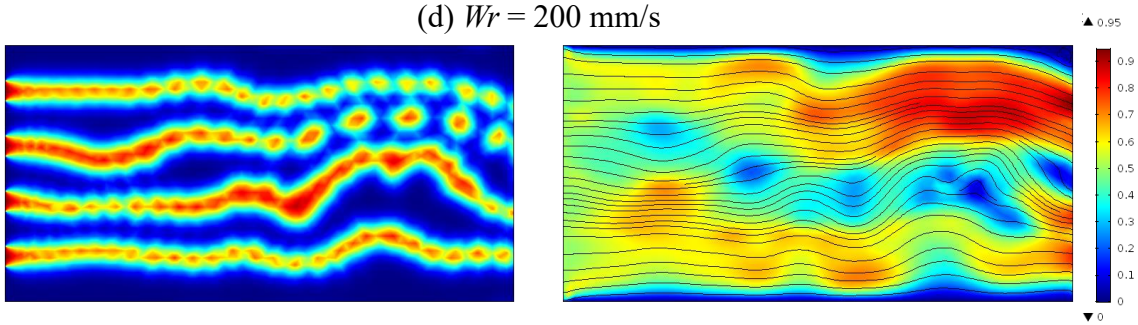

(e) *Wr* = 500 mm/s

Fig. 4-9 The flow structures and velocity distribution, *Or* = 500 mm/s

However, it also shows some characteristics of two-phase flow in porous media. In Figs. 4-7a, b and c, it's obvious that some oil bubbles are trapped and form larger bubbles, which is induced by the capillary force at the areas with a small aperture. In Fig. 4-7c, because the water flow velocity is large, the oil bubbles are more likely to be carried away by water, so oil bubbles are not likely to be trapped. In the circled area in Fig. 4-7c, it is obvious that the flow of some oil phase is redirected. This is induced by the large capillary pressure, which is induced by the small aperture in this area.

Figs. 4-8 and 4-9 show the flow structures and streamlines at different fluid ratios. At an oil injection rate of 100 mm/s, oil phase still flows as bubbles. More oil is trapped to become immobile phase when water is injected at small velocities, because the influence of capillary pressure is larger. When the oil injection rate reaches 500 mm/s, the oil phase becomes continuous, as shown in Fig. 4-9. Note that in the flow structure of continuous flow, the nonwetting phase (oil) still cannot flow into the area marked by the while circle, which is induced by the large capillary pressure on the two-phase interface in this area.

The pictures in the right column show the velocity distribution and streamlines at each gas and water injection velocities. The legends indicate the magnitudes of the velocities. Since the maximum velocity in each case is different, the legends at each water injection rate are respectively attached. It's obvious that at the circled areas, around the coordinate of (150,50), the magnitude of velocity is seriously slowed down compared with neighboring areas. This indicates that the flow of both phases is impeded by the large capillary pressure induced by small apertures in this area.

Compared with Fig. 4-8, the flow structures in Fig. 4-9 are much more stable. It can be found that the flow structures have little difference even though the water injection velocity changes from 20 mm/s to 500 mm/s. This phenomenon is quite similar to the two-phase flow in porous media: the wetting phase and nonwetting phase flow in their own channels respectively due to the influence of capillary pressure, which is induced by the difference of phase wettability. Here, we confirmed the reasonableness of the assumption made by Pruess and Tsang [1990], namely the fractures can be regarded as 2D porous media. The streamlines in the right column of Fig. 4-9 show that the flow velocity is quite small at the circled area, compared with the neighboring areas. This is also induced by the large capillary pressure in this area, which decreases the flow velocity and consequently forms significant interference between two phases.

4.3.2 Quantification of the evolution of saturation and relative permeability

Based on the analysis of the evolution of saturations, we conduct some quantitative analysis on the evolution of saturation and relative permeability. Firstly, the saturation should be calculated from the simulation results. The values of saturation are calculated based on the pictures which show the phase distribution. Since the red parts indicate the oil (φ=0) while the blue parts indicate water (φ=1), in principle, the area occupied by water can be calculated by integrating φ in the whole area. Then the water saturation can be calculated as the ratio between the area occupied by water and the total area (200 mm×100 mm). However, it should be noted that φ on the interface has a value within 0~1. Whether the area occupied by the interface should be included to the area of water or oil remains to be a problem. Here we define a variable T. When φ>0.5, T is 1; while $\varphi \leq 0.5$, T is 0. The area of water is calculated by integrating T in the whole domain.

Fig. 4-11 shows the evolution of the water saturation with respect to water injection rate and oil injection rate. Each individual curve represents the saturation values with a certain oil injection velocity. It shows that the water saturation increases with respect to the water injection flow rate, which is quite reasonable. However, the increase rate differs at different oil injection velocities. For an oil injection rate of 20 mm/s, the water saturation doesn't have obvious changes; while for the oil injection rate of 500 mm/min, the increase of water saturation with respect to water injection velocity is more remarkable. The difference in this increase rate is related to the flow structures. As shown in Fig. 4-7, at an oil injection velocity of 20 mm/s, oil flows as bubbles; Compared with the continuous flow of oil with an injection velocity of 500 mm/s (Fig. 4-9), the bubble flow state has more water-oil interfaces, which means the capillary force play a more important role. Consequently, in this bubble flow state, the flow of oil is retarded more seriously or even trapped as immobile phase. It can be concluded as that the influence of capillary pressure is larger in bubble flow state, the increased viscous force induced by increasing the water injection velocity would play a less role in the bubble flow state. Consequently, the saturation of oil would not have a significant change with respect to the increase of water injection velocity. To conclude, the saturation variation rate is dependent on the flow structures, because the influence of capillary pressure differs in different flow structures.

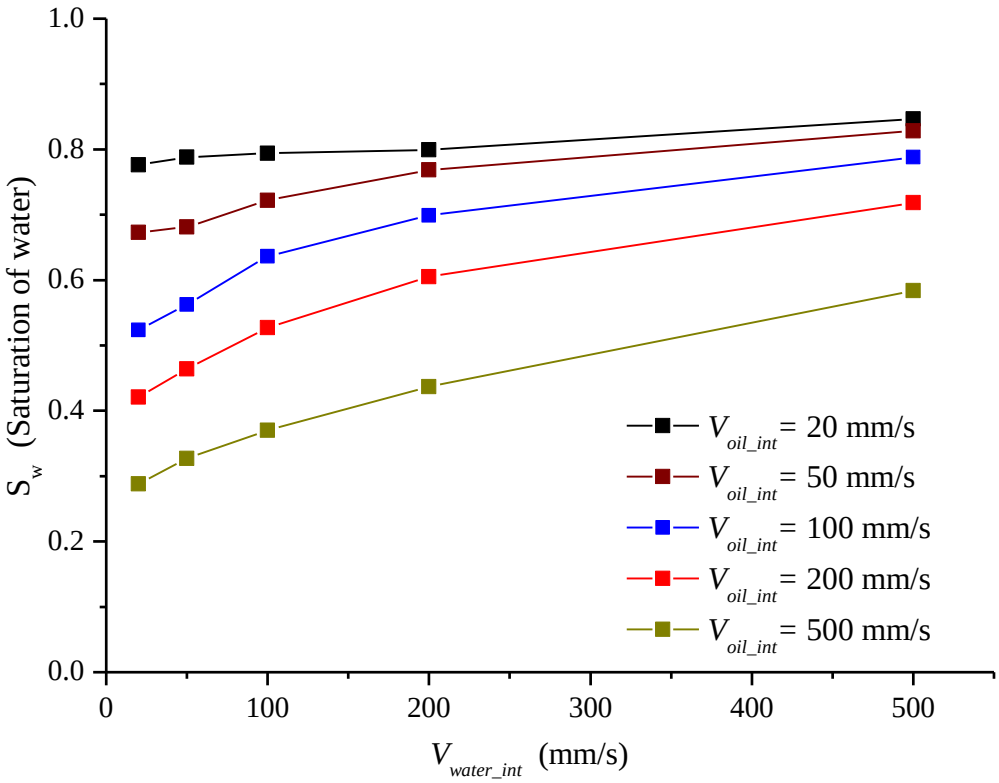

Fig. 4-11 Relationship between the water saturation and injection velocity of two fluids

The evolution of relative permeability with respect to water saturation is shown in Fig. 4-12. The three pairs of curves indicate X model, viscous model and Corey model, respectively. Each pair of curves contain a solid line and a dotted line, and they refer to the permeability of water and oil, respectively. The spots refer to the simulation results. Each group of spots indicate the relative permeability at the same oil injection velocity. The hollow spots refer to the results of water, while the solid spots refer to the results of oil.

As introduced in Chapter 2, Corey model describes the evolution of relative permeability in porous media or fractures when the capillary pressure dominates the flow. The simulation results show that the relative permeability of water follows the Corey model very well, especially when *Or* is 200 mm/s and 500 mm/s. It should be noted that different groups of data with different *Or* values don't fall on the same curve. This is reasonable because the relative permeability in Corey model is also the function residual saturation of nonwetting phase, as indicated by Equation 2-11. In Fig. 4-12, only one curve of Corey model with a certain residual saturation is shown. In our simulation, different flow rates form different flow structures, as shown in Figs. 4-7, 4-8 and 4-9. The

influence of capillary pressure in different flow structures is different. When *Or* is 20 mm/s, oil flows as bubbles; the influence of capillary pressure is significant since there are so many water-oil interfaces. Consequently, the residual saturations with different *Or* values are different from each other. When *Or* is 20 mm/s, both oil and water relative permeabilities are quite small, showing severe interference. With the increase of *Or*, both

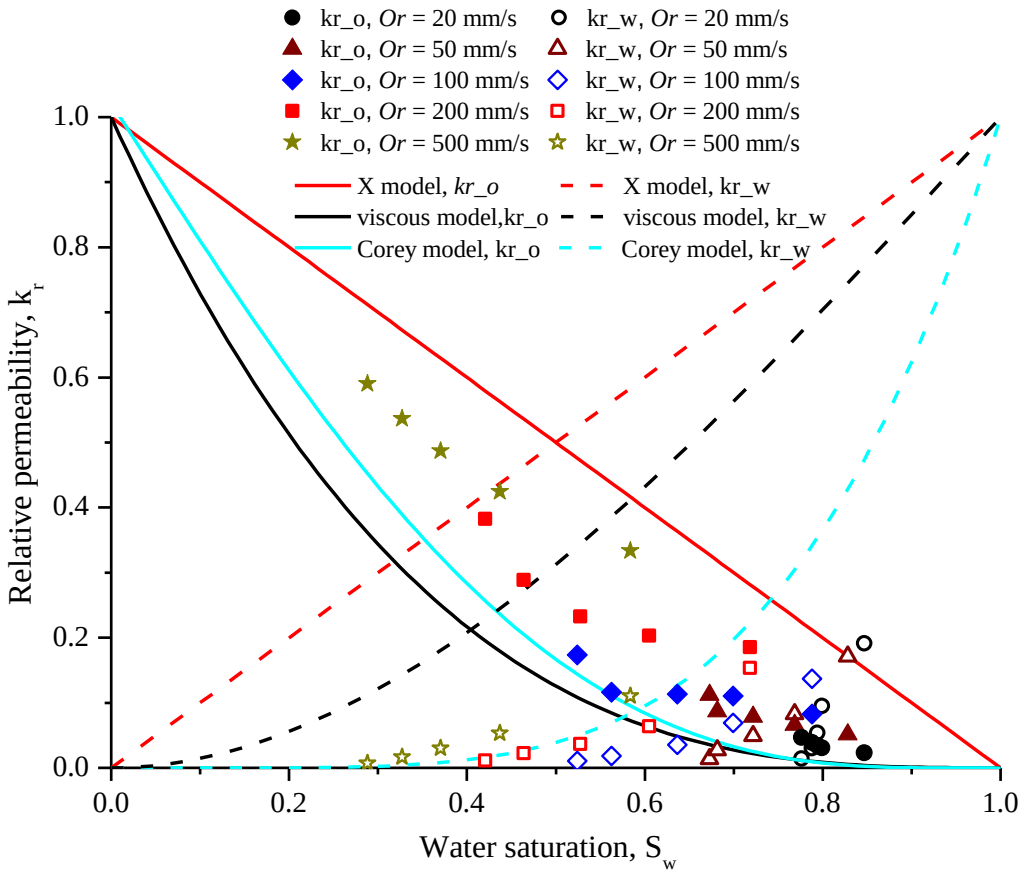

Fig. 4-12 The relationship between relative permeability and water saturation

the water and oil relative permeabilities increase, which indicates that the interference decreases; but each group of data follow the same evolution pattern—to increase nonlinearly as the Corey model.

As mentioned above, the flow structures at *Or* = 500 mm are most similar to that in porous media, meaning that both phases flow in their own channels, respectively. Previous studies indicate that in porous media, when both phases flow respectively in their own channels, the interference between two phases is least, and sometimes can even be neglected. In our simulation, we confirmed that this conclusion is also applicable to

the two-phase flow in fractures. As shown in Fig. 4-12, the flow at *Or* = 500 mm/s shows least phase interference.

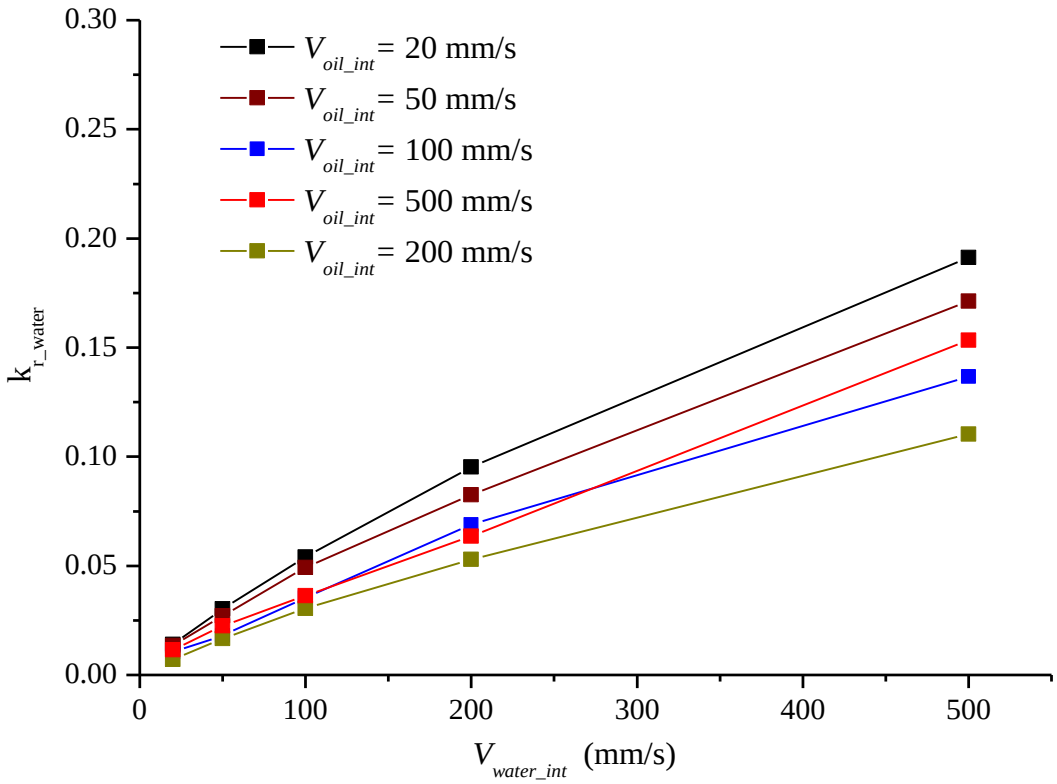

Fig. 4-13 The relationship between relative permeability of water and injection velocity

In engineering applications, the saturation of different phases cannot be directly observed. The classical models, which express the relative permeability as the function of saturation, is difficult to be adopted directly in applications. Consequently, the relationship between the relative permeability and the variables that can be measured in engineering applications should be established. Fig. 4-13 and Fig. 4-14 show the evolution of relative permeabilities of both phases with respect to water and oil velocities. The relative permeability of water increases nonlinear with respect to the water injection velocity, indicating that the phase interference cannot be neglected. In Fig. 4-14, the relative permeability of oil also decreases nonlinearly with respect to water injection velocity. The decrease rate of curves with different *Or* values is also different. As mentioned above, this is induced by different flow structures.

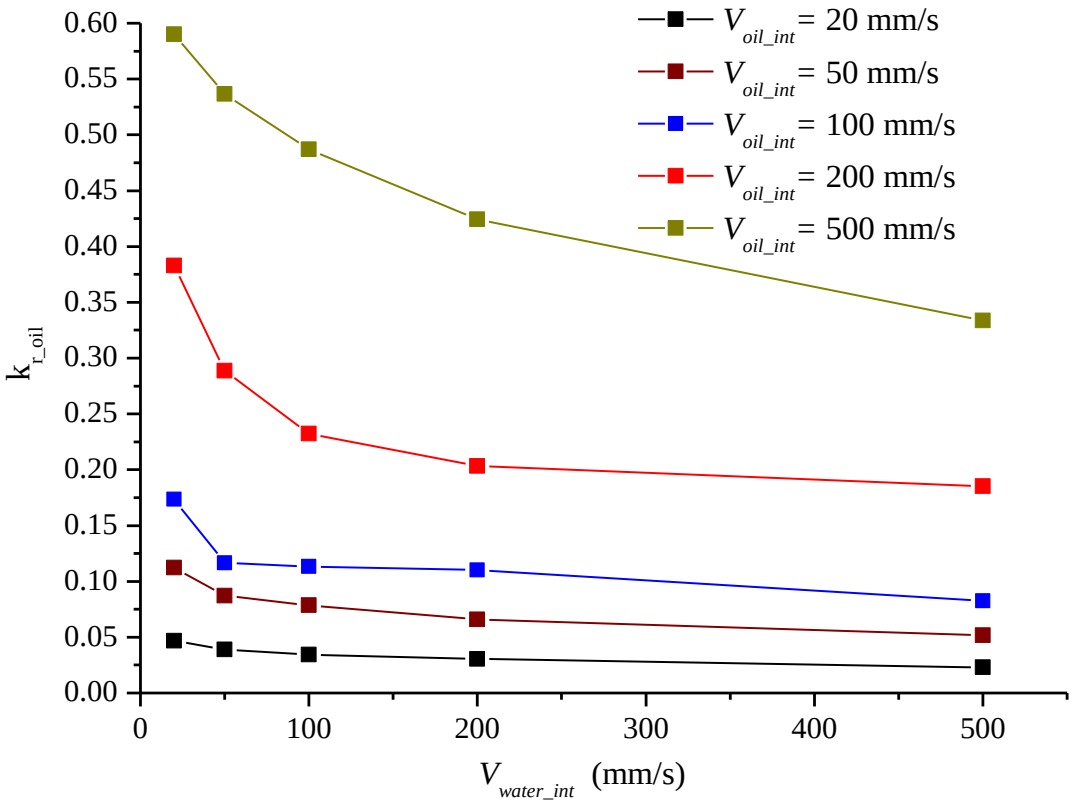

Fig. 4-14 The relationship between relative permeability of oil and injection velocity

4.3.3 The evolution of flow structures in normal distribution fractures

In this section, the simulation results on the fractures with a normal distribution in the aperture are given. Figs. 4-15, 4-16 and 4-17 show the flow structures in the fractures with an average aperture of 0.6 mm, 1.1 mm and 2.1 mm. All the pictures shown here are

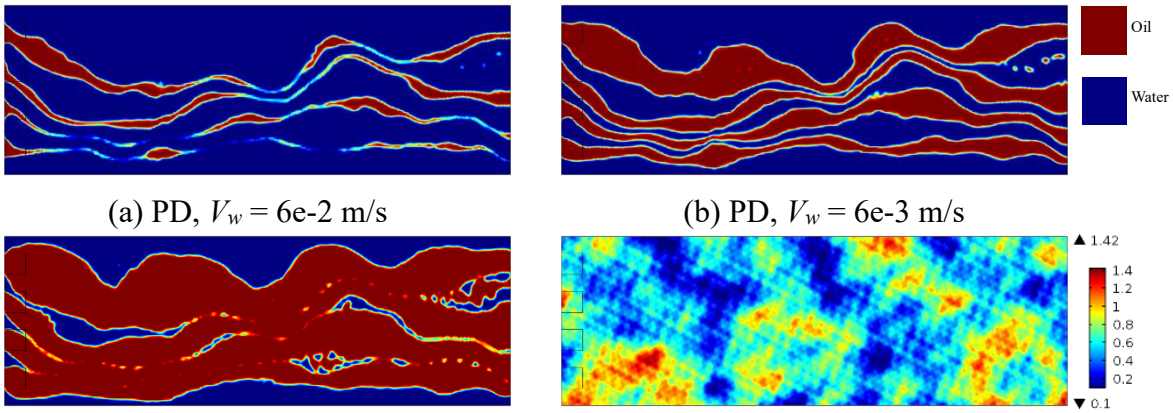

(a) PD, V_w = 6e-2 m/s (b) PD, V_w = 6e-3 m/s

(c) PD, V_w = 6e-4 m/s (d) AD (mm)

(I) μ = 0.5 mm, σ = 0.5

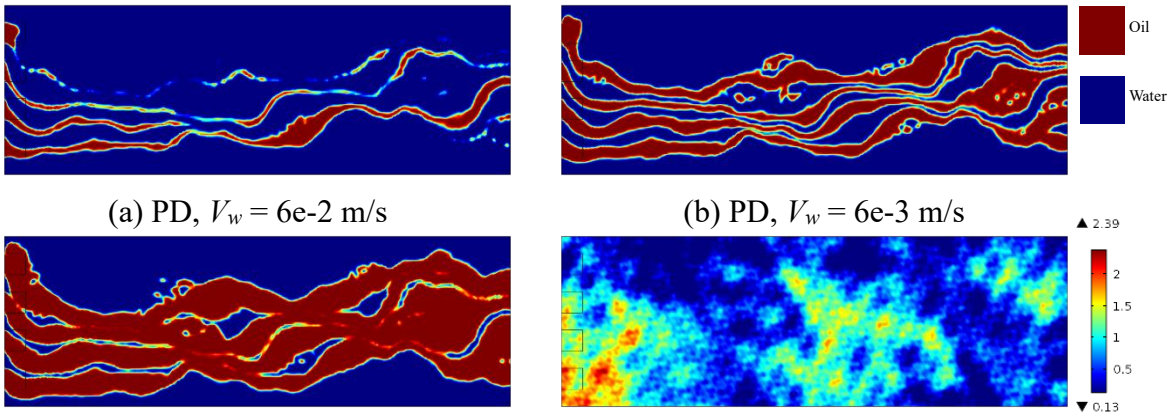

(a) PD, V_w = 6e-2 m/s (b) PD, V_w = 6e-3 m/s

(c) PD, V_w = 6e-4 m/s (d) AD (mm)

(II) μ = 0.5 mm, σ = 1

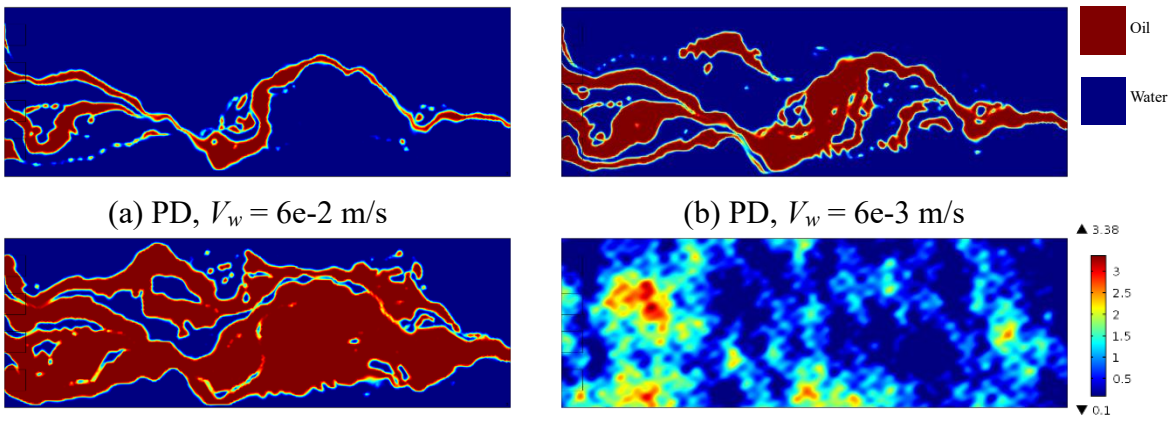

(a) PD, V_w = 6e-2 m/s (b) PD, V_w = 6e-3 m/s

(c) PD, V_w = 6e-4 m/s (d) AD (mm)

(III) μ = 0.5 mm, σ = 1.5

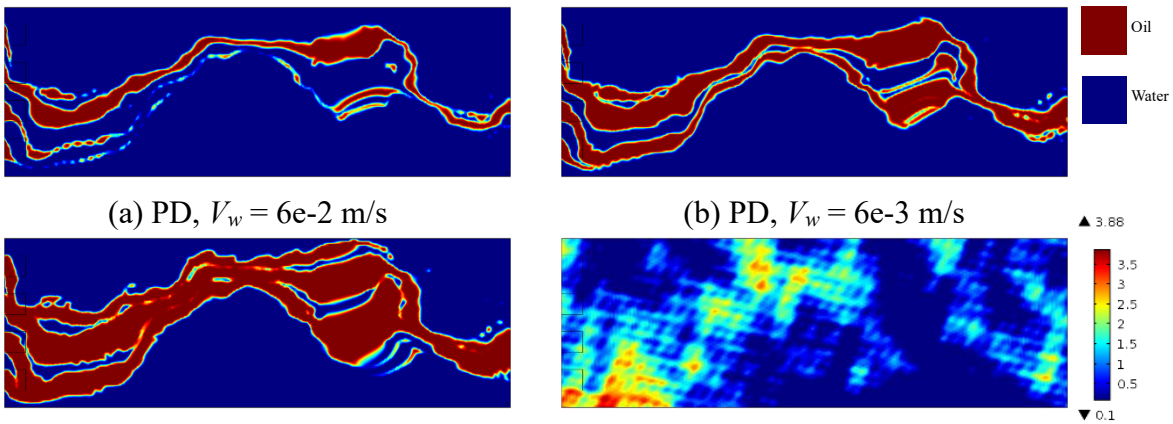

(a) PD, V_w = 6e-2 m/s (b) PD, V_w = 6e-3 m/s

(c) PD, V_w = 6e-4 m/s (d) AD (mm)

(IV) μ = 0.5 mm, σ = 2

Fig. 4-15 The phase distribution (PD) and aperture distribution (AD) of the fractures with an average aperture (μ) of 0.6 mm

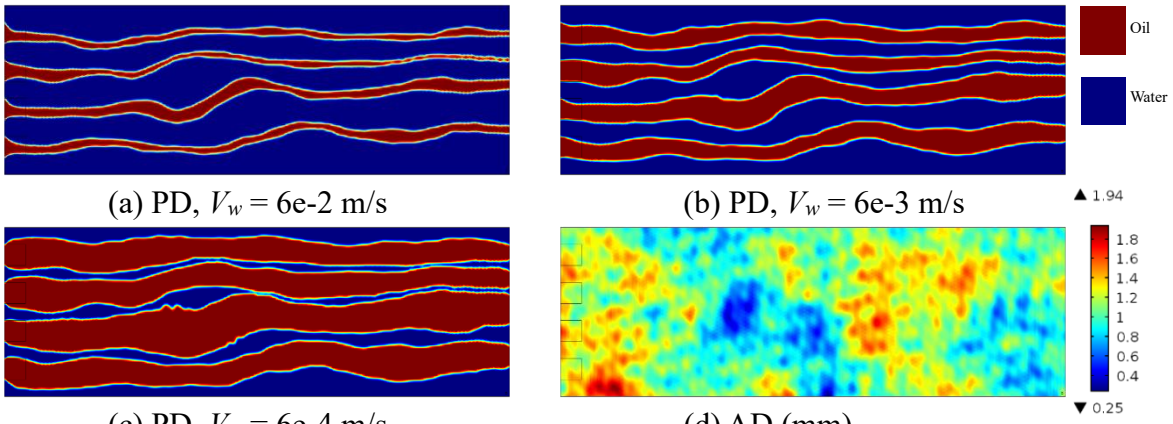

(a) PD, V_w = 6e-2 m/s (b) PD, V_w = 6e-3 m/s

(c) PD, V_w = 6e-4 m/s (d) AD (mm)

(I) μ = 1.1 mm, σ = 0.5

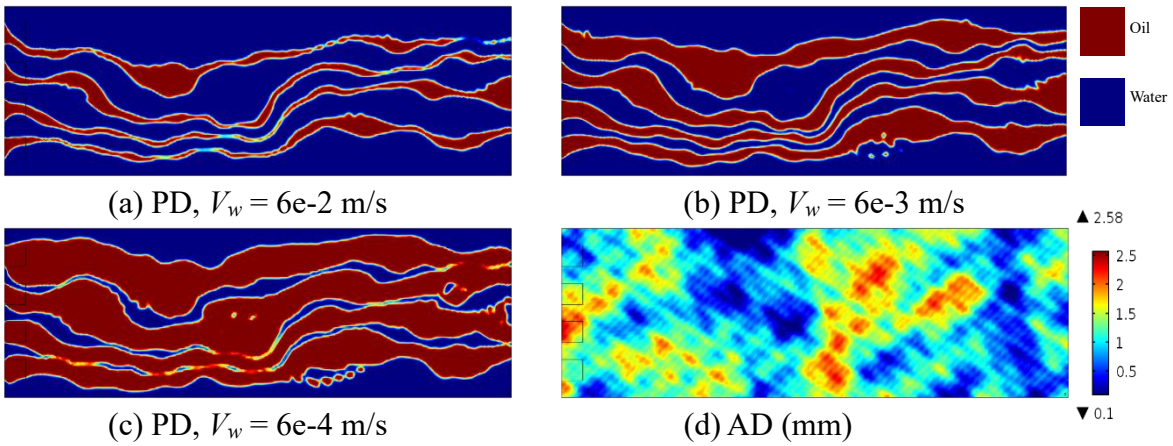

(a) PD, V_w = 6e-2 m/s (b) PD, V_w = 6e-3 m/s

(c) PD, V_w = 6e-4 m/s (d) AD (mm)

(II) μ = 1.1 mm, σ = 1.0

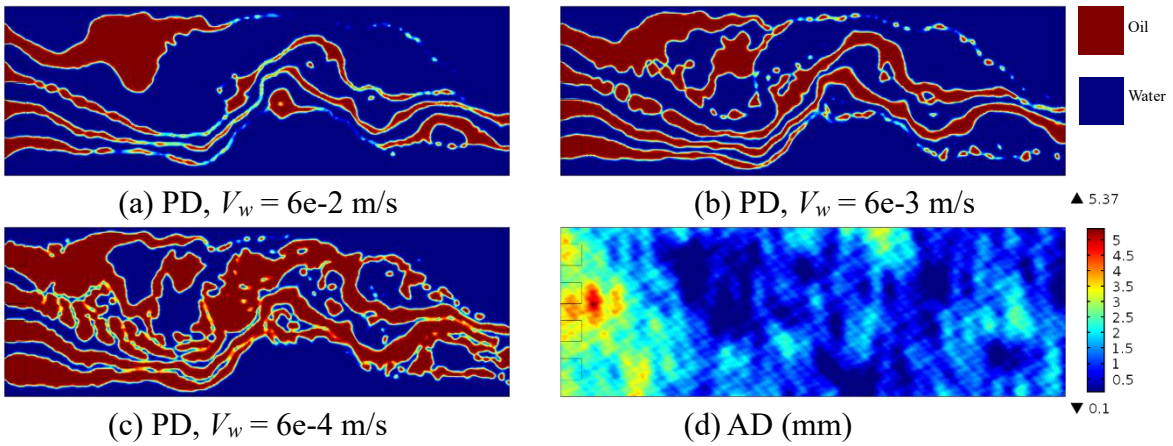

(a) PD, V_w = 6e-2 m/s (b) PD, V_w = 6e-3 m/s

(c) PD, V_w = 6e-4 m/s (d) AD (mm)

(III) μ = 1.1 mm, σ = 1.5

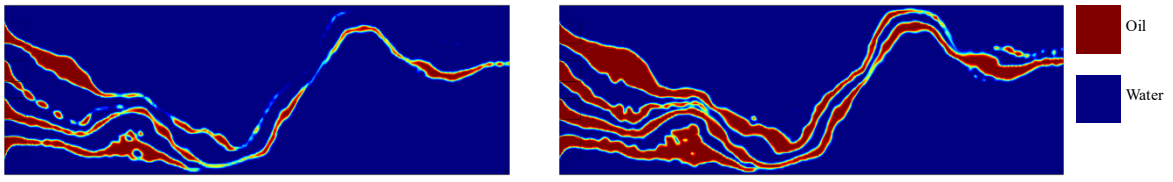

(a) PD, V_w = 6e-2 m/s (b) PD, V_w = 6e-3 m/s

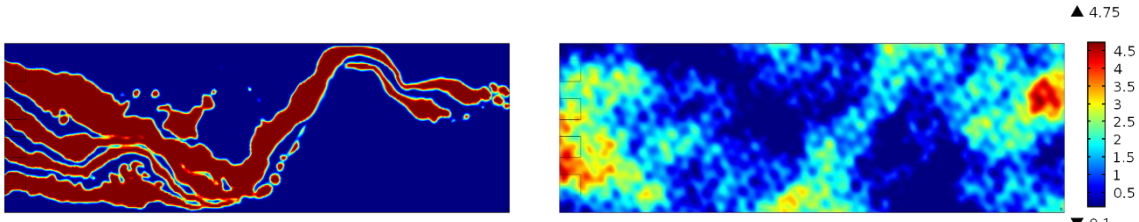

(c) PD, V_w = 6e-4 m/s (d) AD (mm)

(IV) μ = 1.1 mm, σ = 2.0

Fig. 4-16 The phase distribution (PD) and aperture distribution (AD) of the fractures with an average aperture (μ) of 1.1 mm

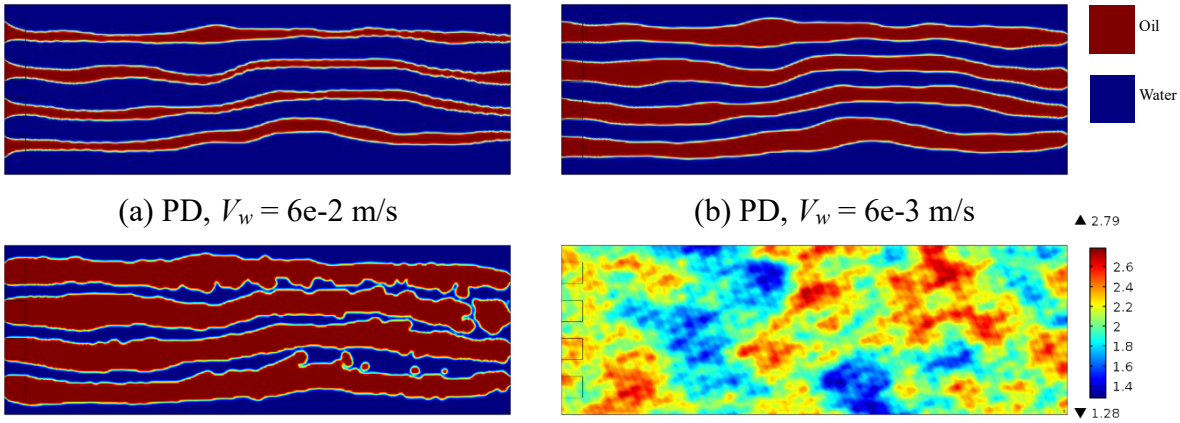

(a) PD, V_w = 6e-2 m/s (b) PD, V_w = 6e-3 m/s

(c) PD, V_w = 6e-4 m/s (d) AD (mm)

(I) μ = 2.1 mm, σ = 0.5

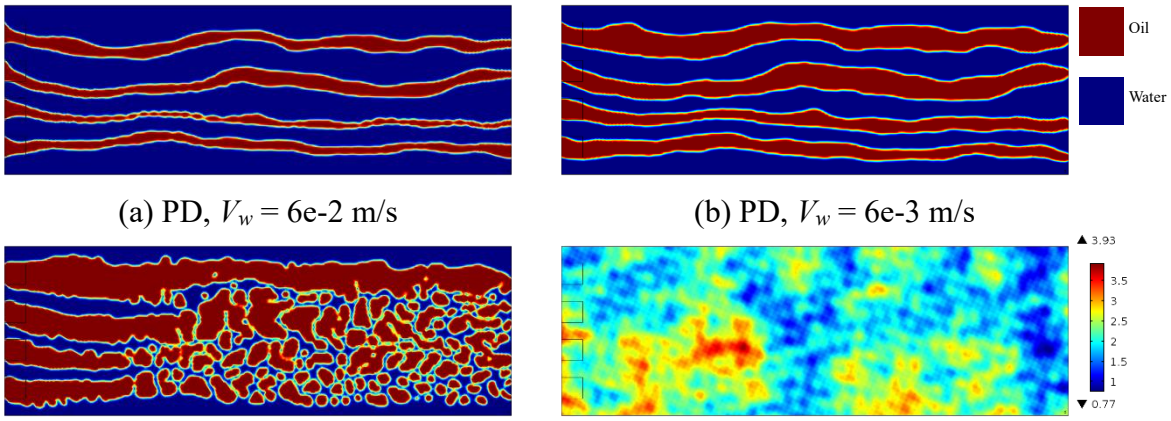

(a) PD, V_w = 6e-2 m/s (b) PD, V_w = 6e-3 m/s

(c) PD, V_w = 6e-4 m/s (d) AD (mm)

(II) μ = 2.1 mm, σ = 1.0

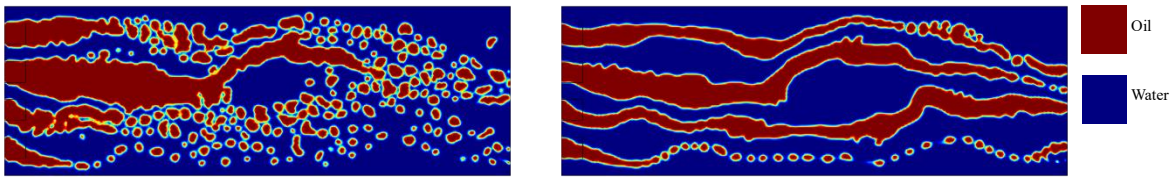

(a) PD, V_w = 6e-2 m/s (b) PD, V_w = 6e-3 m/s

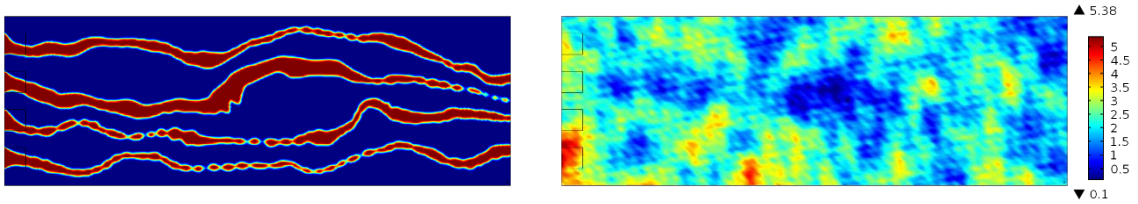

(c) PD, V_w = 6e-4 m/s (d) AD (mm)

(III) μ = 2.1 mm, σ = 1.5

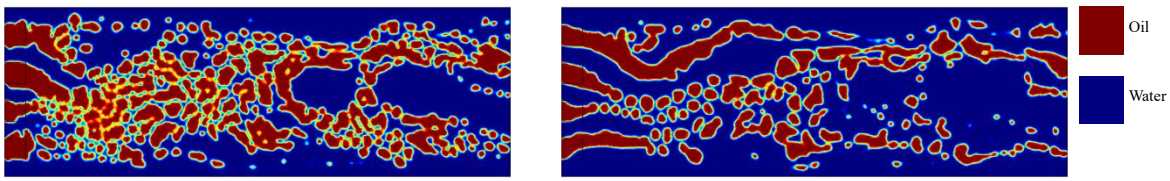

(a) PD, V_w = 6e-2 m/s (b) PD, V_w = 6e-3 m/s

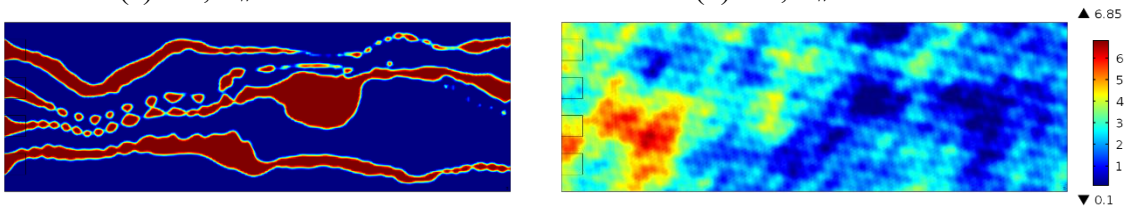

(c) PD, V_w = 6e-4 m/s (d) AD (mm)

(IV) μ = 2.1 mm, σ = 2.0

Fig. 4-17 The phase distribution (PD) and aperture distribution (AD) of the fractures with an average aperture (μ) of 2.1 mm

in the moment when the flow have reached a stable state, namely the saturation and flow channels does not have much variation. It clearly shows that with the increase the aperture standard deviation σ, the flow channels become more tortuous, which consequently add to the pressure drop in the flow process. In Fig. 4-16, in the case of σ = 0.5, the flow channels are regular and the channels are straight, which indicate less interference between phases. In the case of σ = 1.0, the channels tend to be kind of tortuous but both phases can flow without much channel invasion. In the case of σ = 1.5, the channels become chaotic and residual phase exist, which indicates that the capillary pressure becomes important. In the case of σ = 2, it is evident that the oil phase is restricted in the large-aperture areas due to the strong effect of capillary pressure. However, in Fig. 4-15, the flow channels are always tortuous due to the large capillary pressure induced by the small aperture of fractures. In Fig. 4-17, there is a transition from bubble flow to

continuous flow of oil phase, because the weight of capillary pressure has a significant change compare with the viscous force.

Figs 4-18, 4-19 and 4-20 show the evolution of relative permeabilities of water and oil with respect to the water saturation. The relative permeability is also influenced by the standard deviation (σ) of the fracture aperture. With the increase of σ, the relative permeability of water decreases; however, the relative permeability of oil sometimes increases. This may be because sometimes the capillary pressure can act as a drive force to its flow. In addition, the impact of capillary pressure differs in different flow structures due to the different quantities of phase interfaces. The effect of capillary pressure is more significant in bubble flow than in continuous flow. So if there is a transition of flow structures, the evolution of the relative permeability for oil may be more complex since the capillary pressure acts on the non-wetting phase (oil). In addition,

The results clearly indicate that the relative permeabilities of both phases are not only the function of saturation, but also the function of flow velocities and the aperture distributions (especially standard deviations).

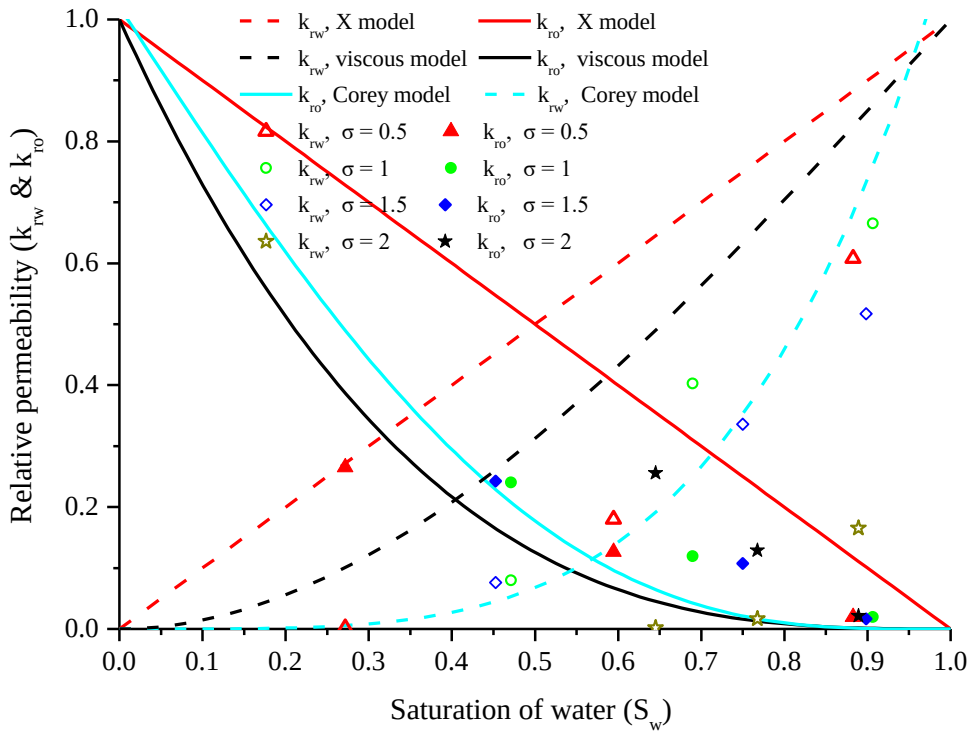

Fig. 4-18 The evolution of relative permeability with respect to water saturation in the fractures of μ = 0.5

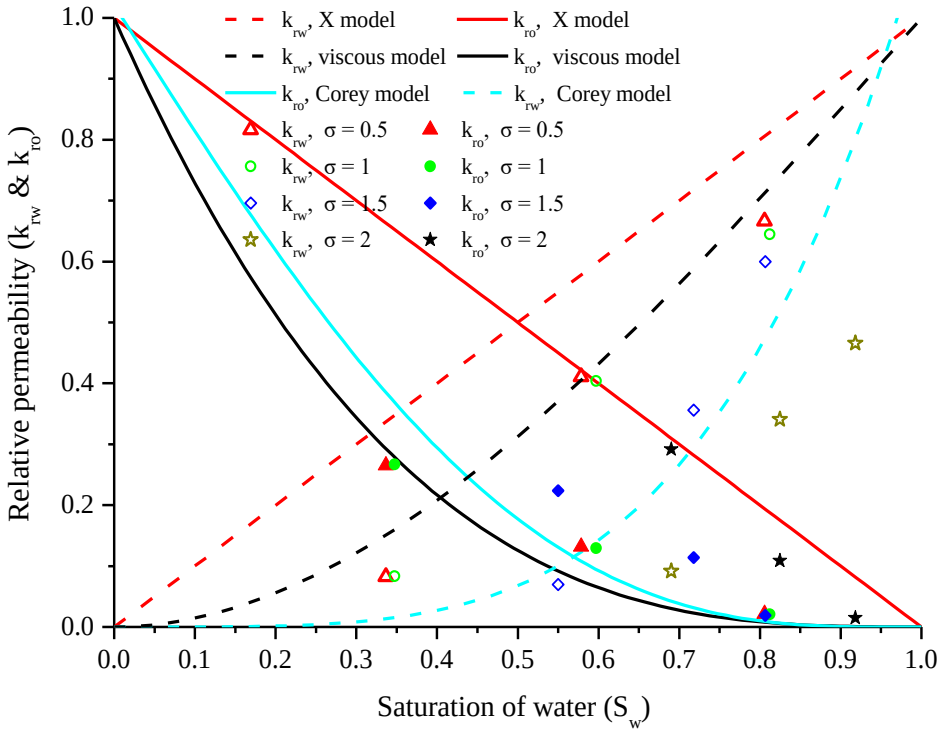

Fig. 4-19 The evolution of relative permeability with respect to water saturation in the fractures of μ = 1

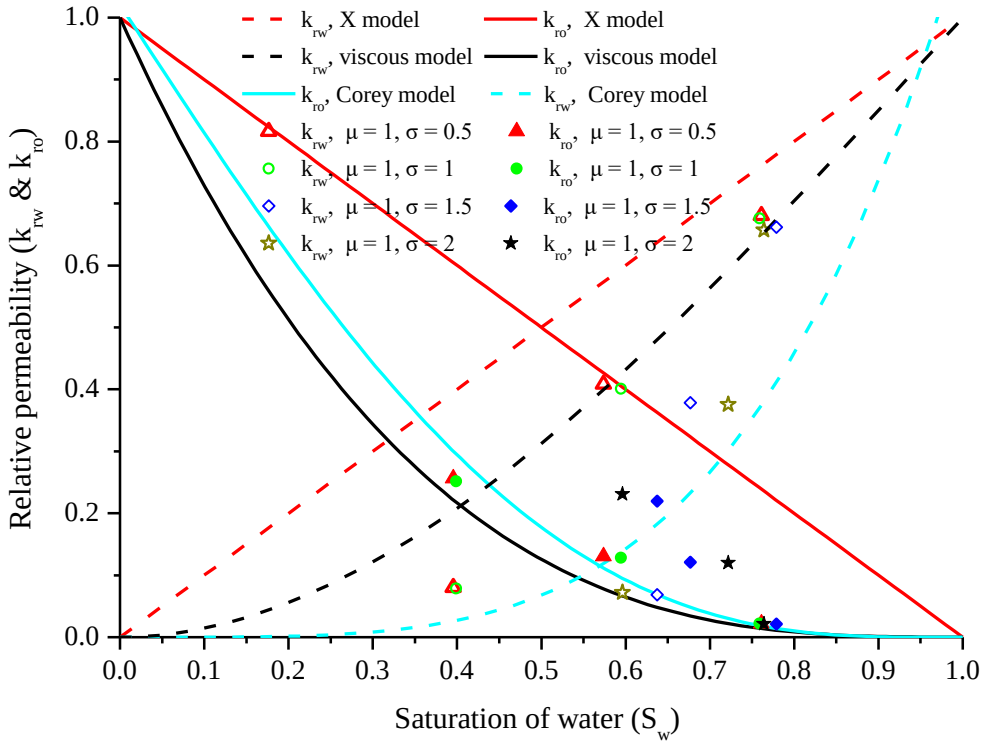

Fig. 4-20 The evolution of relative permeability with respect to water saturation in the fractures of μ = 2

4.4 Summary

In this chapter, a 2D numerical model is established for simulating two-phase flow in a single fracture. The role of capillary pressure is analyzed in two-phase flow in fractures. The evolution of saturation with respect to phase velocity is different, which depends on the flow structures. This is because the influence of capillary pressure differs in different flow structures; the impact of capillary pressure is more significant in bubble flow than in continuous flow.

The simulation results approximately fit with the Corey model. However, the relative permeabilities of both phases are not only the function of saturation, but also the function of flow velocities. This is because the influence of the capillary pressure is different at different flow structures. When both phases become continuous flow, they flow in their respective channels and show least phase interference, which is similar to the two-phase flow in porous media.

The flow structures are also correlated with the fracture morphology. With the increase of the standard deviation, the flow structure becomes more tortuous. The relative permeability is also influenced by the standard deviation of the fracture aperture. This is induced by two reasons: the tortuosity degree of the flow channels and the different effects of the capillary pressure. The flow tortuosity is influenced by the aperture distribution; the larger the standard deviation, the more tortuous the flow channels will be; while the influence of capillary pressure also increases with respect to the roughness of the fracture. In addition, the impact of capillary pressure differs in different flow structures due to the different quantities of phase interfaces. The effect of capillary pressure is more significant in bubble flow than in continuous flow. The relative permeabilities of both phases are not only the function of saturation, but also the function of flow velocities and the aperture distributions (especially standard deviations).

Chapter 5 Experimental study on the two-phase hydraulic properties in the intersecting fracture

In coalbed methane recovery, oil exploitation and geothermal resources utilization, the exploitation is always accompanied with a two-phase flow process in the fracture network. An intersecting fracture is an elementary unit of fracture network. Study on the two-phase flow characteristics in the intersecting fracture offers the basis of studying two-phase flow in fracture network. To quantitatively describe the hydraulic properties of two-phase flow in the intersecting-fracture, in this study, a gas-water two-phase flow experiment was conducted in a smooth 3D intersecting fracture model. The results show that: at a certain water flow rate, the two-phase pressure drop increases nonlinearly with respect to the gas flow rate, which shows kind of difference from previous results of the two-phase flow in rough single fractures. It is believed that this nonlinearity is induced by the strong inertial effect in the intersecting fracture. The Martinelli-Lockhart model is not only effective for describing the two-phase flow in single fractures, but also for the two-phase flow in intersecting fracture. Since the Martinelli-Lockhart model considers the inertial forces, which can't be neglected in the intersecting fracture, the good fitting results are obtained. This study provides basis for further investigation on the two-phase flow characteristics in the fracture network.

5.1 Introduction

Two-phase flow in the rock fracture network occurs in much subsurface space, such as natural gas-oil reservoirs, coal seams and geothermal energy reservoirs. The fluid-conducting capacity of the fracture network is the main concern in such engineering applications. Different from the single-phase flow, two-phase flow in the fracture is not only influenced by the intrinsic properties of fractures, such as the fracture roughness and aperture, but also the gas-water interactions (Corey, 1954; Dana and Skoczylas, 1999; Yang and Zhao, 2008). Two-phase flow in a single fracture is the first step to understand the flow characteristics in the fracture network, and the conventional approach to predict two-phase flow in a single fracture is to extend the Darcy's law for single-phase flow to a generalized Darcy's equation for two-phase flow [Chen, 2005; Watanabe, 2014] with a critical concept-the relative permeability, which is the parameter to measure the flow

interference between two phases. The researchers' main concerning is how the relative permeability evolves, and models are proposed to describe its evolution [Romm, 1966; Fourar and Bories, 1995; Corey, 1954].

In the subsurface, single fractures intersect with each other and constitute the fracture network. Studies on the single-phase flow indicate that fluid flow in the intersecting fractures shows quite different characteristics from that in a single fracture due to the energy loss and inertial effect induced by the fracture intersection [Liu et al, 2016]. Wilson and Withspoon [1976] studied the nonlinearity of fluid transport at the intersection of circular tubes with experiment, and their results indicate that the head loss induced by the intersection is about five times of the tube diameter when the Reynolds number is 100. Kosakowski and Berkowitz [1999] numerically investigated the hydraulic properties of the intersecting fractures with Navier-Stokes equation, and their results indicate that when Reynolds number is within 1~100, the inertial effect occurs and lead to nonlinear flow. Su and Zhan [1997] conducted water flow tests in crossed fractures and established the theoretical model for local loss of head at the intersection; they proposed the correction factor for the theoretical model. All the above-mentioned studies indicate that the hydraulic properties in the intersecting fractures have a nonlinearity and additional pressure drop, and Darcy's law is generally not effective in such situations.

However, the two-phase flow characteristics in the intersecting fractures are still not well understood. The generalized Darcy's equation is derived from the single-phase Darcy's law, which does not account for the nonlinearity of flow induced by the inertial effect or turbulence; this is to say, even though the flow interference between two phases are included in the term of relative permeability of the generalized Darcy's equation, the nonlinearity of two-phase flow, which cannot be neglected in the intersecting fractures, is still not well investigated. With an experimental study, this chapter presents the pressure-drop characteristics of a 3D model with smooth intersecting fractures, and the corresponding interpretation with a two-phase flow model which is initially proposed for two-phase flow in pipes. This study presents a basis for further studies to understand the two-phase flow behavior in the rock fracture network.

5.2 Experiment in the intersecting fractures

5.2.1 Experiment system

The experimental system is shown in Fig. 5-1, which is composed of four subsystems, as introduced as the following:

(1) The water supply subsystem. In this subsystem, the peristaltic pump is used for injecting water at a specified flow rate within 0~2000 mL/min. Since the pressure and flow rate of the injected water is always fluctuating, a pulse damper is connected to the pump to decrease the pulse in order to uniformly inject water into the 3D model.

(2) The gas supply subsystem. In this subsystem, nitrogen is supplied from a gas cylinder. The initial gas pressure in the cylinder is as large as 10 MPa, so a pressure regulator is connected to the cylinder to decrease the gas pressure to be under 0.3 MPa in order to protect the mass flow controller. The mass flow controller can specify the gas flow rate to a value within 0~5000 mL/min.

(3) The 3D fracture model. This model is made of acrylic materials and transparent, as shown in Figure 5-2. The schematic of the model from a vertical view is shown as Figure 5-3. The model has five smooth fractures: the apertures of Fractures 1~5 are 0.6 mm, 0.3 mm, 0.3 mm, 0.6 mm and 1 mm. The length of Fracture 5 is 10 cm while the other four fractures have a length of 5.78 cm. The model has two inlets connected to Fracture 1 and Fracture 2 respectively, two outlets connected to Fracture 3 and Fracture 4 respectively. By opening or closing different tanks, different combinations of fractures can be established. In this experiment, we established two cases for testing, as shown in Fig. 5-3, the red lines indicate the activated fractures, while the black lines indicate the fractures in which no flow occurs.

(4) The measurement subsystem. This subsystem includes the camera, the pressure sensors, the separation bottle, the electronic balance and the flowmeter. The flow structures are captured by the camera. One pressure sensor is connected to the gas inlet, one is connected to the water inlet, and one is connected to the outlet. Pressure data are transmitted and recorded in a digital recorder (not shown in the Fig. 5-1). The separation bottle, which is put on the electronic balance, is used to separate water and gas. Gas flows out of the separation bottle and water remains in the bottle. The water mass is measured by the electronic balance, and the data are transmitted to the computer simultaneously.

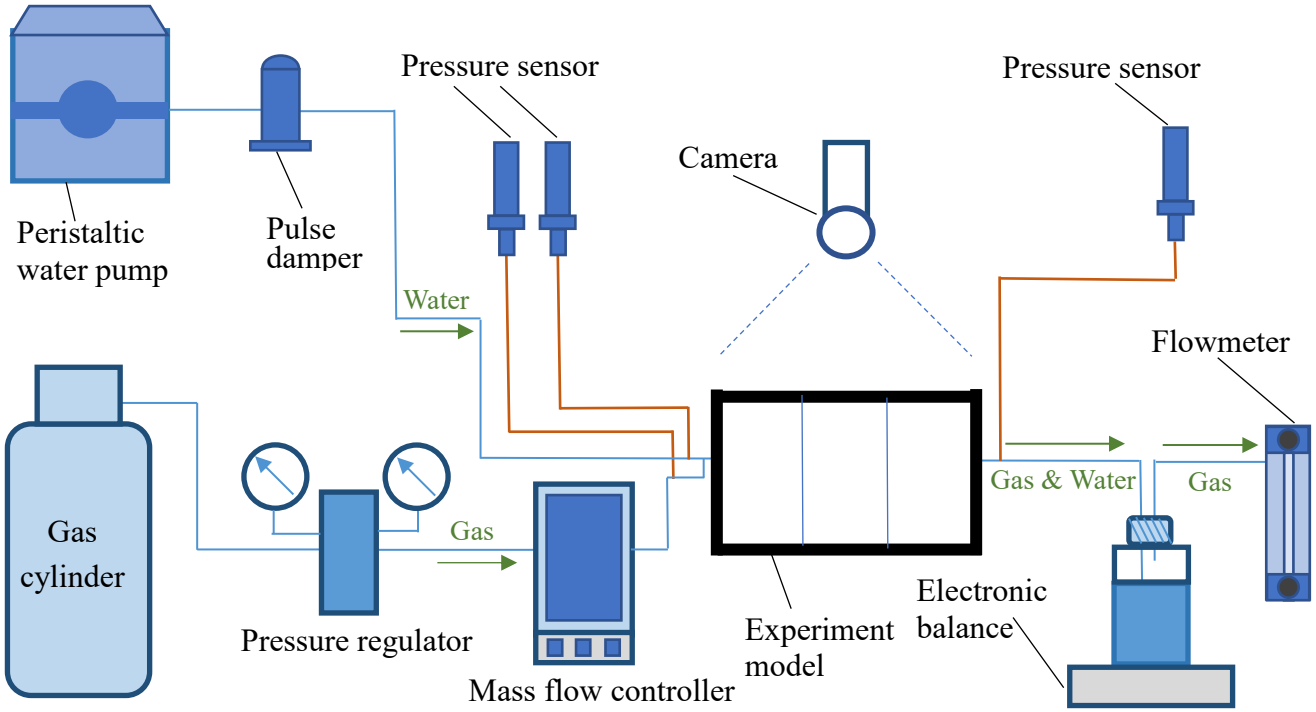

Fig. 5-1 Schematic of the experimental system

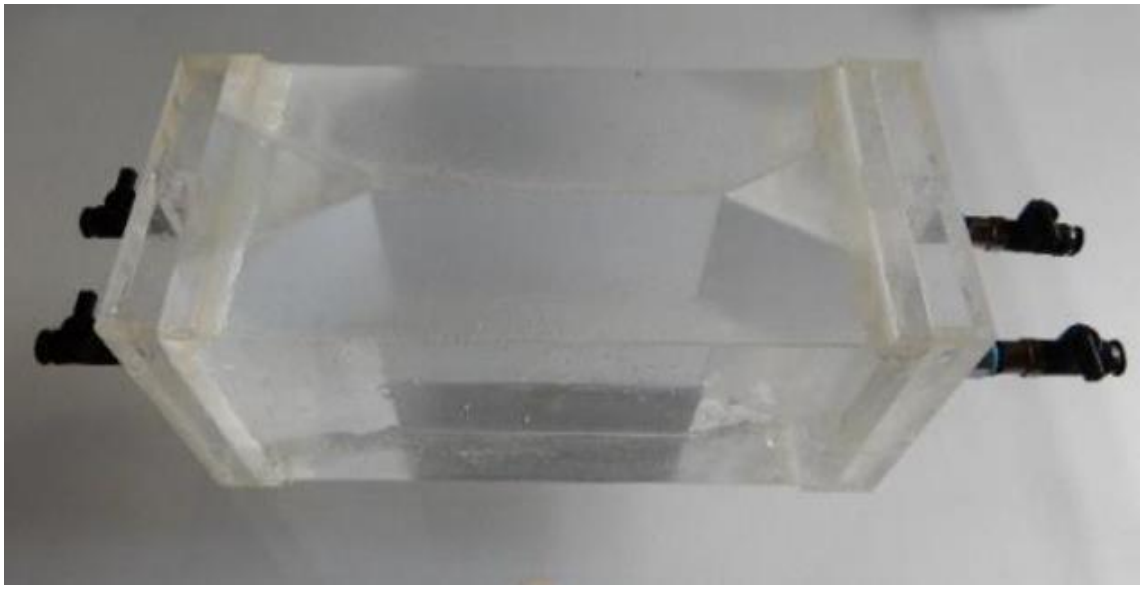

Fig. 5-2 The 3D-fracture model [Liu et al, 2015]

It should be noted that the water flow rate can be indicated in the peristaltic water pump, but without enough accuracy. That's why we set up an electronic balance to measure the water flow rate. On the contrary, the gas flow rate indicated by the mass flow controller is accurate enough according to our test. The gas flow rate indicated by the

flowmeter is identical to that displayed by the mass flow controller. Consequently, the flowmeter can be removed.

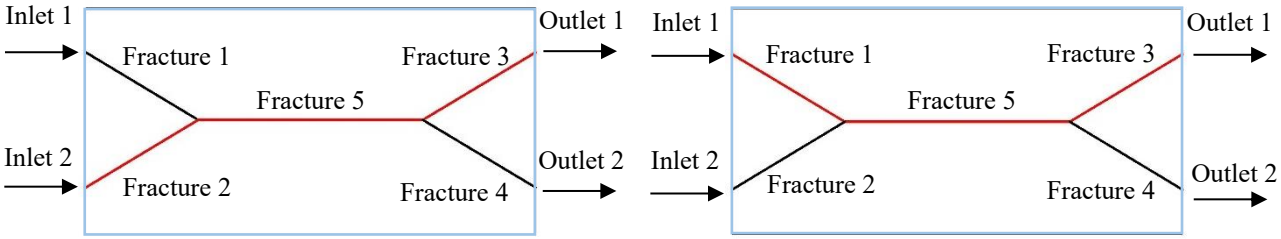

(a) Case 1 (b) Case 2

Fig. 5-3. Schematic of the 3D-fracture model (vertical view)

5.2.2 Experiment procedures

As mentioned above, this experiment was conducted with two cases. In each case, the tests were conducted in the following procedures:

(1) Adjust the levelness of the 3D model with a level gauge.

(2) Conduct the preliminary test to check the tightness of the system and the accuracy of the measurement subsystem. The flowmeter connected to the separation bottle is used to check the accuracy of the gas flow rate indicated by the mass flow controller, and the electronic balance is used to check the accuracy of the water flow rate indicated by the peristaltic pump. The test results showed that the accuracy of the peristaltic pump is not good, but the gas flow rate indicated by the flowmeter is identical to that displayed by the mass flow controller. However, we found that the flowmeter brought a large resistance to the flow of fluids. It means that compared with the resistance of the model, the resistance of flowmeter cannot be neglected, and this may cause burden to the pump. Consequently, in the formal experiment we removed the flowmeter.

(3) Conduct a single-phase flow test of water to obtain the single-phase hydraulic properties of the intersecting fracture model. Water was injected at different flow rates within 0~1000 mL/min.

(4) Conduct the two-phase flow test. In each case, five groups of two-phase flow tests were conducted. In each group, the water flow rate was kept constant while gas was injected at a series of flow rates within 0~2000 mL/min. In each test, when water and gas were injected at their respective flow rates, five minutes are waited for the flow to reach

a stable state. Then the pressure and the water mass in the separation bottle were recorded with the pressure sensors and electronic balance, respectively. At the same time, the flow structures were captured by the camera. Since the pressure and the flow rates were always fluctuating, in each test, the data recording lasted one minute in order to obtain the average values of data; ten photos were taken to acquire the flow structures and average saturation.

5.3 Potential models for describing two-phase flow in the intersecting fractures

5.3.1 The generalized Darcy's law

As introduced in Chapter 2, the generalized Darcy's law is widely used for describing two-phase flow in single fractures [Wyckoff and Botset, 1936; Corey, 1986], as indicated in Equations 5-1 and 5-2:

$$V_{ws} = -\frac{k_0 K_{rw}}{\mu_w}\frac{dP_w}{dx} \tag{5-1}$$

$$V_{gs} = -\frac{k_0 K_{rg}}{\mu_g}\frac{dP_g}{dx} \tag{5-2}$$

in which P_w and P_g are the pressure of water and gas, respectively; V_{ws} *and* V_{gs} are the superficial velocities of water and gas; k_0 is the intrinsic permeability of the fracture; K_{rw} and K_{rg} are the relative permeabilities of water and gas, respectively; μ_w and μ_g are the viscosities of water and gas, respectively; the subscripts *w* and *g* represent water and gas. The above two equations indicate the relationship between the flow rate and the pressure drop of two phases, which is similar to Darcy's law in single-phase flow. The relative permeabilities are critical parameters that indicate the interference between two phases, and they are dependent on the saturations of each phase. Since it is not known whether this method is applicable to intersecting fractures, it is selected as an alternative.

5.3.2 The Lockhart-Martinelli model

The Lockhart-Martinelli model was initially proposed to describe the two-phase flow in pipes (Lockhart and Martinelli, 1949). It proposed two important parameters-the water phase multiplier Φ_w and the gas phase multiplier Φ_g to assess the flow resistivity induced by two-phase interactions. They are defined as Equations 5-3 and 5-4, in which dP/dx refers to the two-phase pressure drop of both fluids; $(dP/dx)_w$ refers to the single-phase

pressure drop of water at the same water flow rate as in the two-phase flow, and $(dP/dx)_g$ refers to that of gas. It should be noted that in pipe flow, the capillary pressure does not exist, so the gas pressure drop and the water pressure drop in two-phase flow are equal, namely $dP_w/dx = dP_g/dx = dP/dx$. Because at the same flow rate, the pressure drop of each phase in two-phase flow is always larger than that in single-phase flow, there two parameters represent the extra resistivity induced by the two-phase flow interactions.

It should be noted that Φ_w and Φ_g are originally defined as the square root of the ratio between the two-phase pressure gradient and single-phase one. For the convenience of comparison with the definition of relative permeability, Fourar and Bories [1993] redefined them as Equations 5-3 and 5-4, and in this dissertation we followed this revised definition. The definition of Φ_w and Φ_g is similar to that of relative permeability in the aspect that both of them represent a comparison between two-phase pressure drop and single-phase pressure drop. However, the difference lies in the fact that Φ_w and Φ_g account for the flow nonlinearity induced by inertial effect or turbulence. If the single-phase flow is nonlinear, this nonlinearity is included in the term of single-phase pressure drop $(dP/dx)_w$ and $(dP/dx)_g$.

The Martinelli parameter—χ is used to analyze the evolution of frictional multipliers. It is defined as Equation 5-5. $(dP/dx)_w$ refers to the single-phase pressure drop of water, whose corresponding flow rate is identical to that in the two-phase flow state, and $(dP/dx)_g$ refers to that of gas. It represents the relative importance of the flow of water to gas.

$$\Phi_w = \frac{dP/dx}{(dP/dx)_w} \tag{5-3}$$

$$\Phi_g = \frac{dP/dx}{(dP/dx)_g} \tag{5-4}$$

$$\chi = \frac{(dP/dx)_w}{(dP/dx)_g} \tag{5-5}$$

5.4 Hydraulic characteristics of two-phase flow in the intersecting fractures

5.4.1 Results of single-phase flow test

In the single-phase flow test of water, the relationship between the flow rate Q and pressure drop P is shown in Figure 5-4. The results show that the pressure drop increases

nonlinearly with respect to the flow rate. The experiment data are fit with a quadratic relationship, which can be described by the Forchheimer's law as indicated by Equation 5-6 (Zimmerman et al., 2004). Here, a is the parameter related to the aperture of the fracture, and b is a parameter that indicates the nonlinearity of flow, which is correlated to the fracture morphology. The equation is found to be applicable to flow in porous media (Temeng and Horne, 1988) and in rough fractures (Schrauf and Evans, 1986). It has been demonstrated that in intersecting fractures, this equation is also effective due to the existence of inertial effect of water flow (Liu et al, 2008).

$$-\nabla P = aQ + bQ^2 \tag{5-6}$$

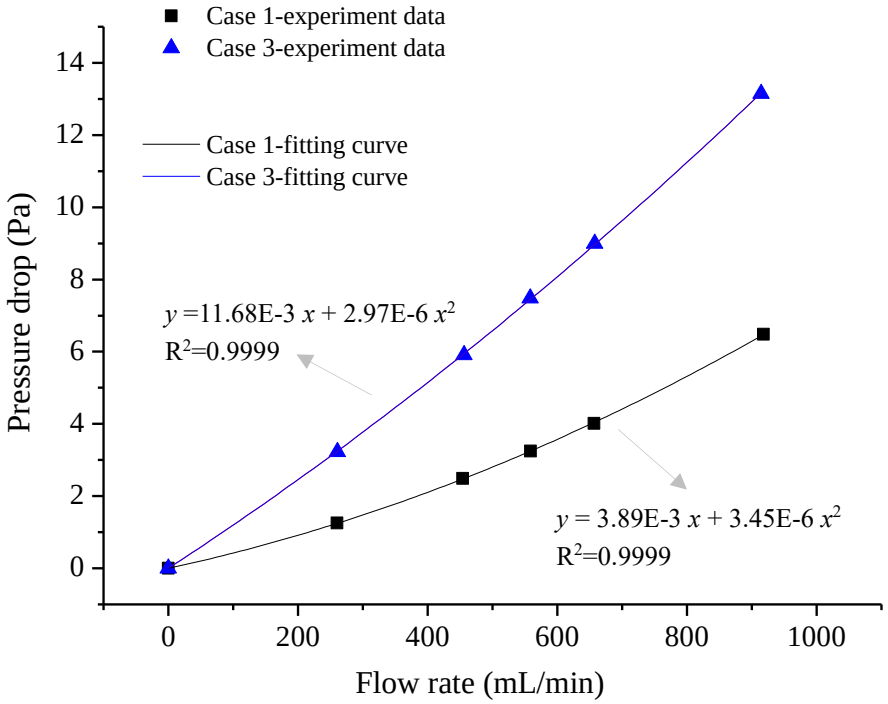

Fig. 5-4 The hydraulic characteristics of single-phase flow (water)

The fitting results show that single-phase flow in both cases follow the Forchheimer's law very well, which means that the flow nonlinearity cannot be neglected. With the results of single-phase flow test, the two-phase flow hydraulic characteristics can be calculated, as introduced in the next section.

5.4.2 Hydraulic characteristics of the two-phase flow in the intersecting fractures

Figures 5-5 and 5-6 show the evolution of two-phase pressure drop with respect to gas flow rate. Each curve represent the test with the same water flow rate. Here the pressure

drop refers to the pressure difference between the inlet and outlet, which indicates the energy loss in the simultaneous flow of two fluids through the intersecting fractures.

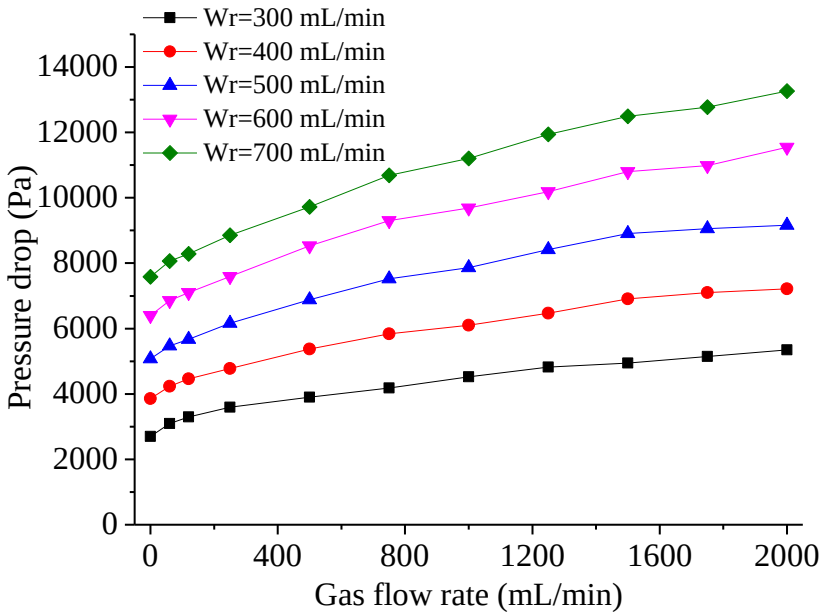

Fig. 5-5 Evolution of the two-phase pressure drop with respect to the water flow rate and gas flow rate in Case 1

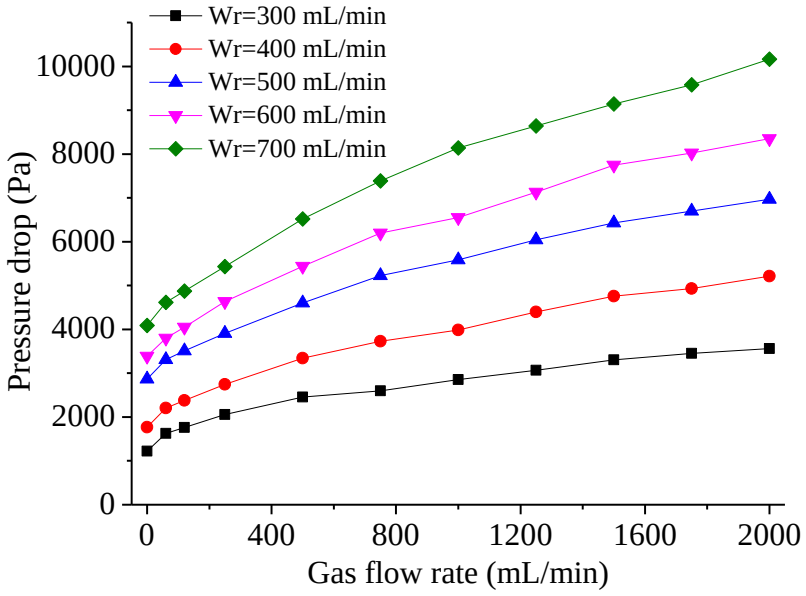

Fig. 5-6 Evolution of the two-phase pressure drop with respect to the water flow rate and gas flow rate in Case 2

Both cases show that at a certain water flow rate, each curve indicates a nonlinear relationship between the pressure drop and the gas flow rate. This result is quite different from that of the two-phase flow test in rough single fractures (Fourar and Bories, 1995).

In their experiment, at each water velocity, the pressure gradient increases almost linearly with respect the gas flow rate. It is believed that this nonlinearity is induced by the stronger inertial effect of water in the intersecting fractures. Since the density of water is much larger than that of gas, the inertial effect of water is more severe. That is to say, in our experiment the pressure drop of water contributes more to the total pressure drop due to the strong inertial effect of water, while the pressure drop induced by gas accounts for a smaller percentage compared with the experiment of Fourar and Bories. Consequently, at a constant water flow rate, the increase of pressure drop induced by increasing the gas flow rate in our experiment is smaller than that in single fractures, and accordingly leads to the flow nonlinearity.

In two-phase flow in pipes, there are usually sharp variations in the P-Q (pressure drop-flow rate) relationship if the flow structure changes from one to another. In our test, no sharp variations were observed in Figures 5-5 and 5-6. We tried to seek for the reasons from the flow structures. This is because in our tests the fractures in the 3D model were vertical to the horizontal plane, and all the gas gathered in the upper space of the fracture due to buoyancy, consequently formed a stratified flow. In stratified flow, there is not an obvious transfer of flow structures from bubble flow to continuous flow, so there are no sharp variations in the evolution of pressure drop with respect to the flow rate.

As introduced in Section 5.3.1, the generalized Darcy's law has been adopted to describe two-phase flow in single fractures. However, the generalized Darcy's law does not account for the inertial effect. As we know, in single-phase flow, the Darcy's law is not applicable if the flow nonlinearity cannot be neglected. This nonlinearity can be induced by the inertial effect or turbulence. Consequently, revised laws such as Forchheimer's law are proposed to account for the nonlinearity [Irmay, 1958]. As for two-phase flow in our experiment, due to the existence of inertial effect induced by the fracture intersection, which will contribute to flow nonlinearity, the generalized Darcy's law is not expected to fit the pressure drop data very well. However, we still analyzed the flow structures and measured the saturation to discuss the applicability of generalized Darcy' law in detail.

Figs. 5-7 shows the flow structures of Case 2 when water flow rate (W_r) was 600 mL/min and gas flow rate (G_r) was 1500 mL/min. The photos were all taken from the lateral view. It shows that the saturation of gas kept fluctuating with respect to time, which

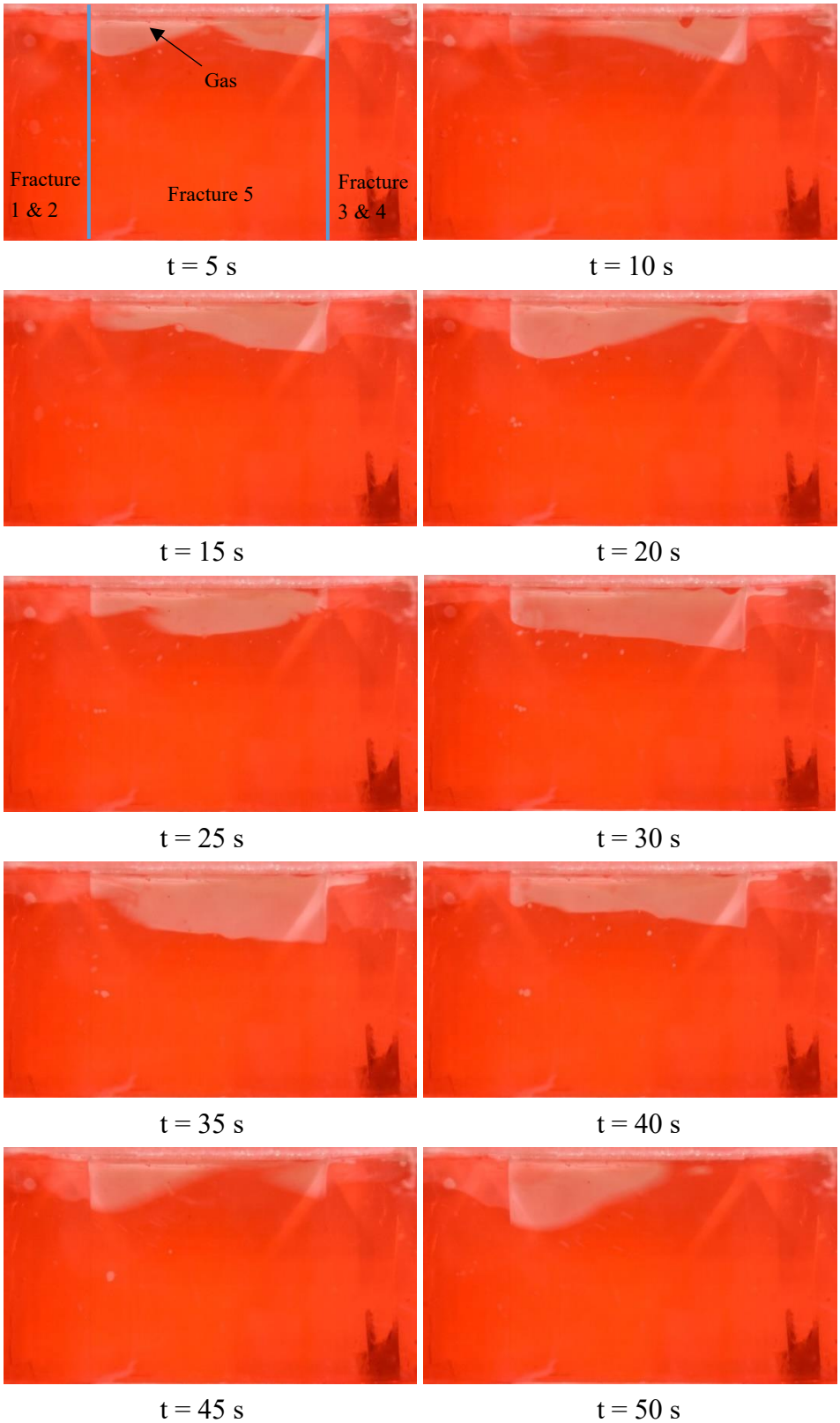

Fig. 5-7 The flow structures at W_r = 600 mL/min, G_r = 1500 mL/min in Case 2

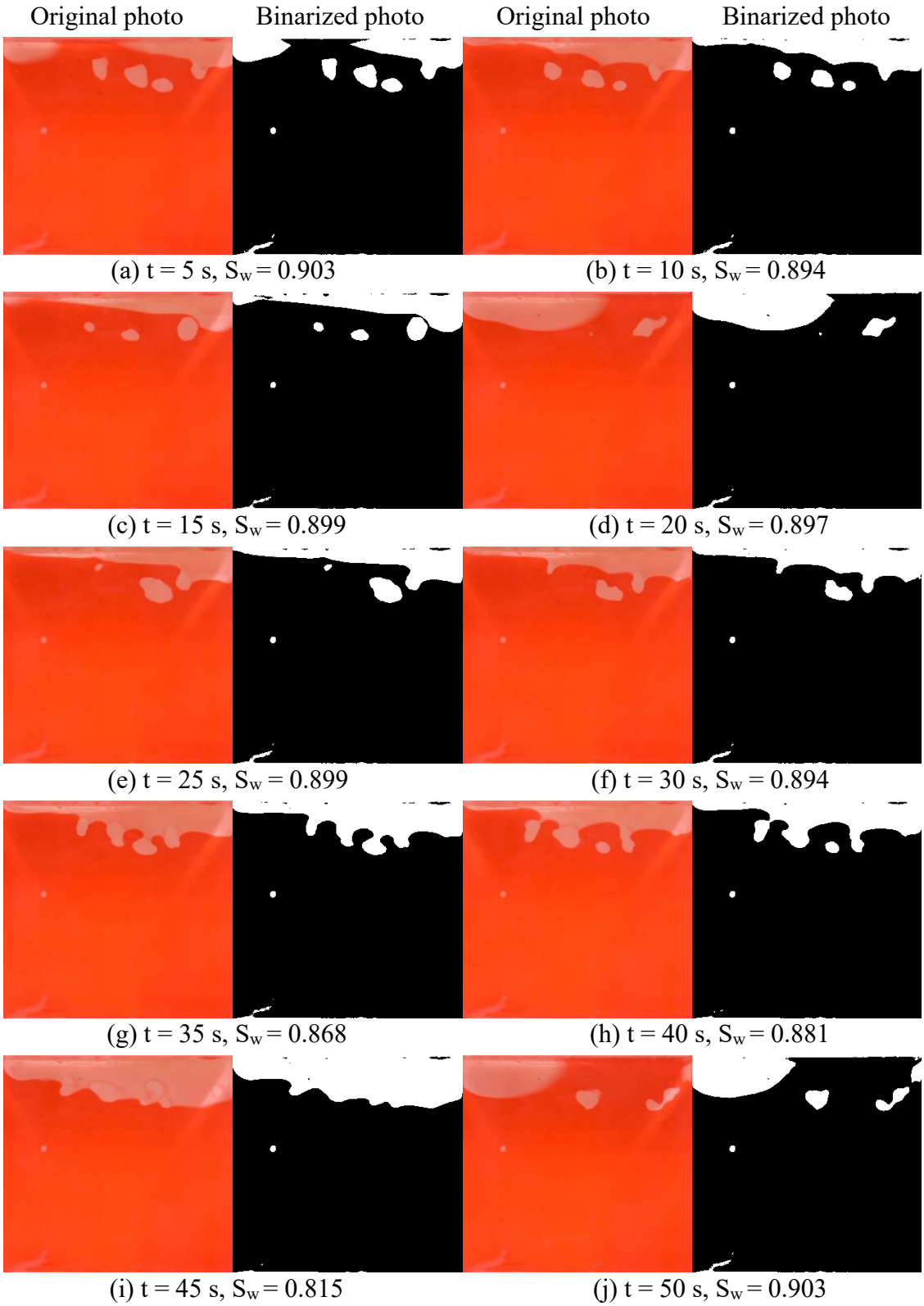

Fig. 5-8 The saturations in Fracture 5 at different moments when W_r = 500 mL/min, G_r = 500 mL/min in Case 2

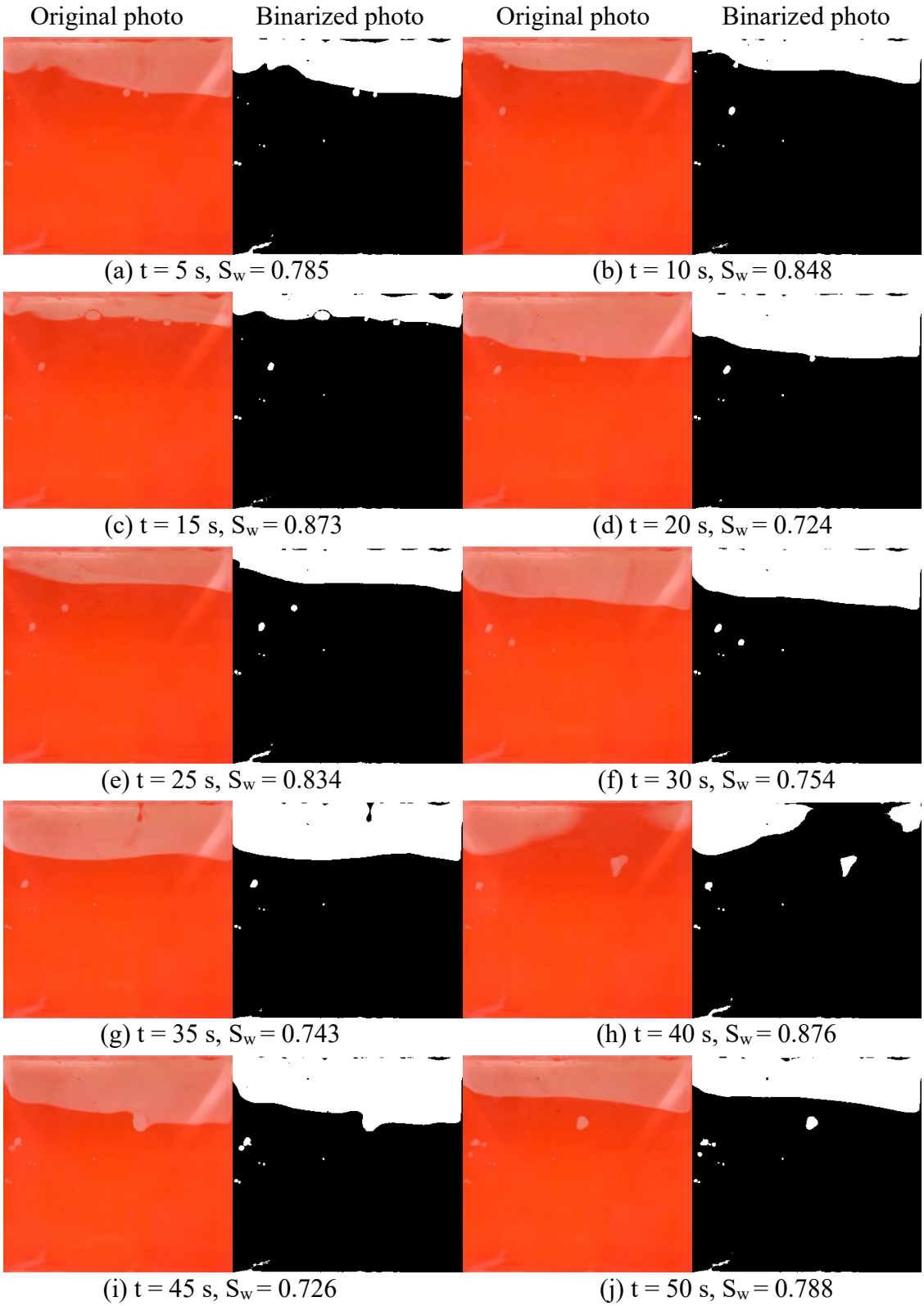

Fig. 5-9 The saturations in Fracture 5 at different moments when W_r = 500 mL/min, G_r = 1000 mL/min in Case 2

is more similar to the stratified wavy flow in pipes. This gives information that the generalized Darcy's law, which is originally proposed for porous media, may be not effective for this experiment. In order to confirm this, the saturation should be calculated. Since the Fractures 1~4 were not vertical to the camera, to avoid refraction in taking photos, only the flow structures and saturations in Fracture 5 are analyzed. The photos of Fracture 5 are extracted from the original photos for saturation calculation, as shown in Figures 5-8 and 5-9. Figure 5-8 shows the flow structures in Fracture 5 when W_r is 500 mL/min, G_r is 500 mL/min in Case 2; in Figure 5-9, W_r is 500 mL/min, G_r is 1000 mL/min. The red pictures are the original photos taken by the camera, in which the light-colored parts indicate the gas and dark-colored parts indicate the water. The black-while pictures were converted from the original photos by binarization with MATLAB in order to calculate the water saturation $S_{w.}$ It is indicated that the saturation was also fluctuating with respect to time, though the flow rates of water and gas were kept constant. When gas flow rate increased from 500 mL/min to 1000 mL/min, there was not an obvious variation in the flow structures, but always kept as stratified flow. This confirmed that in Figures 5-5 and 5-6 the pressure increases with respect to gas injection rate without sharp variations.

Table 5-1 The evolution of water saturations in Case 2

W_r / G_r	300 mL/min	400 mL/min	500 mL/min	600 mL/min	700 mL/min
250 mL/min	0.862569	0.857369	0.875392	0.881016	0.896558
500 mL/min	0.821236	0.879957	0.855444	0.854149	0.851789
750 mL/min	0.802358	0.866676	0.810348	0.813873	0.810044
1000 mL/min	0.785123	0.815105	0.803772	0.792381	0.824783
1250 mL/min	0.764371	0.776926	0.803066	0.790732	0.807058
1500 mL/min	0.751457	0.773134	0.779215	0.809707	0.809978

Table 5-1 shows the saturation at different flow rates of water and gas in Case 2. The saturation at each flow rate is the averaged value from ten pictures. It shows that the water saturation decreases with respect to gas flow rate. But some exceptions may exist, such as the case when G_r is 500 mL/min and W_r is 400 mL/min. In addition, the variation of water saturation is not obvious. When W_r is 700 mL/min, the G_r increases from 250 mL/min to 1500 mL/min, the water saturation decreased only 10%. This also indicates

that the generalized Darcy's law may not work well in describing the two-phase flow pressure drop in the intersecting fractures.

Consequently, the Lockhart-Martinelli model is selected to analyze the two-phase hydraulic characteristics of the intersecting fractures. The evolution of Φ_w and Φ_g in the two cases is shown in Figures 5-10 and 5-11. $\chi(1+\chi)$ is selected as the X-axis instead of χ for convenience, since in this way the X-axis varies from 0 to unity. It shows that all the experiment data fall on the same curve, indicating that the Martinelli-Lockhart model is not only effective for describing the two-phase flow in a single fracture, but for the two-phase flow in the intersecting fractures. Because the Martinelli-Lockhart model considers the nonlinearity of flow, which can't be neglected in the intersecting fractures, the good fitting results are obtained. In nature, the Martinelli-Lockhart model is similar to the generalized Darcy's law, which is based on concept of relative permeability (Chen, 2005). Both models are established by considering the extra resistivity induced by the two-phase interactions. However, the extended Darcy's law does not consider the nonlinearity of single-phase flow, and sometimes lead to deviations (Fourar and Bories, 1993).

The values of Φ are usually very large, so the difference of Φ values at different water flow rates cannot be clearly shown. In order to see the difference in the values of Φ in different water flow rates, the evolution of $1/\Phi$ with respect to $\chi(1+\chi)$ are shown in Figs. 5-12, 5-13 and 5-14. They show that there is a little difference in the values of $1/\Phi$ with different water flow rates.

Delhaye et al [1981] proposed an empirical relationship between Φ_w, Φ_g and χ, as shown in Equations 5-7 and 5-8. *C* is a parameter that indicates the flow regime of each phase. When *C* is 5, both water and gas flow are laminar; when *C* is 10, water is turbulent and gas is laminar; when *C* is 12, liquid is laminar and gas is turbulent; when *C* is 20, both water and gas flow are turbulent. However, this method is initially proposed for describing the two-phase flow in pipes. Fourar and Bories [1993] used this method to fit two-phase flow data in single fractures, and they found that this model can work well for rough calculations. Since the two-phase flow in intersecting fractures has similarity to that in the rough single fracture in the aspect that the flow has nonlinearity induced by the inertial force, it is believed that this model may be also effective for the intersecting fractures. Therefore, the experiment data are fit with these two equations.

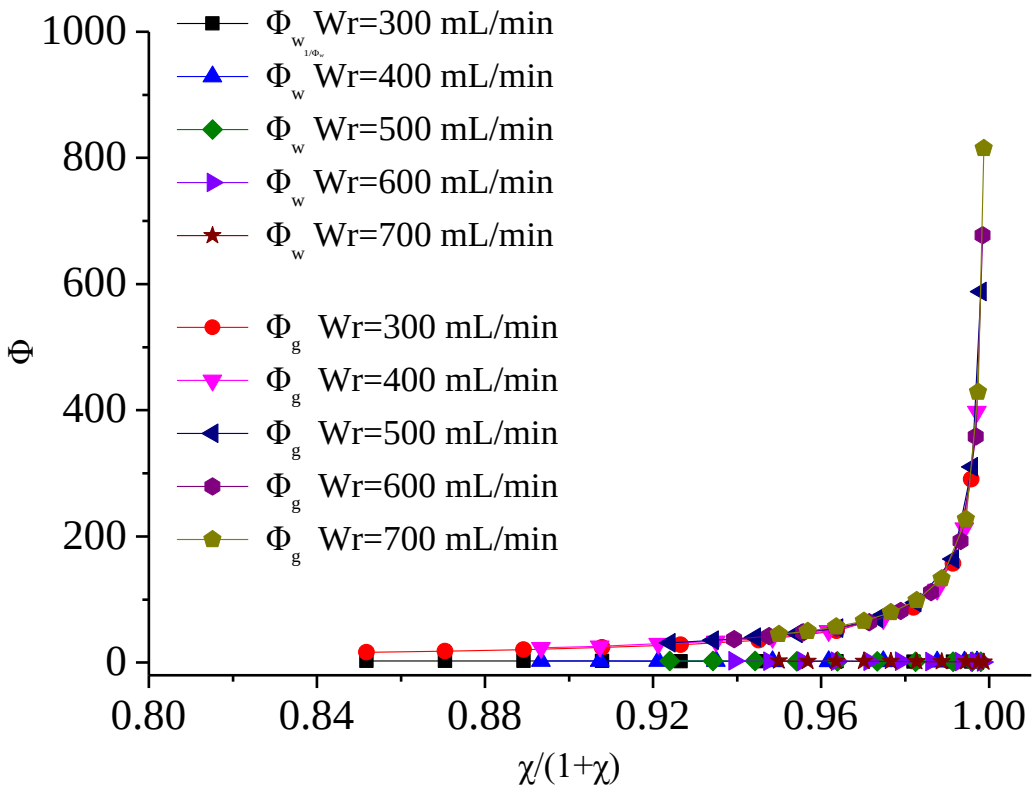

Fig. 5-10 The relationship between Φ_w, Φ_g and $\chi(1+\chi)$ in Case 1

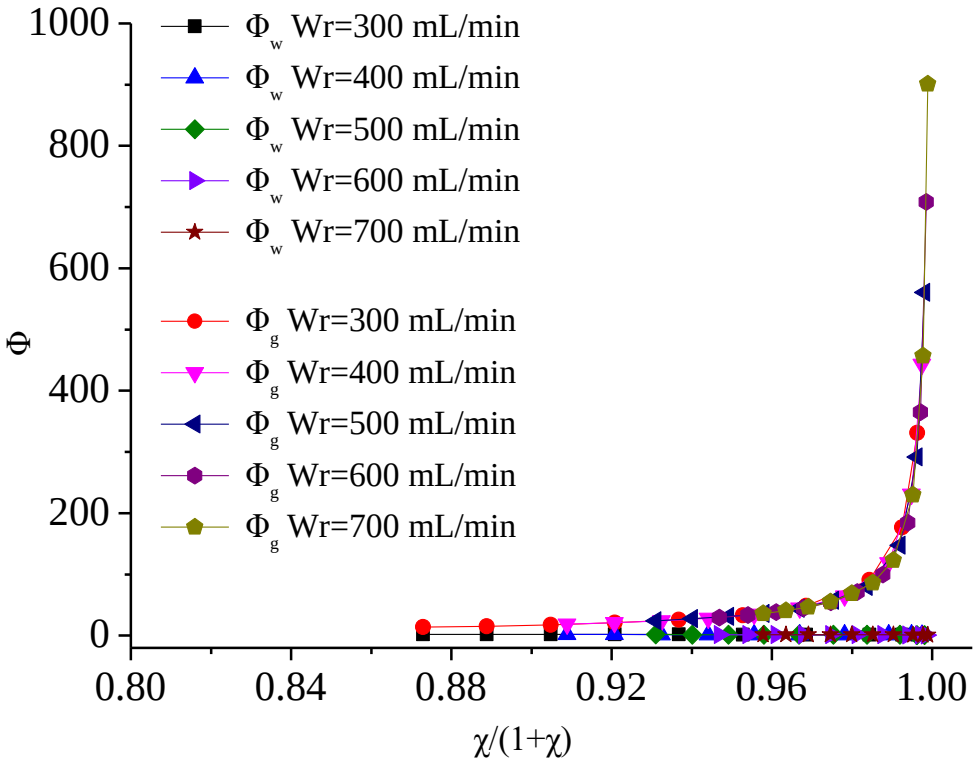

Fig. 5-11 The relationship between Φ_w, Φ_g and $\chi(1+\chi)$ in Case 2

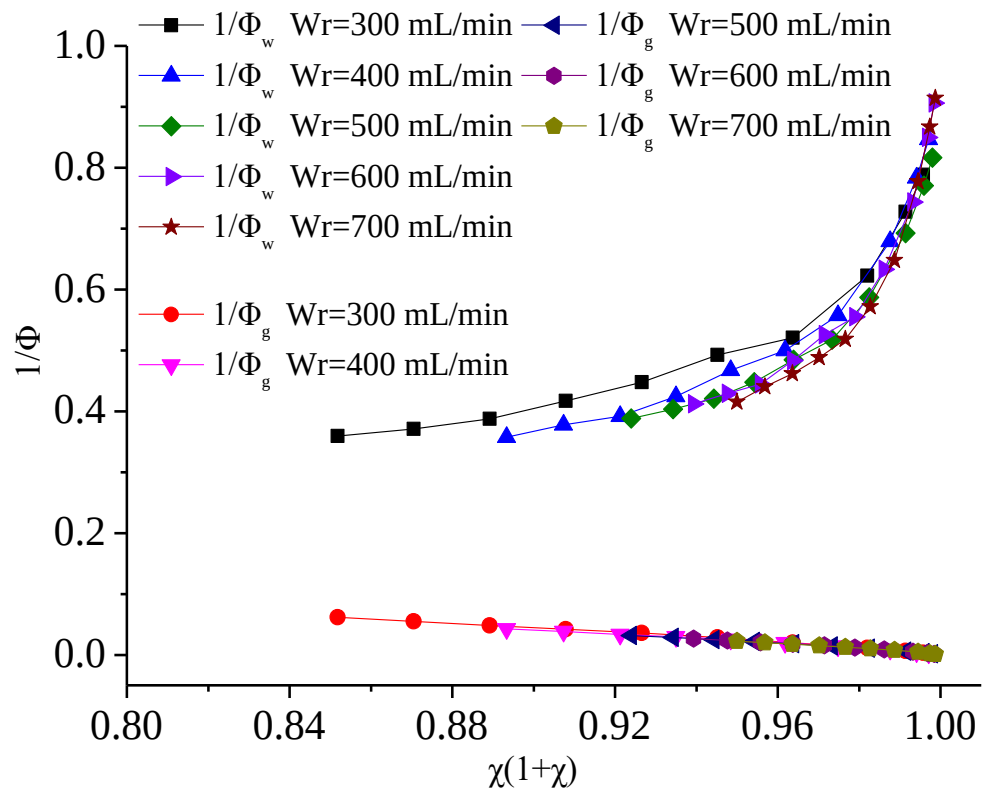

Fig. 5-12 The relationship between $1/\Phi_w$, $1/\Phi_g$ and $\chi(1+\chi)$ in Case 1

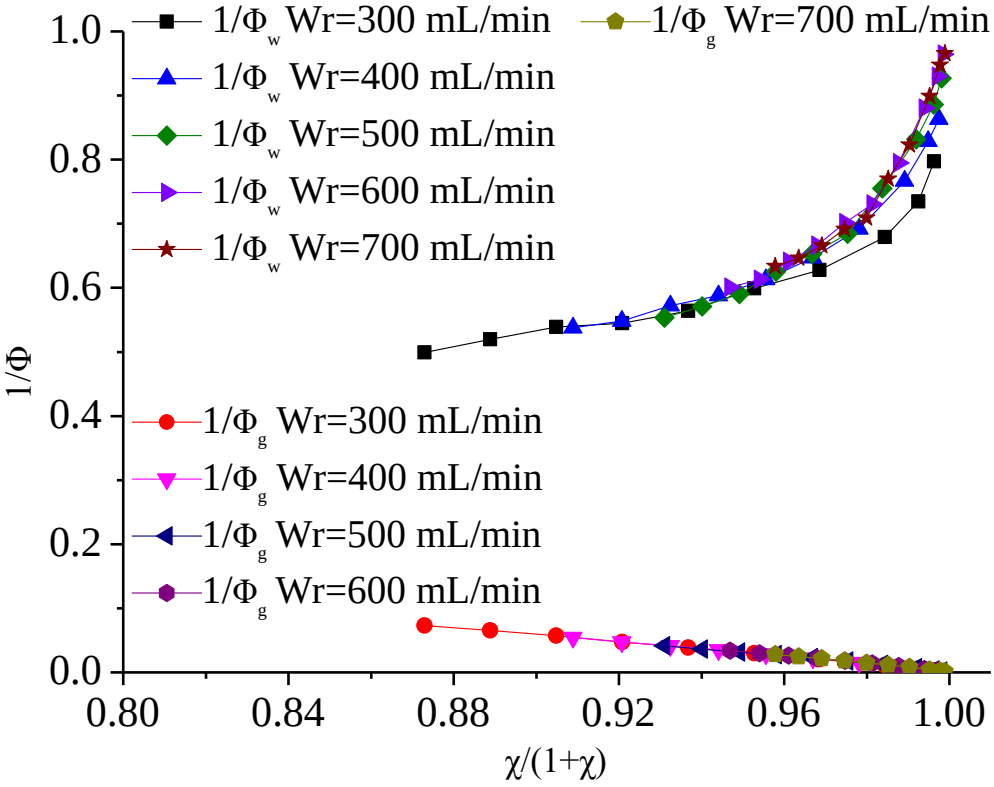

Fig. 5-13 The relationship between $1/\Phi_w$, $1/\Phi_g$ and $\chi(1+\chi)$ in Case 3

$$\Phi_w = 1 + \frac{C}{\sqrt{\chi}} + \frac{1}{\chi} \tag{5-7}$$

$$\Phi_g = 1 + C\sqrt{\chi} + \chi \tag{5-8}$$

Fig. 5-14 and Fig. 5-15 show the evolution of Φ_w and Φ_g with respect to Sqrt (χ) in Case 1, and the corresponding fitting values of *C*. The curves of Equation 5-7 or 5-8 with $C = 5$, $C = 10$, $C = 12$, $C = 20$ are also plotted for reference. The five curves are close to $C = 5$, namely the water laminar-gas laminar flow state. To be accurate, when the water flow rate is 300 mL/min, 400 mL/min, 500 mL/min, 600 mL/min, 700 mL/min, the corresponding *C* is 4.048530, 4.80857, 5.29730, 5.32033, 5.65830, respectively. The corresponding R^2 is 0.99303, 0.99037, 0.9958, 0.99256 and 0.96893. With the increase of the water flow rate, the value of *C* increases. This indicates that with the increase of the flow rate, the flow regime tends to vary from water laminar to water turbulent. However, the Delhaye's model may be not totally applicable to intersecting fractures, because our experiment data show that the pressure fluctuates very seriously in most of the cases. In our experiment, there are hardly laminar flow states. However, the fact that the turbulence increases with respect to the water flow rate is reasonable.

By fitting the testing data in to Equation 5-8, the corresponding *C* is 3.92972, 3.62245, 3.34231, 2.95531, 2.78059, respectively. The corresponding R^2 is 0.99964, 0.99807, 0.99955, 0.99585, 0.99486. The fitted values of *C* in Fig. 5-15 are also close to C=5, which is consistent with the fitting values of *C* with Equation 5-7. This indicates that Delhaye's model is approximately applicable to the intersecting fractures, but the values of *C* in the intersecting fractures may have differences with that in pipe two-phase flow. If Delhaye's model is modified, it can better fit the two-phase flow data in intersecting fractures.

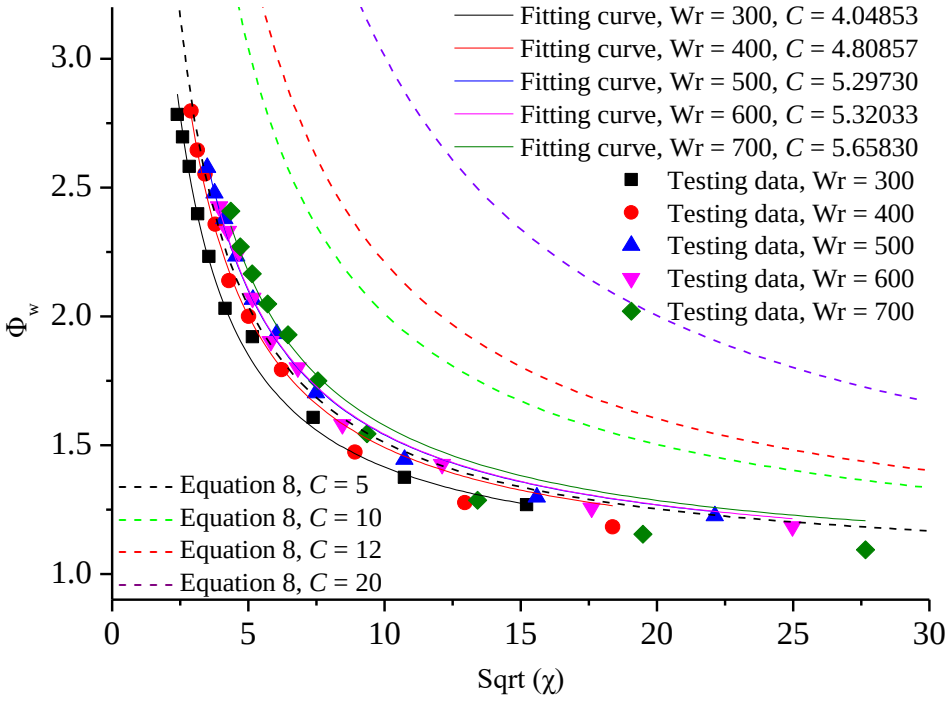

Fig. 5-14 The relationship between Φ_w and Sqrt (χ) in Case 1

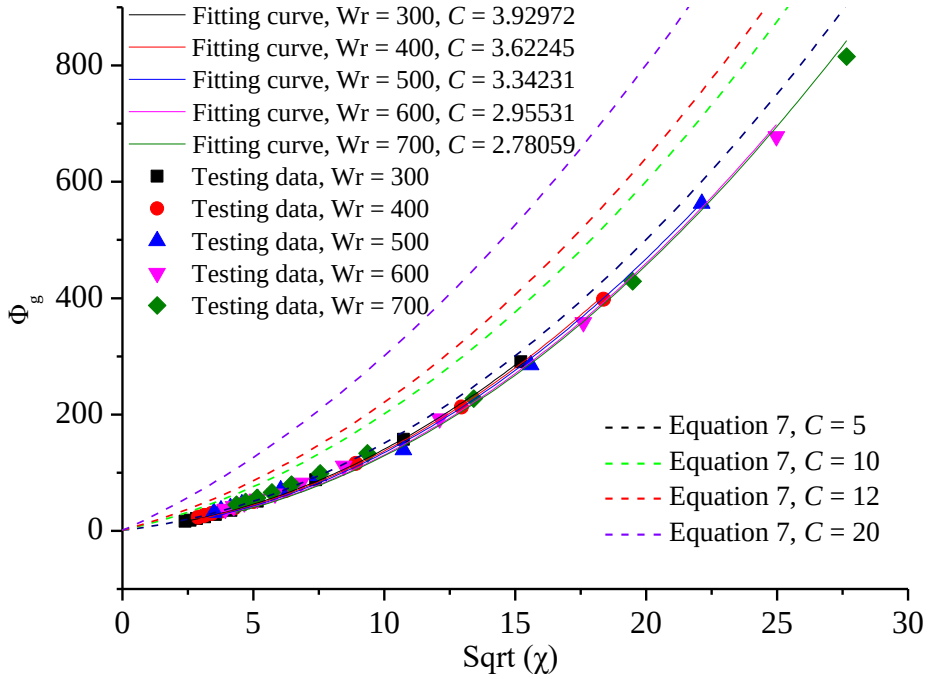

Fig. 5-15 The relationship between Φ_g and Sqrt (χ) in Case 1

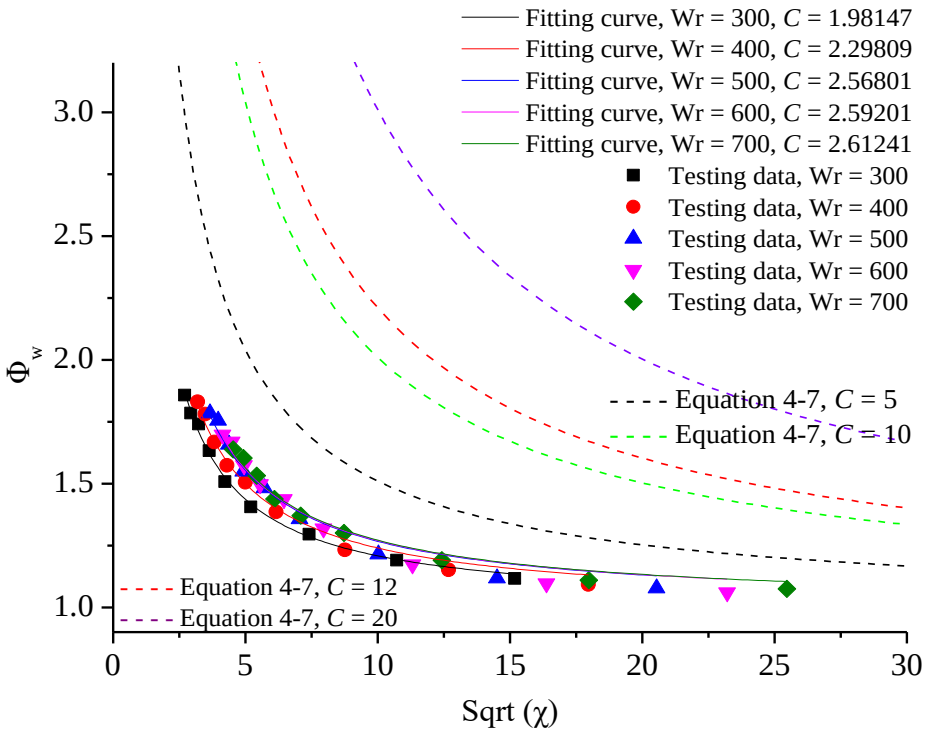

Fig. 5-16 The relationship between Φ_w and sqrt (χ) in Case 2

Figs. 5-16 and 5-17 show the fitting results of Case 2. When the water flow rate is 300 mL/min, 400 mL/min, 500 mL/min, 600 mL/min, 700 mL/min, the fitted values of *C* with Equation 5-7 are 1.98147, 2.29809, 2.56801, 2.59201, 2.61241; the fitted values of *C* with Equation 5-8 are 1.76394, 1.81044, 1.70312, 1.55409, 1.04640. Both groups of fitted values of *C* indicated that the turbulence in Case 2 is smaller than that in Case 1. This is reasonable since Case 1 is composed of three fractures with an aperture of 0.3 mm-1 mm-0.3 mm, while Case 2 is composed of three fractures with an aperture of 0.6 mm-1 mm-0.3 mm. The average fracture of Case 2 is larger than that of Case 1, and in Case 2 the superficial velocity is smaller, and consequently the turbulence is also small. In addition, the aperture change at the first intersection of Case 2 (from 0.6 mm to 1mm) is smaller than that of Case 1 (from 0.3 mm to 1mm), so in Case 1, the turbulence induced by the aperture change at the fracture intersection is also serious.

In Fig. 5-16, when the water flow rate increases from 300 mL/min to 700 mL/min, *C* increases from 1.98147 to 2.61241, which also indicates the increase of water turbulence. However, the evolution of fitted *C* in Fig. 5-17 doesn't show much regularity with respect to the increase of water flow rate. This indicates that the applicability of Delhaye's model

is better for evaluating the water phase in two-phase flow in the intersecting fractures. Since the density of gas is much smaller than that of water, in such conditions the inertial force of water would be larger compared to the viscous force, and water is more likely to reach turbulent flow state. Therefore, with the increase of water flow rate, the increase of the turbulence for water is more obvious, while the turbulence of gas (indicated by *C*) shows less regularity.

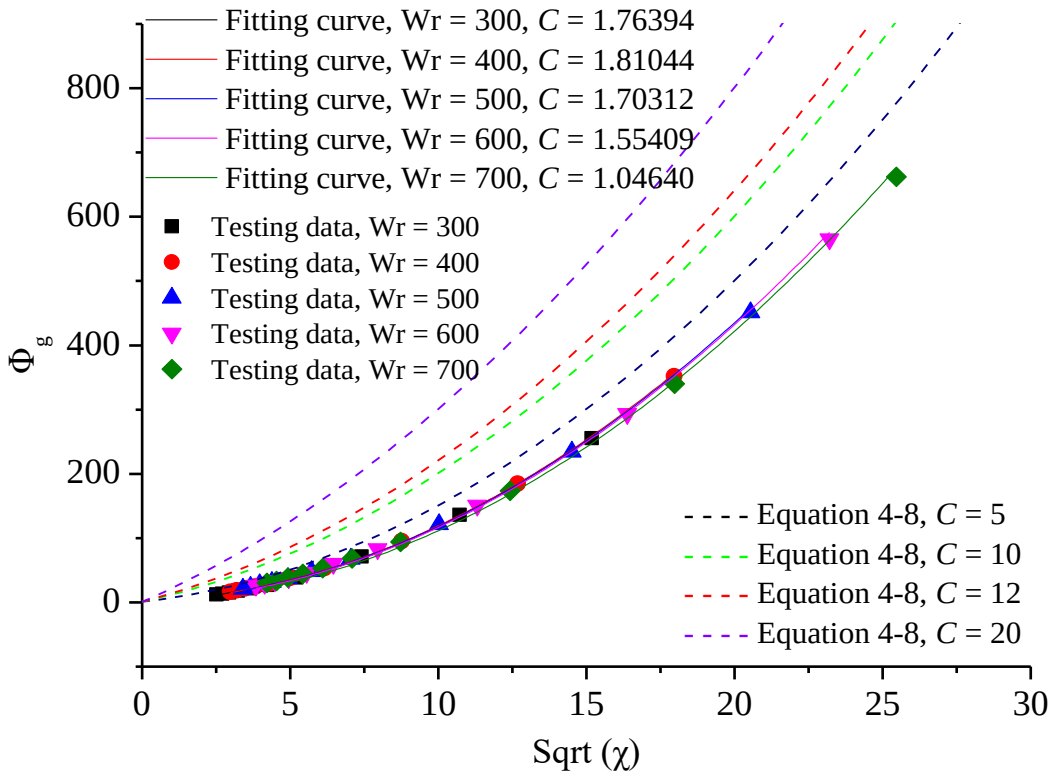

Fig. 5-17 The relationship between Φ_g and Sqrt (χ) in Case 2

However, it should be noted that in Delhaye's [1981] study, the values of *C* calculated by Equation 5-7 and Equation 5-8 should be identical. In our test, there is a little difference between the values of *C* calculated by these two equations. This may be due to the fact that Equation 5-7 and Equation 5-8 are not completely suitable for describing the two-phase flow in such intersecting fractures. They are supposed to be improved in future studies. In addition, Φ_w and Φ_g are believed to be related to the parameters of the intersecting fractures. Further researches are to be extended in these aspects.

5.5 Summary

In this chapter, a two-phase flow experiment is conducted in the 3D model with smooth intersecting fractures, in order to investigate its hydraulic characteristics. The following conclusions are supported by the results:

(1) The flow structures in the intersecting fractures show more similarity to that of stratified wavy flow in pipes, and the saturation kept fluctuating with respect to time. In addition, the nonlinearity induced by inertial force and turbulence in the intersecting fractures cannot be neglected in the two-phase flow. Due to these two reasons, the generalized Darcy's law cannot well describe the hydraulic characteristics of the intersecting fractures; but the Lockhart-Martinelli model can fit the experiment data very well.

(2) For a rough calculation of the pressure drop in the intersecting fractures, the Delhaye's model is effective. The degrees of turbulence in different cases can be well indicated by the average values of the parameter C. However, in each case, the evolution of the parameter C for water shows more regularity than that for gas. C increases with respect to the water flow rate, indicating an increase of turbulence degree.

(3) For intersecting fractures, there is an inconstancy between the flow-state parameter C for water and C for gas in the Delhaye's model. This indicates that the even though the Delhaye's model can be used for rough calculations of the two-phase pressure drop in the intersecting fractures, but not completely suitable for evaluating the turbulence of fluid, especially for gas. It should be modified for better fit.

The phase multipliers Φ_w and Φ_g are believed to be related to the parameters of the intersecting fractures, such as the intersecting angle, the aperture change of the fractures. These aspects are to be further investigated in future studies.

Chapter 6 Experimental investigation on the phase distribution characteristics of gas and water in the intersecting fracture

As introduced in Chapter 1, in coalbed methane recovery, water is generally drained out together with gas at the initial stage of gas exploitation. In order to quantify the evolution of distribution of gas and water in intersecting fractures and hence understand the two-phase fluid flow behavior in fracture network, an experiment system was developed and then an experimental study was conducted on three artificial models with two fractures intersecting at 30°, 60° and 90°, which are manufactured with glasses for convenience of visualization. The results show that the evolution of water and gas can be classified into three stages. In each stage, the dominant factor is different. The effect of different gas-water ratios, fracture intersecting angles, and gas desorption positions on the gas and water distributions is analyzed quantitatively.

6.1 Introduction

In coalbed methane exploitation, there is usually a gas-water two-phase flow stage. This is because the coal seams are generally abounded with water. As the exploitation progresses, the water storage decreases, and correspondingly the water flow rate also decreases. On the other hand, as the gas desorbs from the coal matrix, the gas flow rate will increase. In the above-mentioned process, there is a transition from single-phase flow of water to gas-water two-phase flow in the fracture network, and the gas desorption rate varies with respect to time. Consequently, a two-phase flow with different gas-water ratios will be formed, so the flow behavior with different gas-water ratios requires to be well understood.

On the other hand, the parameters of the fracture network such as the fracture intersecting angle also have an impact on the flow behavior. As a basis, a study on the fracture intersections is needed to seek for the influence of fracture parameters such as the intersecting angle on the flow behavior. In applications of coalbed methane recovery, by investigating the statistical parameters in the coal seam fracture network and based on the field data such as the water or gas percentage and the pressure depletion curve, the flowing state can be evaluated, and the optimal exploitation scheme can be determined.

The gas-water ratio is a critical and fundamental parameter. Different gas-water ratios will lead to different flow structures such as bubble flow, slug flow or stratified flow, and correspondingly lead to different influences of viscosity and capillary pressure. Therefore, there will be different pressure drop characteristics [Reimann and Seeger, 1986; Fourar and Bories, 1993]. This is also confirmed in our numerical study in Chapter 4. However, the diversity of two-phase models and experimental results in fractures indicates that a more generalized model to describe the multiphase behavior is still absent. Fundamental problems, such as whether the contributions of viscous force or capillary pressure dominate the flow in different kinds of fractures, still require to be investigated.

In addition, many present studies on the two-phase flow in fractures were carried out in a single fracture, while the two-phase flow behavior in combined fractures or fracture network still require to be further investigated. On the distribution characteristics of gas-water two-phase flow, many studies have been conducted in T-junctions [Azzi et al, 2010; Wang et al, 2011; He et al, 2011; Chen et al, 2012], and the distribution of water and gas is influenced by the effect of inertial effect and gravity [Bhagwat and Ghajar, 2017; Liu et al, 2017]. It is reported that gas and water can be separated due to the difference of inertial effects [Tabe et al, 2009; Seeger et al, 1986; Bhagwat and Ghajar, 2017; Mohamed et al., 2011]. Small bubbles or solid particles are more likely to be carried by fluid flow, while large bubbles or solid particles are likely to deviate from the streamline of the fluid, and small bubbles or slug bubbles show different inertial effects [Li et al, 2017; Kim and Lee, 2015; Chen et al, 2013; Sun et al, 2018]. Therefore, the gas-water ratio plays an important role in two-phase flow behavior. Inertia separator is developed based on this mechanism, and in fractures, it is indicated that the inertial effect cannot be neglected in many conditions [Radilla et al, 2013; Fourar and Lenormand, 1998], so such effects still require to be quantitatively investigated. In addition, the flow characteristics in single fractures and fracture intersections provide basis for deeply understanding the fluid flow behavior in the fracture networks. The fractures can intersect at different angles. The intersecting angle is a critical parameter that influences the flow characteristics because the fluid is redistributed at the intersection. Li et al. [2016] studied the influence of the intersecting angle on nonlinear flow at fracture intersections. They reported that the larger intersecting angle results in the stronger nonlinearity of flow regimes. The phase separation is influenced by the intersecting angle between the two outlets due to the

different inertias of the phases. Therefore, the influence of intersecting angle should be investigated.

In the present study, a series of two-phase flow tests were conducted in artificial smooth intersecting fractures with the developed experimental system. Then the influence of different gas-water ratios, fracture intersecting angles, and gas injection positions on the gas and water distributions was analyzed. This experiment simulates the evolution of water flow rate with respect to different gas desorption rates in coal seams, with the expectation that by evaluating the water flow rate the gas desorption state can also be forecast. This experiment provides a basis for further studies to understand the distribution of gas and water in the two-phase flow in fracture networks.

6.2 Experimental study on the distribution of two phases

6.2.1 Experimental system

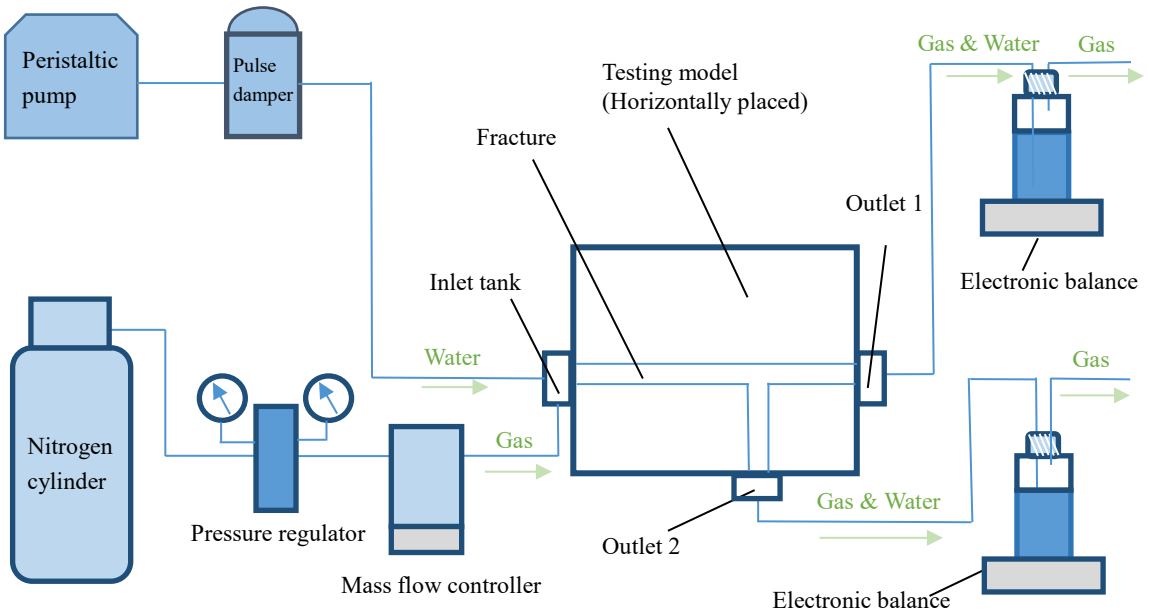

Fig. 6-1 The experimental system

In order to investigate two-phase fluid flow behavior through intersecting fractures, an experimental system was developed. It consists of three main subsystems: the fluids supply subsystem, the fracture model and the data measurement subsystem. The detailed schematic of the experiment system is shown in Fig. 6-1. Gas (Nitrogen) is supplied from the gas cylinder, in which the initial gas pressure is about 15 MPa. Since the mass flow

controller which was connected to the cylinder cannot bear the pressure over 1 MPa, the pressure is decreased to the range of 0.1-0.3 MPa with a pressure regulator. With the mass flow controller, gas was injected into the testing model with a constant flow rate in a range of 0-2000 mL/min. Gas injection rate can be displayed on the digital screen of mass flow controller. Water was injected with a peristaltic pump with a constant flow rate. In this experiment, water was injected with 500 mL/min, 700 mL/min, 900 mL/min, 1100 mL/min. Gas and water were injected into the inlet tank of the fracture model simultaneously, and flowed out from the two outlet tanks, which are named as Outlet 1 and Outlet 2, respectively. At the two outlets, gas was released to the atmosphere while water was collected in a bottle and the weight of water was measured by an electronic balance. The data of water mass in each bottle was transmitted into the computer in real-time. Consequently, the water flow rate can be obtained.

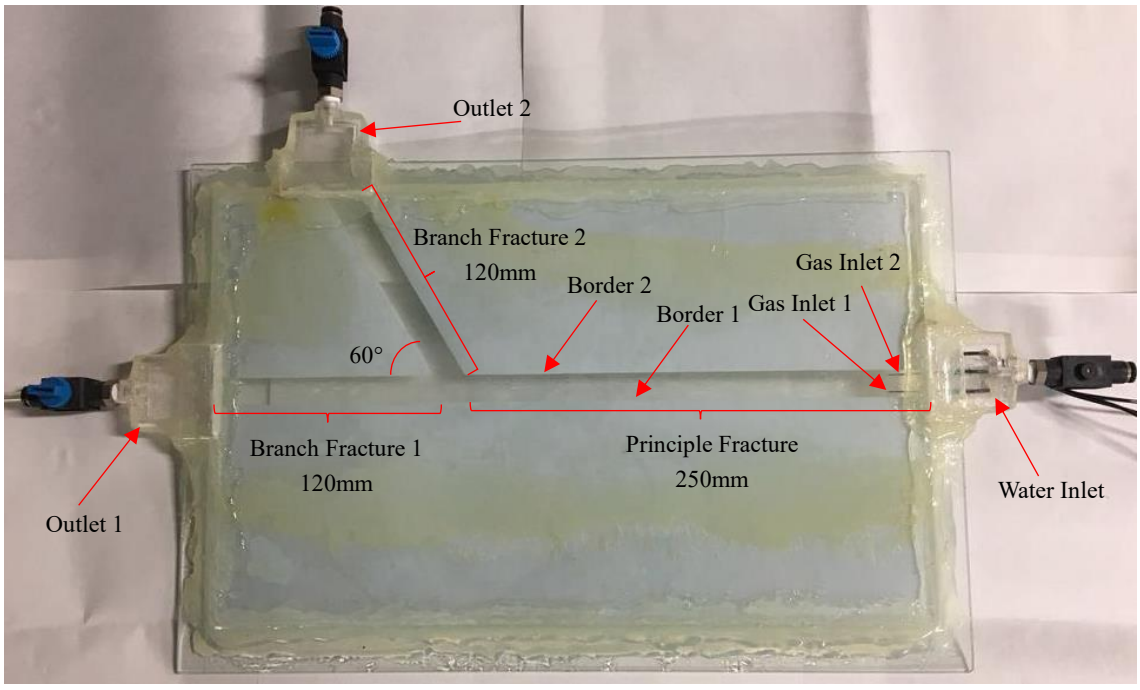

Fig. 6-2 The testing model with fracture intersecting angle of 60°

Three testing models were manufactured with toughened glasses and resin plates. In each model, two fractures intersect at a certain angle (30°, 60° or 90°). Fig. 6-2 shows the testing model in which fractures intersect at 60°. Each testing model consists of three layers. Two toughened glasses were used as upper and lower layers, respectively, for purpose of visual observation. Resin plates with a thickness of 1 mm was set as the middle

layer. The resin plates have three separate parts to form an artificial fracture with a thickness of 1 mm. The aperture of the fractures is 15 mm. Compared with the aperture of natural fractures, the adopted aperture in the experiment is larger for the purpose of visually observing the two-phase flow phenomenon within the void spaces of a fracture. If the fracture aperture is in the natural scale, i.e., 0.01 ~ 1 mm, it is quite difficult to capture images of fluid flow and bubble distributions using the current visualization techniques. However, we accept that to simulate the real two-phase flow at the fracture intersection, the fracture that has a real-scale aperture should be used. Therefore, in the future works, we will investigate the influence of fracture aperture size on the two-phase flow behaviors.

Here we define the Principle Fracture, Branch Fracture 1 and Branch Fracture 2, as indicated in Fig. 2. In each model, both Branch Fracture 1 and Branch Fracture 2 has a length of 120 mm to achieve identical conductivity in two branch fractures. The principle fracture has a length of 250 mm. The only difference between these testing models is the intersecting angle, while all the other sizes are identical. Grease were coated on the resin to restrain the water and gas from flowing into the areas beyond the fractures. At the boundaries of the testing model, silicone sealant was used to fix the glasses and the plate, and it is also for sealing up the model. Near the water inlet tank, there were two needles with an inner diameter of 0.8 mm acting as gas inlets, as shown in Fig. 2. This is designed to estimate the influence of gas injection positions on the water and gas distribution. The two boundaries of the principle fracture are designated as Border 1 and Border 2, respectively.

6.2.2 The testing procedures

If the testing model was not horizontally placed in the test, the two outlets will be of different elevations, and the flow rates of liquids will be seriously influenced. Consequently, prior to the flow test, the testing model was horizontally laid, and the horizontality was checked with a level gauge. In each testing model, Branch Fracture 1 and Branch Fracture 2 have the same fracture thicknesses and widths. Therefore, theoretically they should have identical permeabilities if the inertial effects can be neglected when fluids transport at small velocity. To further test the horizontality, water was injected to the specimen at very small flow rates. The test results show that the flow

rates of water from 2 outlets were approximately identical, which indicate that the horizontality was enough.

After that, water was injected to the specimen at a constant flow rate of 500, 700, 900, 1100 mL/min, respectively. Nitrogen was injected with a constant flow rate in the range of 0-2000 mL/min. The gas flow rate of 0-2000 mL/min in this study corresponds to a superficial velocity of 0-2 m/s, and the water flow rate of 500-1100 mL/min corresponds to a superficial velocity of 0.55-1.2 m/s. The gas velocity and flow velocity are in the same order of magnitude as those reported in the literature. For example, to investigate the two-phase flow pressure drop characteristics in fractures, a gas superficial velocity of 0-5 m/s and a water superficial velocity of 0-0.41 m/s were adopted by Fourar and Bories [1995]. In each test round, the flow of two different phases of fluid was kept for 1-2 min to achieve a stable flow state prior to the measurement of flow rates in each outlet.

6.3 Quantification of the phase distribution

According to the testing results, the distribution of water in the two outlets was seriously influenced when gas was injected at different rates. On the other hand, the water injection rate also had an impact on the distribution of gas in the two outlets. In this study, the evolution of water flow rates in the two outlets was quantitatively measured and analyzed along with the gas flow structures which were qualitatively measured with the visualization photos. The 60°-model is firstly selected as an example for analyzing the effect of the gas injection rate.

6.3.1 The effect of gas injection rate

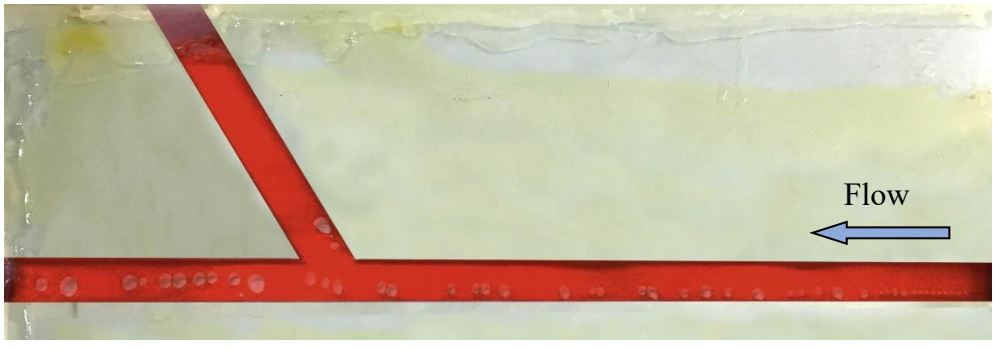

(a) *Gr*=100 mL/min

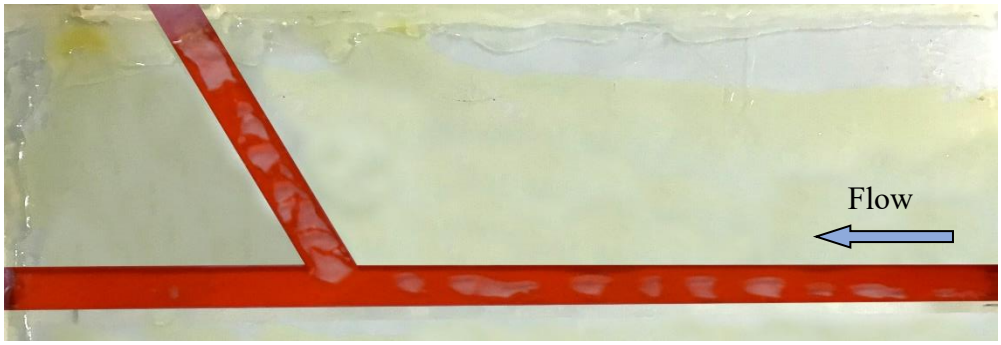

(b) *Gr*=500 mL/min

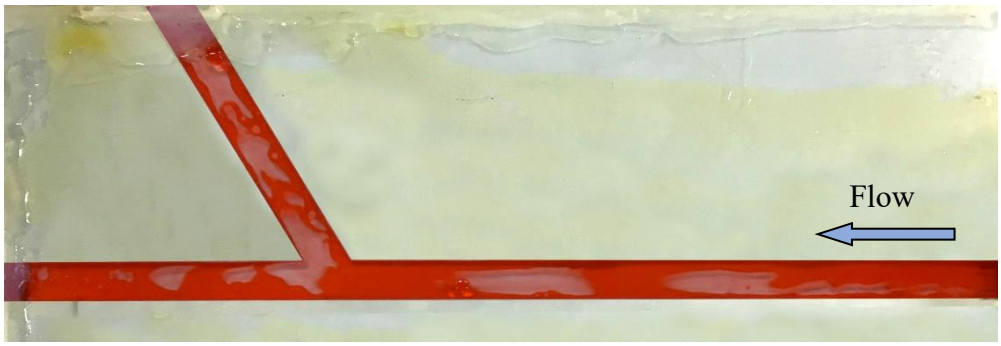

(c) *Gr*=1000 mL/min

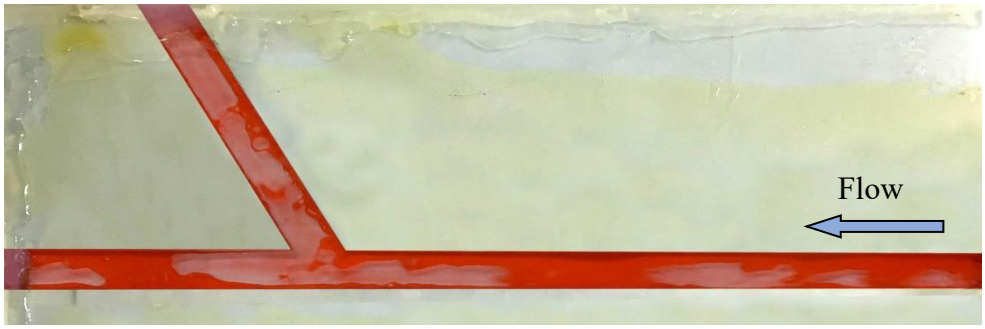

(d) *Gr*=2000 mL/min

Fig. 6-3 The flow structures at the water injection rate of 1100 mL/min with gas injected from Gas Inlet 1

Fig. 6-3 shows the cases in which water was injected at 1100mL/min and gas was injected from Gas Inlet 1. The gas injection rate was increased step by step. The evolution of the flow characteristics can be divided into 3 stages. In the first stage, gas was injected at a small rate, as shown in Fig. 6-3(a). Gas bubbles transported at a stable state, and the morphology of gas bubbles was regular. This indicates that the turbulence was not serious, which is similar to the laminar state in single-phase flow. Since gas was injected from Gas Inlet 1 which is close to Border 1, the gas bubbles flowed along the Border 1 of the principle fracture, and consequently almost all the gas transported to Branch Fracture 1.

Therefore, more water was driven to Branch Fracture 2. Corresponding to the transport of gas in this stage, the transport characteristics of water can be indicated in Fig. 6-8. As shown in Fig. 6-8(a), gas was injected from Inlet 1, when water was injected at 500mL/min (*W*r=500), the water flow rate in Outlet 1 decreased when gas injection rate increased from 0 to 100 mL/min. This is because all the gas bubble transported into Branch Fracture 1 and more water was driven into Branch Fracture 2. That's why the water flow rate in Outlet 2 increased as indicated in Fig. 6-8(b), while the water flow rate in Outlet 1 decreased as indicated in Fig. 6-8(a). When gas was injected from Gas Inlet 2, gas totally flow into Outlet 2, as shown in Fig.4(a); water flow rate in the Outlet 1 increased with respect to the increase of gas injection rate, as shown in Fig. 6-8(a). This is totally contrary to the case when gas was injected from Gas Inlet 1.

To summarize, gas transported stably as small bubbles in this stage. The turbulence was not serious, which was similar to the laminar flow. The difference in gas injection positions would lead to totally contrary flow conditions of both water and gas: when gas was injected from different positions, the gas bubbles flowed into different branch outlets (Fig. 3a and Fig. 4a), and the water flow rates in Outlet 1 (Fig. 7a) would also evolve in opposite trends, as well as that in Outlet 2 (Fig. 7a).

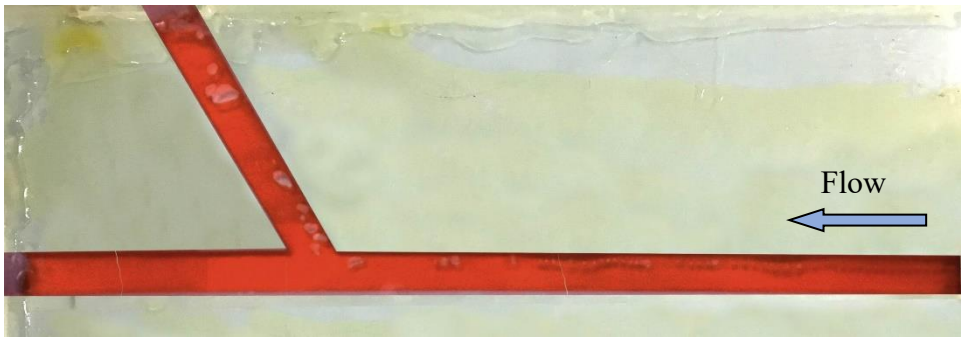

(a) *G*r=200 mL/min

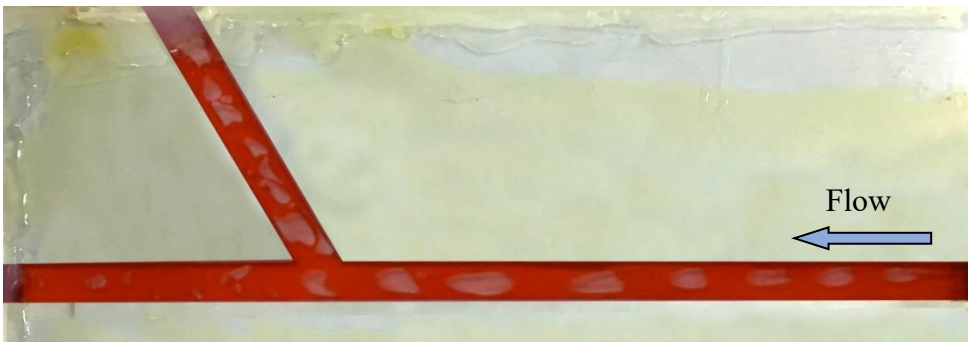

(b) *G*r=500 mL/min

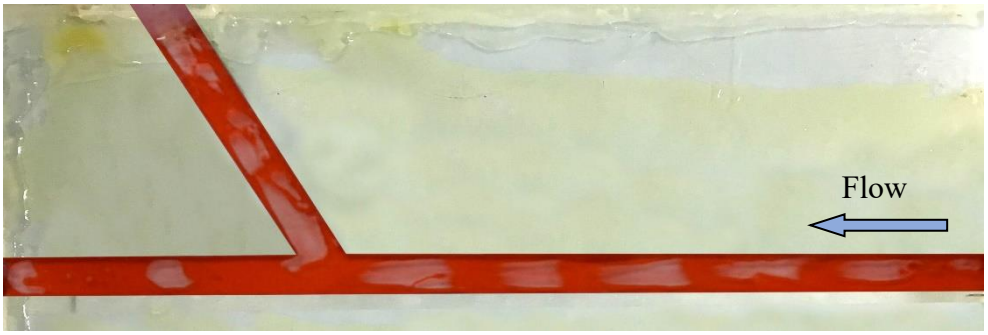

(c) *G*r=1000 mL/min

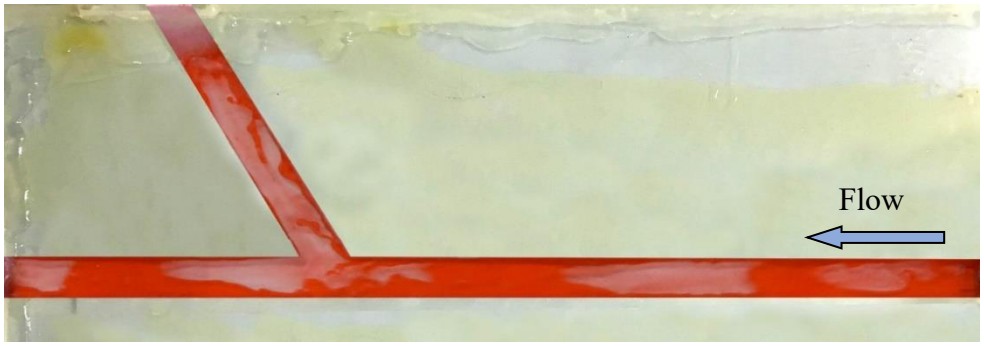

(d) *G*r=2000 mL/min

Fig. 6-4 The flow structures at the water injection rate of 1100 mL/min with gas injected from Gas Inlet 2

In the second stage, because gas was injected with a lager rate, larger bubbles were formed, as shown in Fig. 6-3(b) and Fig. 6-4(b). By comparing Fig. 6-3(b) and Fig. 6-4(b), it can be indicated that no matter gas was injected from Gas Inlet 1 or Gas Inlet 2, almost all gas bubbles transported into Branch Outlet 2, which is quite different from the first stage. Correspondingly, as shown in Fig. 6-8(a), when water flow rate was 500 mL/min, when the gas injection rate was increased from 300-900 mL/min, the evolution of water flow rate (with gas injected from Gas Inlet 1) was identical to the evolution of water flow rate (with gas injected from Gas Inlet 2). In Fig. 8(b), the same phenomenon is indicated. In this stage larger bubbles were formed, and the morphology of gas bubbles was no longer regular. The turbulence became significant due to the drastic interactions between water and gas, and consequently the gas bubbles no longer remained close to the border. The distribution of water and gas was dominated by the different inertias of water and gas. Both Fig. 6-3(b) and Fig. 6-4(b) show that almost all the gas transported to Branch Fracture 2. In such conditions, the reason why most gas bubbles moved into Branch Outlet 2 is that the density of water is about 800 times as that of gas, and thus

there is a significant difference in the inertial effects. In such conditions, water, the liquid with a larger inertial effect, would be more likely to transport into Branch Outlet 1, which is connected to the principle fracture without diversion angle, and drove gas into Branch Outlet 2.

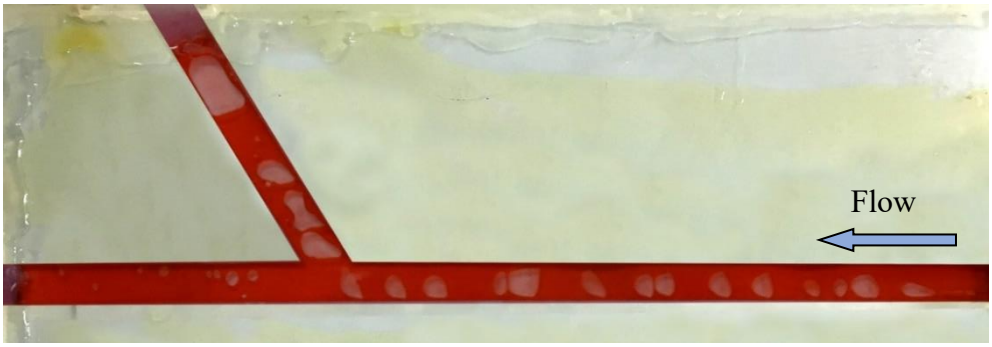

(a) *Gr*=200 mL/min

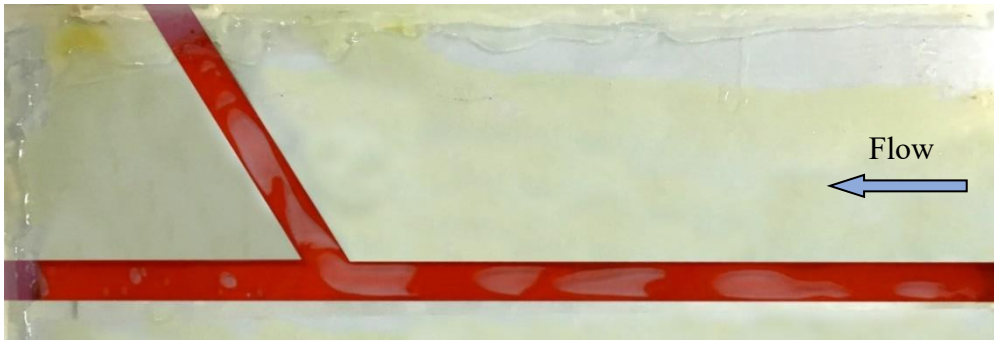

(b) *Gr*=500 mL/min

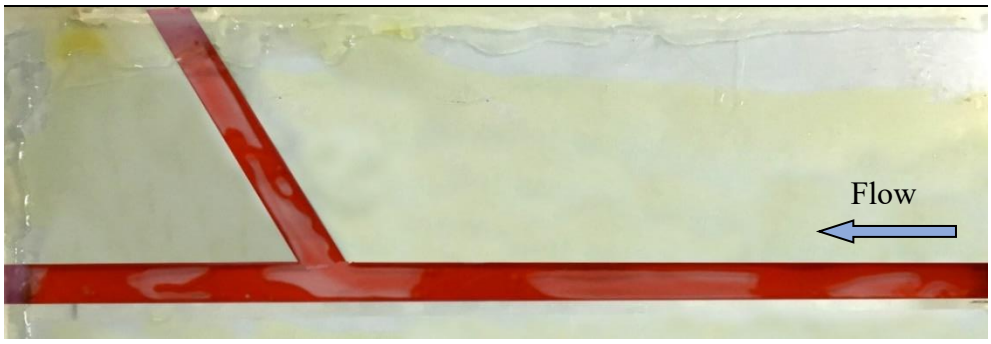

(c) *Gr*=1000 mL/min

Fig. 6-5 The flow structures at the water injection rate of 500 mL/min with gas injected from Gas Inlet 1

To summarize, in this stage the transport of water and gas was quite turbulent with serious interactions between water and gas. The distribution of water and gas was dominated by the different inertias between water and gas, and the gas injection positions

didn’t take much effect on the water and gas distribution when the water flow rate was small.

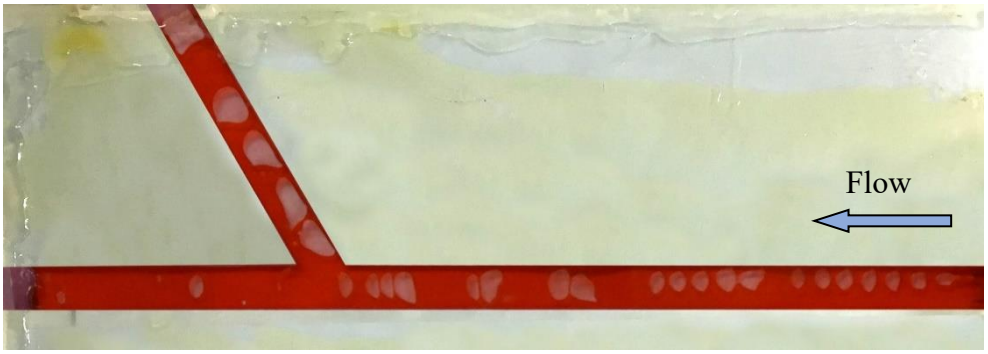

(a) *Gr*=200 mL/min

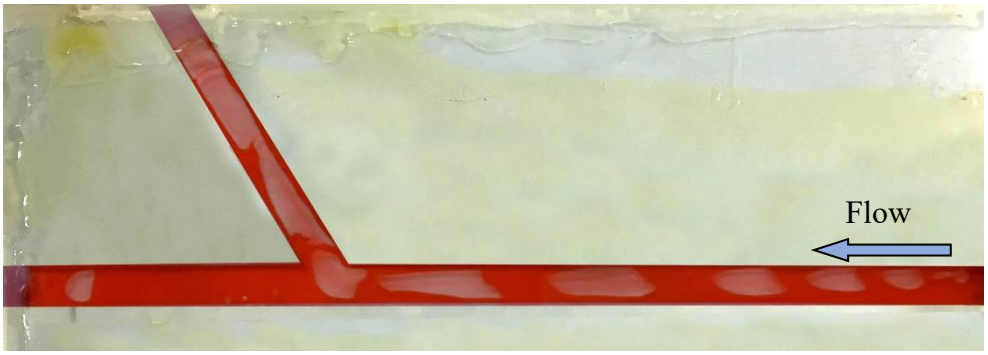

(b) *Gr*=500 mL/min

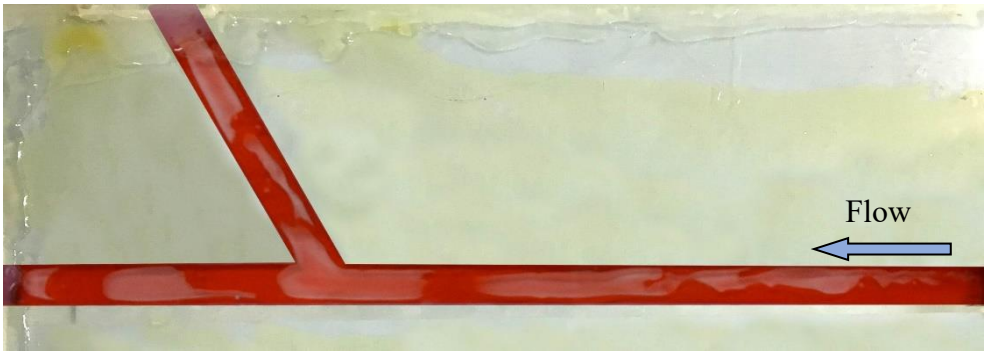

(c) *Gr*=1000 mL/min

Fig. 6-6 The flow structures at the water injection rate of 500mL/min with gas injected from Gas Inlet 2

In the third stage, because gas injection rate was further increased, slug bubbles were formed, as shown in Fig. 6-3(c), Fig. 6-3(d), Fig. 6-4(c) and Fig. 6-4(d). The gas injection rate was larger, and the flow of both water and gas was more turbulent, and there are many factors that influence the distribution of water and gas. The distribution of gas into two

outlets became more even, but it's still that more gas transported to Branch Fracture 2, indicating that the effect of different inertias on distribution was still important. By comparing Figs. 6-3(b), 6-3(c) and 6-3(d), it can be noticed that the flow structures evolved from bubble flow to slug flow, and the percentage of gas that transported into Branch Fracture 1 also increased, meaning that the distribution behavior was also influenced by the flow structures. The evolution of the water flow rates in two outlets went into a stable state when gas injection rate increased from 1000 to 2000 mL/min, as shown in Fig. 6-8(a) and Fig. 6-8(b). Different from that in the second stage, the difference between the cases in which gas was injected from different positions became obvious. This means that in this stage, though the effect of different inertias was still important, some other factors also had influence and lead to this difference if gas was injected from different gas injection inlets.

The results of 30°-model and 90°-model also show same evolution process, as shown in Fig. 6-7 and Fig. 6-9.

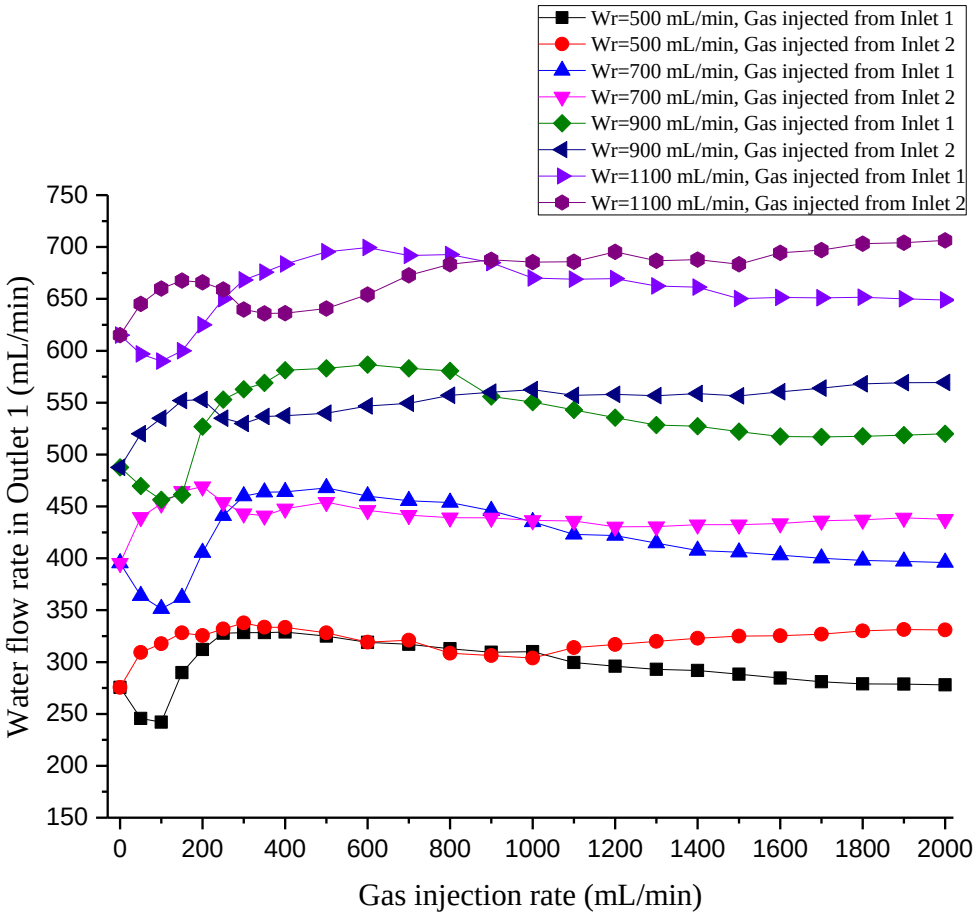

Fig. 6-7(a) The water flow rate in Outlet 1 in the 30° testing model

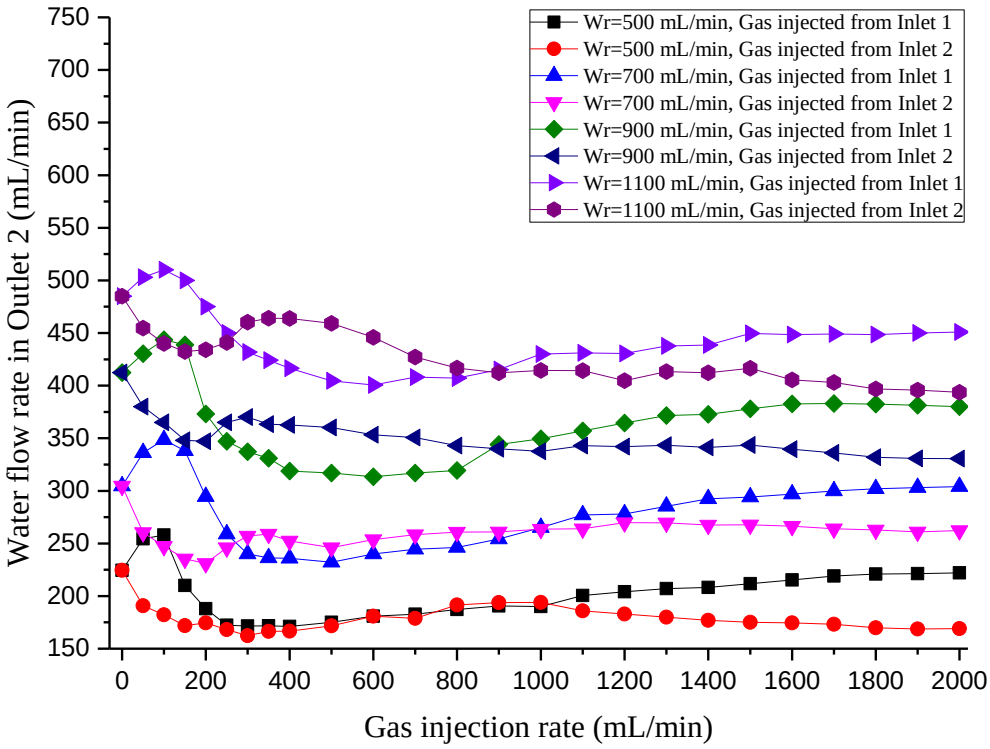

Fig. 6-7(b) The water flow rate in Outlet 2 in the 30° testing model

6.3.2 The effect of water injection rate and fracture intersecting angle

The 90°-model is selected as an example for analyzing the effect of water injection rate. Fig. 6-9(a) shows the evolution of water flow rate in Outlet 1 when water was injected with different injection rates at the water inlet, and Fig. 6-9(b) shows that in Outlet 2. As mentioned above, the evolution of gas and water in each outlet can be divided into three stages. It can be indicated in Fig. 6-9(a) and Fig. 6-9(b) that no matter water was injected at which rate (500 mL/min, 700 mL/min, 900 mL/min, 1100 mL/min), the evolution of the water flow rate in Outlet 1 or Outlet 2 always has these three stages. But at different water injection values, some differences can be noticed. In the second stage, as shown in Fig. 9(a), when water was injected at 500 mL/min, the difference between the cases when gas was injected from different positions can be neglected. When water was injected at 700 mL/min, this difference became larger but still not significant. When water was injected at 900 mL and 1100 mL, this difference became obvious. This is because in the second stage, when water was injected at small rates, such as 500 mL/min, the distribution of water and gas is dominated by the different inertias between water and gas, as

mentioned previously. When the water injection rate went higher, the flow became more turbulent and some other factors took more effect which would lead to such a difference. In the third stage, despite that water was injected at different rate, the difference between

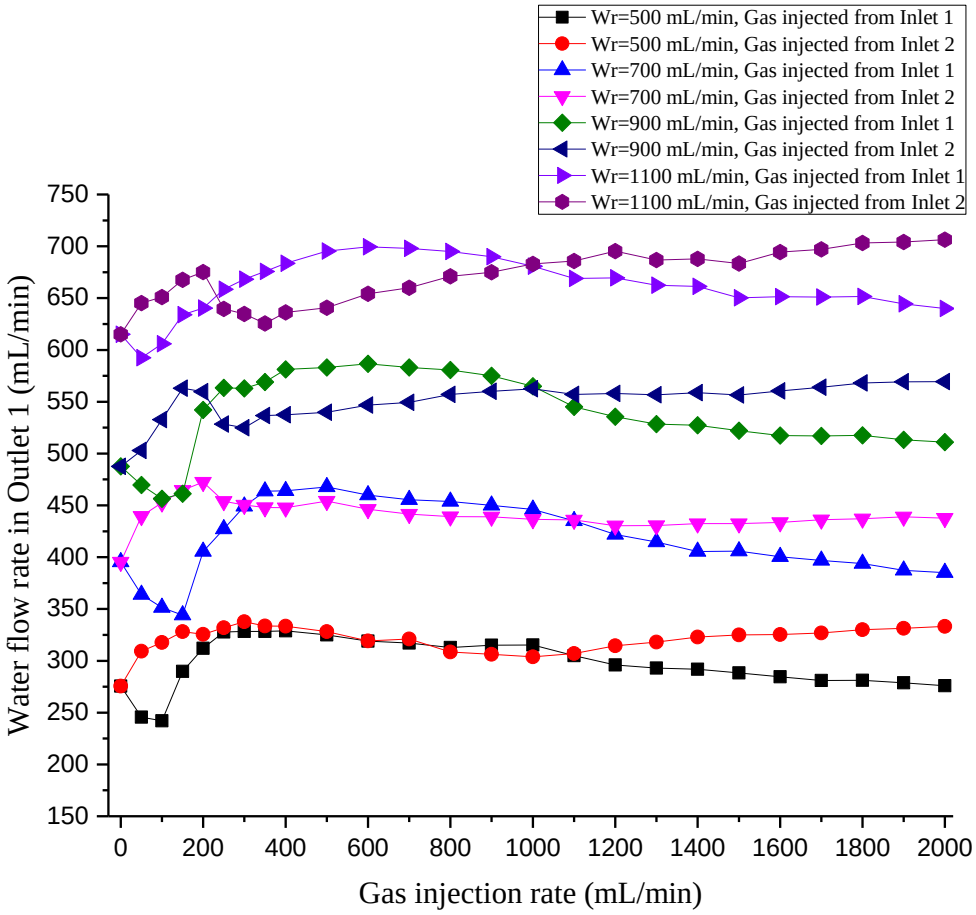

Fig. 6-8(a) The water flow rate in Outlet 1 in the 60° testing model

each case in which gas was injected from different positions was similar.

By comparing Figs. 6-7, 6-8 and 6-9, it can be noticed that with the increase of intersecting angle, there is some difference in the evolution of water flow rates in the outlets. As mentioned above, the evolution of water flow rates in the two outlets can be divided into three stages. As indicated by Fig. 6-7, for the 30°-model, in the cases of *Wr* = 500 mL/min and *Wr* = 700 mL/min, when the gas injection rate passed 900 mL/min, the flow of water transferred from the second stage to the third stage. For *Wr* = 900 mL/min and *Wr* = 1100 mL/min, this transferring point is 1000 mL/min. For the 60°-model, in the cases of *Wr* = 500 mL/min and *Wr* = 700 mL/min, this transferring point is 1000 mL/min. For *Wr* = 900 mL/min and *Wr* = 1100 mL/min, this transferring point is

1100 mL/min. For the 90°-model, in the cases of Wr = 500 mL/min and Wr = 700 mL/min, Wr = 900 mL/min and Wr = 1100 mL/min, this transferring point is 1200 mL/min. This indicates that with the increase of the intersecting angle of fractures, the transferring point of the gas injection rate, which indicates the transfer from the second stage to the third stage, would increase. This is because the second stage is dominated by the inertial effect of water and gas. With a lager intersecting angle of the two fractures, the difference of the inertial effects between phases will play a more significant role. Consequently, the second stage would be extended in the model with a larger fracture intersecting angle since the second stage is inertial effect dominated.

Actually, the mentioned factors which would influence the distribution of water and gas into two outlets, including the gas injection rate, water injection rate, gas injection positions, fracture intersecting angle etc., are coupled with each other, meaning that any variation in one factor will contribute to changes in the magnitudes of the influence by the other factors. It has to be addressed that this study is a preliminary study for the distribution of two flowing phases through two intersecting fractures using the newly-

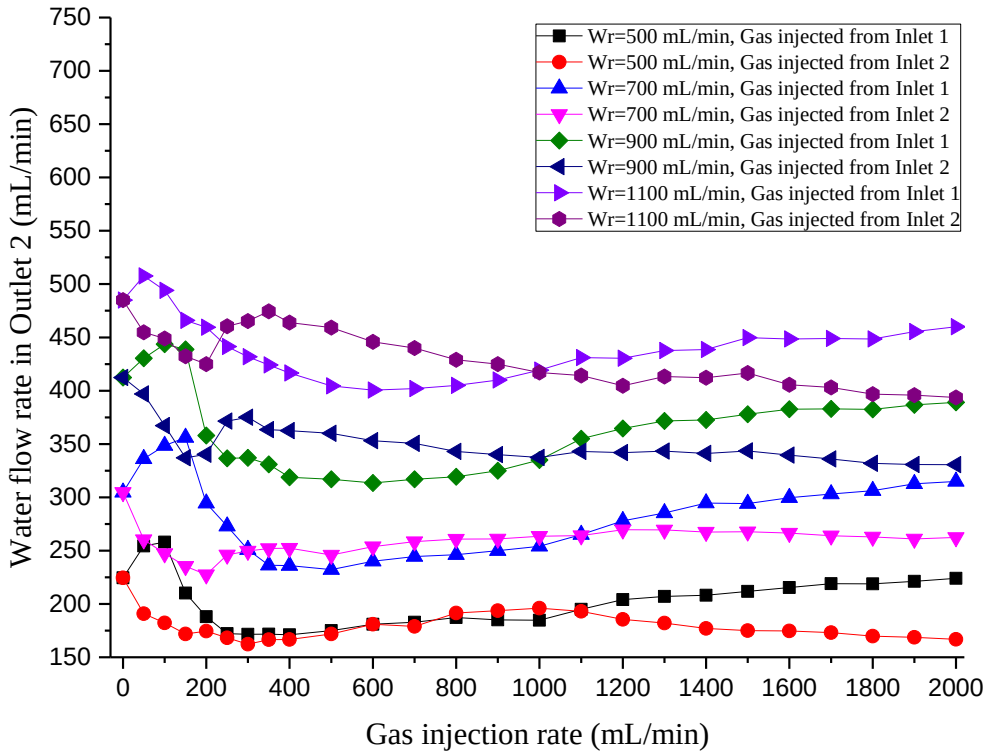

Fig. 6-8(b) The water flow rate in Outlet 2 in the 60° testing model

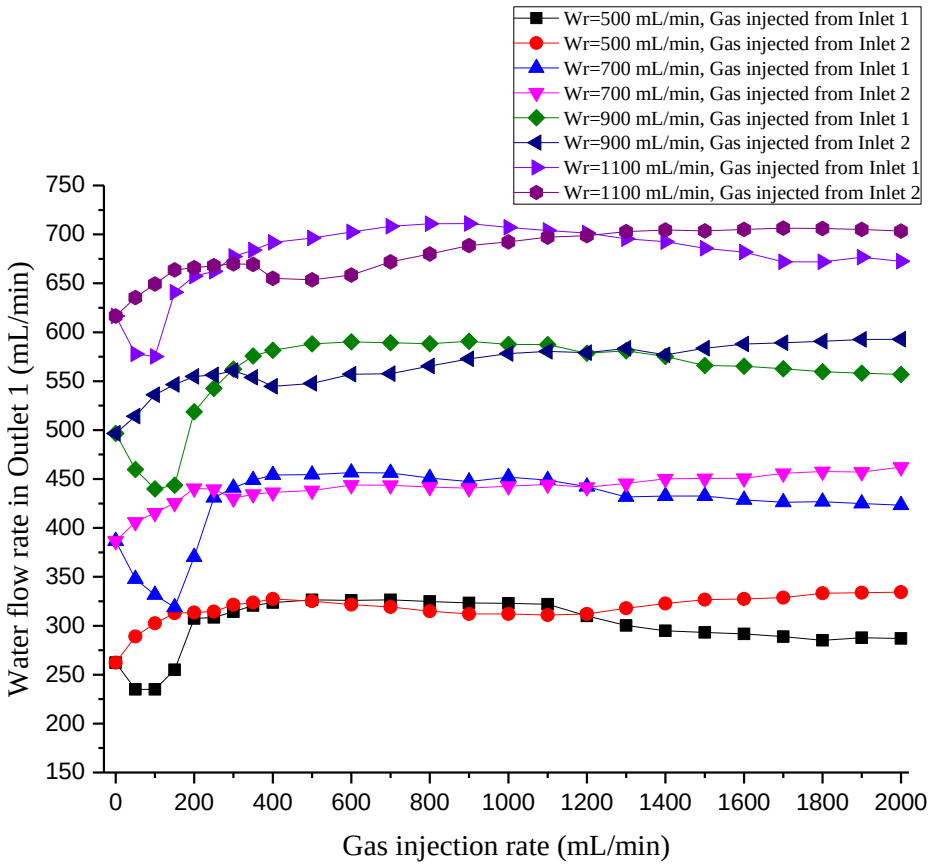

Fig. 6-9(a) The water flow rate in Outlet 1 in the 90° testing model

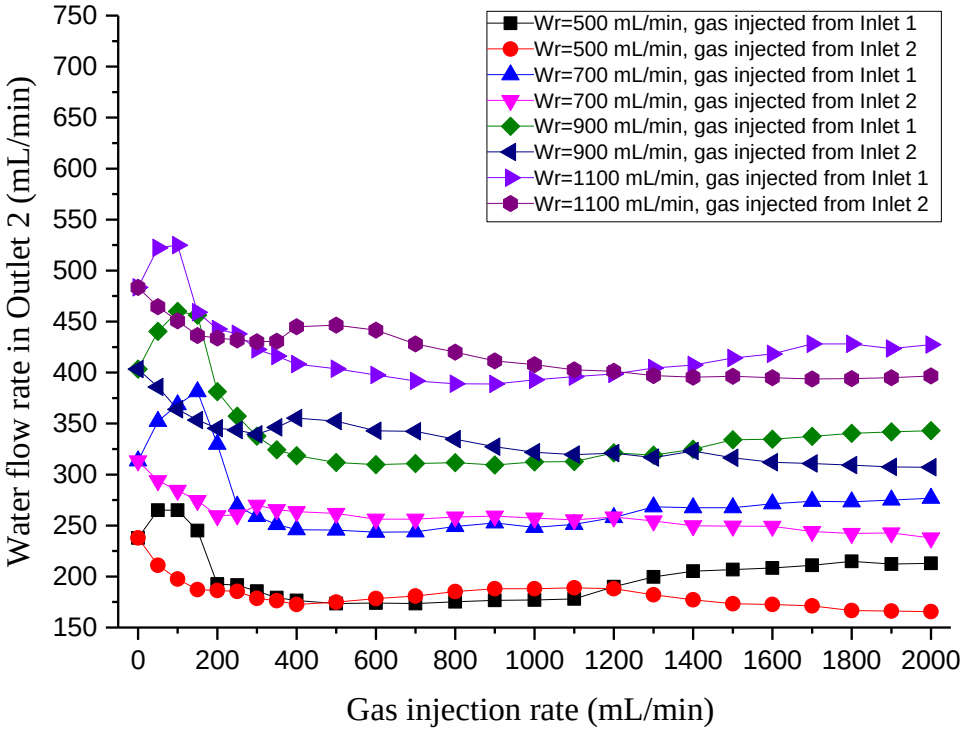

Fig. 6-9(b) The water flow rate in Outlet 2 in the 90° testing model

developed visualization testing system of two-phase fluid flow. In the present study, the reason why the flow has three stages is that different physical effects take turns to be the dominate factors, so in future studies we will focus on the quantitative analysis of different physical factors including the inertial effect, the viscous effect, the capillary pressure etc. to seek more accurate quantitative description methods for describing such flow phenomenon.

6.4 Summary

With the developed visual experimental system, the two-phase flow through different intersecting fractures at different water and gas injection rates is investigated. The results can be concluded as following.

With gas and water injected at different rates, the flow of both water and gas can be classified into three stages. In the first stage, gas flowed at small bubbles, and the transport of gas and water was stable. The turbulence was not serious, which is similar to the single-phase laminar. The difference in gas injection positions would lead to totally contrary flow conditions of both water and gas: when gas was injected from different positions, the gas bubbles flowed into different branch outlets, and the water flow rate in Outlet 1 or Outlet 2 would also evolve in opposite trends.

In the second stage, because larger bubbles were formed, and the turbulence became significant due to the drastic interactions between water and gas. The difference of the inertial effects between water and gas dominates the distribution of water and gas. In such conditions, most gas bubbles transported into Branch Outlet 2 and drove more water into Branch Outlet 1. In this stage, the difference in the gas injection positions did not take much effect on the water and gas distribution.

In the third stage, the turbulence became more significant and the interactions between water and gas were more serious. Though the effect of different inertias was still important, some other factors also became to taking more effect. The difference of the gas injection positions would lead to different evolution curves of water flow rates in each outlet.

The water injection rate also has impact on the distribution of the water flow rate in each outlet, particularly in the second stage. In the second stage (gas injection rate between 200 to 1000 mL/min), when water was injected in small flow rates (500 mL/min,

700 mL/min), the difference between the cases in which gas was injected from different positions can be neglected. When the water was injected in larger flow rates (900 mL/min, 1100 mL/min), this difference became obvious. This indicates the transformation from an inertial effect dominated process to a multi-effect influenced process. The intersecting angle of the fractures also influences the distribution of water and gas. The larger the intersecting angle, the larger the inertial effect will be. Consequently, the intersecting angle influences the range of the second stage, which is dominated by the inertial effect.

The factors which influence the distribution of water and gas into two outlets, including the gas injection rate, water injection rate, gas injection positions, fracture intersecting angle etc., are coupled with each other, meaning that any variation in one factor will contribute to changes in the influence magnitudes of the other factors, so in future studies more accurate quantitative description methods for such flow phenomenon are supposed to be developed.

Chapter 7 Conclusions and Future Work

7.1 Conclusions

This research has investigated the hydraulic characteristics of two-phase flow in fractures with both experiments and numerical simulation. It is composed of two aspects: studies in the single fracture and the intersecting fracture, which aims at forms basis for studying the two-phase flow in the fracture network.

First, we developed an experimental system. The two-phase flow box is the core element in this system, which can seal up the specimens without using glue. With this flow box, we conducted the experiments in both a smooth fracture specimen and a rough fracture specimen. The results show that the flow structures in the smooth fracture are similar to that of two-phase flow in pipes; while the flow structures in the rough fracture show more similarity to that in porous media, namely that the flow structures didn't experience much change with respect to different gas-water ratios; both water and gas tend to flow in their own channels. The two-phase pressure drop in the rough fracture is dominated by both the capillary effect and the inertial effect. The relative permeability is not only the function of saturation, but also the function of flow velocities. This is found by the results that curves with different water flow rates fail to fall on the same curve. The Lockhart-Martinelli model is also applicable to the test results. For the smooth fracture, all the groups of data with different water flow rates fall on the same curve; while in the rough fracture, the value of C changes with respect to the gas flow rate, which means that the flow regime was changing. In addition to that, the increase of water flow rate also leads to the increase of turbulence of two-phase flow. To conclude, the pressure drop characteristics of two-phase flow in the single fracture is influenced by multiple factors, and the flow turbulence and two-phase interference in the rough fracture are more likely to be influenced by the flow rates of water and gas than that in the smooth fracture.

Since there are multiple factors that influence the two-phase flow in the experiment in the single fracture, we tried to quantify the effect of one certain factor—the role of capillary pressure. We established a 2D numerical model with the level set method. The simulation is conducted in a randomly rough fracture, which is generated with cosine function series. The simulation results show that the evolution of saturation with respect to phase velocity is different, which depends on the flow structures. This is because the

influence of capillary pressure differs in different flow structures; the impact of capillary pressure is more significant in bubble flow than in continuous flow since in the bubble flow there are more phase interfaces. In addition, Corey model can work well in the two-phase flow in this simulation. However, the relative permeabilities of both phases are not only the function of saturation, but also the function of flow velocities. This is because the influence of the capillary pressure is different at different flow structures. When both phases become continuous flow, they flow in their respective channels and show least phase interference, which is similar to the two-phase flow in porous media.

Besides the flow in the single fracture, the two-phase flow in the intersecting fracture is also a critical step for understand the two-phase flow behavior in the fracture network. Consequently, a water-gas two-phase flow experiments were conducted in the 3D intersecting fracture model. The testing results shown that: at a certain water flow rate, the two-phase pressure drop increases nonlinearly with respect to the gas flow rate. It is believed that this nonlinearity is induced by the strong inertial effect in the intersecting fracture. The Martinelli-Lockhart model is no only effective for describing the two-phase flow in single fractures, but also for the two-phase flow in intersecting fracture. Because the Martinelli-Lockhart model considers the inertial forces, which is quite serious in the intersecting fracture, the good fitting results are obtained.

The phase distribution behavior at the fracture intersection is also important for understanding two-phase flow process in the fracture network. With the developed experimental system, the two-phase flow experiment through different intersecting fractures was conducted. The results show that with gas and water injected at different rates, the flow of both water and gas can be classified into three stages. In the first stage, gas flowed at small bubbles, and the transport of gas and water was stable. The turbulence was not serious, which is similar to the single-phase laminar flow. In the second stage, because larger bubbles were formed, and the turbulence became significant due to the drastic interactions between water and gas. The difference of the inertial effects between water and gas dominates the distribution of water and gas. In the third stage, the turbulence became more significant and the interactions between water and gas were more serious. Though the effect of different inertias was still important, some other factors also became to taking more effect. The intersecting angle of the fractures also influences the distribution of water and gas. The larger the intersecting angle, the larger the inertial

effect will be. Consequently, the intersecting angle influences the range of the second stage, which is dominated by the inertial effect.

7.2 Recommended future studies

The factors which influence the two-phase flow are multiple, and they are coupled with each other, meaning that any variation in one factor will contribute to changes in the influence magnitudes of the other factors, so in future studies more accurate quantitative description methods are supposed to be developed. The numerical model in our simulation only considers the effect of capillary pressure, which is created for quantifying the capillary effect. In the future, a more general model should be established.

The evolution patterns of both saturation and relative permeability are related to the fracture morphology. This means that the relative permeability models should not only be the function of saturation, but also the function of the morphology parameters (such as JRC and fracture aperture distribution parameters) of a rough fracture. This is going to be further investigated in the future works.

In the field of two-phase flow in the intersecting fracture, the hydraulic characteristics, such as the phase multipliers in the Lockhart-Martinelli model, Φ_w and Φ_g are believed to be related to the parameters of the intersecting fracture, such as the intersecting angle, the aperture of each individual fracture that constitutes the intersecting fracture. Further researches are to be extended in these aspects.

Based on the establishment of appropriate models for both single-phase fracture and intersecting fracture, it is expected that a general model for describing two-phase flow in the fracture network can be established in the future.

References

Azzi A, Al-Attiyah A, Liu Q, Cheema W, Azzopardi B J. Gas–liquid two-phase flow division at a micro-T-junction. *Chemical Engineering Science*, vol.65, no.13, pp.3986-3993, 2010.

Babadagli T, Ren X, Develi K. Effects of fractal surface roughness and lithology on single and multiphase flow in a single fracture: an experimental investigation. *International Journal of Multiphase flow*, vol.68, pp.40-58, 2015.

Bachu S and Bennion B. Effects of in-situ conditions on relative permeability characteristics of CO2-brine systems. *Environmental geology*, vol.54, pp.1707-1722, 2008.

Bhagwat S M and Ghajar A J. Experimental investigation of non-boiling gas-liquid two phase flow in downward inclined conduit. *Experimental Thermal and Fluid Science*, vol.89, pp.219-237, 2017.

Brennen C E. Fundamentals of multiphase flows. Cambridge University Press. 2005.

Brooks R and Corey A. Hydraulic properties of porous media. Hydrology Paper No.3, Colorado State University, Fort Collins, 1964.

Chen C Y. Liquid-Gas Relative Permeabilities in Fractures: Effects of Flow Structures, Phase Transformation and Surface Roughness. Stanford University, 2005.

Chen J, Wang S, Cheng S. Experimental investigation of two-phase distribution in parallel micro-T channels under adiabatic condition. *Chemical Engineering Science*, vol.84, no.24, pp.706-717, 2012.

Chen J, Wang S, Ke H, Cai S and Zhao Y. Gas–liquid two-phase flow splitting at microchannel junctions with different branch angles. *Chemical Engineering Science*, vol.104, pp.881-890, 2013.

Comsol, Use's Guide of the CFD module, 2011.

Corey A T. The interrelation between Gas and Oil Relative Permeabilities. *Producers Monthly*, pp.38-41, 1954.

Corey A T. Mechanics of immiscible fluids in porous media, *water resources publications*, Littleton, Colorado, 1986.

Dana E and Skoczylas F. Gas relative permeability and pore structure of sandstones, *International Journal of Rock Mechanics and Mining Science,* vol.36, no.5, pp.613-

625, 1999.

Delhaye J M, Giot M and Riethmuller M L. Thermohydraulics of two-phase systems for industrial design and nuclear engineering. McGraw-Hill, New York, 1981.

Detwiler R L, Rajaram H and Glass R J. Interphase mass transfer in variable aperture fractures: Controlling parameters and proposed constitutive relationships. *Water Resources Research*, vol.45, W08436, 2009.

Diomampo G P. Viscous Coupling in Two-phase flow in porous media and its effect on relative permeabilities. *Transport in Porous Media*, vol.11, no.3, pp.201-218, 1993.

Diomampo G P. Relative permeability through fractures. PhD. Dissertation, Stanford: Stanford University, 2001.

Fan L, Wang H and Ma G. An experimental apparatus and test method for two-phase flow in fracture network (in Chinese). China, 201710432090.5, 2017.06.09.

Feng W. Coalbed methane reservoir engineering. Beijing: Science Press, 2009.

Fourar M and Bories S. Two-phase flow in smooth and rough fractures: measurement and correlation by porous-medium and conduit flow models. Water resources research. vol.29, no.11, pp.3699-3708. 1993.

Fourar M and Bories S. Experimental Study of Air-Water Two-phase Flow Through a Fracture (Narrow Channel). *International Journal of Multiphase Flow*, vol.21, no.4, pp. 621-637,1995.

Fourar M and Lenormand R. A viscous coupling model for relative permeabilities in a fracture. SPE Annual Technical Conference and Exhibition, New Orleans, Louisiana, USA, 1998.

Fourar M and Lenormand R. Inertial effects in two-phase flow through fractures. *Oil and gas science and technology*, vol.55, no.3, pp.259-268, 2000.

Fumagalli A and Scotti A. A numerical method for two-phase flow in fractured porous media with non-matching grids. *Advances in Water Resources*, vol.62, pp.454-464, 2013.

Gilman J R and Kazemi H, “Improvements in simulation of naturally fractured reservoirs,” *Society of petroleum engineers Journal*, vol.23, no.4, pp.695-707, 1983.

Hauge V L and Aarnes J E. Modeling of Two-Phase Flow in Fractured Porous Media on Unstructured Non-Uniformly Coarsened Grids. *Transport in porous media*, vol.77, no.3, pp.373-398, 2009.

He K, Wang S, Huang J. The effect of flow pattern on split of two-phase flow through a micro-T-junction. *International Journal of Heat and Mass Transfer*, vol.54, no.15-16, pp.3587-3593, 2011.

Irmay S. On the theoretical derivation of Darcy and Forchheimer formulas. *Transactions American Geophysical Union*, vol.39, no.4, pp.702-707, 1958.

Ishii M and Hibiki T. Termo fluid dynamic of two-phase flow. Paris: Eyrollers. 2010.

Kim S and Lee S. Split of two-phase plug flow with elongated bubbles at a microscale branching T-junction. *Chemical Engineering Science*, vol.134, pp.119-128, 2015.

Kimura S. Geothermal energy development and multiphase flows. *Japanese Journal of Multiphase Flow*, vol.11, no.3, pp.11-14, 1997.

Kosakowski G and Berkowitz B. Flow pattern variability in natural fracture intersections. *Geophysical research letters*, vol.26, no.12, pp.1765-1768, 1999.

Li B, Liu R, Jiang Y. Influences of hydraulic gradient, surface roughness, intersecting angle, and scale effect on nonlinear flow behavior at single fracture intersections. *Journal of Hydrology*. vol.538, pp.440-453, 2016.

Li H, Li J, Zhou Y, Liu B, Sun B, Yang D and Fan X. Phase split characteristics of slug and annular flow in a dividing micro-T-junction. *Experimental Thermal and Fluid Science*, vol.80, pp.244-258, 2017.

Liang Y, Zhang Z, Chen J et al. A visualized experimental system for two-phase flow in fractured rocks. China, CN105547954A, 2016.05.04.

Liu, R, Li B and Jiang Y. Experimental and numerical study on hydraulic properties of 3-D crossed fractures, *Chinese Journal of Rock Mechanics and Engineering*, vol.A02, pp.3813-3821, 2016.

Liu Y, Sun W, Wu W, Wang S. Gas-liquid two-phase flow distribution in parallel micro-channels with different header and channels' orientations. *International Journal of Heat and Mass Transfer*, vol.112, pp.767-778, 2017.

Lockhart W and Martinelli R. Proposed correlation of data for isothermal two-phase, two-component flow in conduit, *Chemical Engineering Pro*gress, vol.45, no.1, pp.39-48, 1949.

Mahoney D and Doggandt K. Multiphase flow in fractures. *Proceedings of the Meanding of the Sociandy of Core Analysts*, Calgary, Canada.

Mohamed M A, Soliman H M and Sims G E. Experimental investigation of two-phase

flow splitting in an equal-sided impacting tee junction with inclined outlets. *Experimental Thermal and Fluid Science*, vol.35, no.6, pp.1193-1201, 2011.

Nuske P, Faigle B, Helmig R, Niessner J and Neuweiler I. Modeling gas-water processes in fractures with fracture flow properties obtained through upscaling. *Water Resources Research*, vol.46, no.9, pp.201-210, 2010.

Peitgen H-O and Saupe D (editors). The science of fractal images. Springer Science & Business Media, 2012.

Persoff P and Pruess K. Two-phase flow visualization and relative permeability measurement in natural rough-walled rock fractures. *Water resources research*, vol.31, no.5, pp.1175-1186, 1995.

Pruess K, and Tsang Y W. On two-phase relative permeability and capillarity in rough-walled rock fractures. Water Resour. Resources, 26(9), 1915-1926, 1990.

Pruess K, Bodvarsson G S, and Stefansson V. Analysis of production data from the Krafla geothermal field, Iceland. *Ninth workshop on Geothermal reservoir Engineering*, Stanford university, Stanford, California, 1983.

Radilla G, Nowamooz A and Fourar M. Modeling non-Darcian single- and two-phase flow in transparent replicas of rough-walled rock fractures. *Transport in porous media*, vol.98, pp.401-426, 2013.

Reimann J and Seeger W. Two-phase flow in a T-junction with a horizontal inlet. Part II: Pressure differences. *International Journal of Multiphase Flow*, vol.12, no.4, pp.587-608, 1986.

Romm, E.S., Fluid flow in fractured rocks (in Russian), Nedra Publishing House, Moscow, 1966. (English Translation, Blake W R, Bartlesville, Oklahoma, 1972)

Scheidegger A E. The physics of flow through porous media. University of Toronto Press, Toronto and Buffalo, 3rd Edition, 1974.

Schrauf W and Evans D. Laboratory studies of gas flow through a single natural fracture, *water resources research*, vol.22, pp.1038-1050, 1986.

Seeger W, Reimann J, Müller U. Two-phase flow in a T-junction with a horizontal inlet. Part I: Phase separation. *International Journal of Multiphase Flow*, vol.12, no.4, pp.575-585, 1986.

Sjodin B. How to generate random surfaces in COMSOL Multiphysics. https://www.comsol.jp/blogs/how-to-generate-random-surfaces-in-comsol-

multiphysics, 2017.

Soong Y, Goodman A L, Jones M and Baltrus J P. Experimental and simulation studies on mineral trapping of CO_2 with brine. *Energy conversion and management*, vol.45, pp.1845-1859, 2004.

Su B and Zhan M. Experimental study on fluid flow in crossed fractures. *Journal of hydraulic engineering*, vol.5, pp.1-6, 1997.

Sudicky E A and Frind E O. Contaminant transport in fractured porous media: analytical solutions for a system of paralled fractures. *Water resources research*, vol.18, no.6, pp.1634-1642, 1982.

Sun W, Liu Y, He K, Wang S. The phase distribution of gas-liquid two-phase flow in microimpacting T-junctions with different branch channel diameters. *Chemical Engineering Journal*, vol.333, pp.34-42, 2018.

Tabe Y, Lee Y, Chikahisa T, Kozakai M. Numerical simulation of liquid water and gas flow in a channel and a simplified gas diffusion layer model of polymer electrolyte membrane fuel cells using the lattice Boltzmann method. *Journal of Power Sources*, vol.193, no.1, pp.24-31, 2009.

Temeng O and Horne R. The effect of high pressure gradients on gas flow, *63rd Annual technical conference and exhibition*, SPE, Houston, 1988.

Thomas L K, Dixon T N and Pierson R G, "Fractured reservoir simulation," *Society of Petroleum Engineers Journal*, 1983.

Wang J. Research on the dynamic behavior of gas-liquid two-phase flow [M]. Shanghai: Shanghai Jiao Tong University Press, 2012.

Wang S, He K and Huang J. Phase splitting of a slug–annular flow at a horizontal micro-T-junction. *International Journal of Heat and Mass Transfer*, vol.54, no.1-3, pp.589-596, 2011.

Watanabe N, Sakurai K, Ishibashi T et al. New v-type relative permeability curves for two-phase flows through subsurface fractures. *Water Resources Research*, vol.51, no.4, pp.2807-2824, 2014.

Whitaker S. Flow in porous media I: A theoretical derivation of Darcy's law. Transport in porous media, vol. 1, no.1, pp.3-25, 1986-I.

Whitaker S. Flow in porous media II: The governing equations for immiscible, two-phase flow. *Transport in porous media*, pp.105-125, 1986-II.

Wilson C R and Withspoon P A. Flow interference effects at fracture intersections. Water resources research, 1976, vol.12, no.1, pp.102-104.

Wu Y, Di Y, Kang Z and Fakcharoenphol P. A multiple-continuum model for simulating single-phase and multiphase flow in naturally fractured vuggy reservoirs. *Journal of petroleum science and engineering*, vol.78, pp.13-22, 2011.

Wyckoff R D and Botset H G. The flow of gas-liquid mixtures through unconsolidated sands. *Physics*, vol.7, pp. 325-345, 1936.

Yang D and Zhao Y. Gas-liquid two-phase critical seepage law in single fracture and its random and compound mathematical model, *Chinese Journal of Rock Mechanics and Engineering,* vol.27, no.1, pp.84-89, 2008.

Zimmerman W, Al-yaarub A, Pain C et al. Non-linear regimes of fluid flow in rock fractures, *International Journal of Rock Mechanics and Mining Science*, vol.41, pp.163-169, 2004.